Doctoral Thesis

CIRCULATING TUMOR CELLS ENRICHMENT AND SINGLE CELL ANALYSIS IN NON-SMALL CELL LUNG CANCER

Minji Lim

Department of Biomedical Engineering

Graduate School of UNIST

2020

CIRCULATING TUMOR CELLS ENRICHMENT AND SINGLE CELL ANALYSIS IN NON-SMALL CELL LUNG CANCER

Minji Lim

Department of Biomedical Engineering

Graduate School of UNIST

Circulating tumor cells enrichment and single cell analysis in non-small cell lung cancer

A thesis/dissertation
submitted to the Graduate School of UNIST
in partial fulfillment of the
requirements for the degree of
Doctor of Philosophy

Minji Lim

06. 16. 2020
Approved by

Advisor
Yoon-Kyoung Cho

Circulating tumor cells enrichment and single cell analysis in non-small cell lung cancer

Minji Lim

This certifies that the thesis/dissertation of Minji Lim is approved.

06. 16. 2020

Advisor: Yoon-Kyoung Cho

Semin Lee: Thesis Committee Member #1

Taejoon Kwon: Thesis Committee Member #2

Mi-Hyun Kim: Thesis Committee Member #3

Dong Uk Kim: Thesis Committee Member #4

Abstract

Compared to general-used tissue biopsy, less invasive "liquid biopsy" can provide insight which related to the real-time dynamics of cancer by more frequent analysis of circulating biomarkers including circulating tumor cells (CTCs) and circulating tumor DNA (ctDNA). Furthermore, liquid biopsy is expected to offer a more comprehensive information of the disease, because circulating biomarkers may include cancer-associated materials from multiple disease sites in the body. However, the extreme rarity of cancer-associated circulating biomarkers in blood has been a great challenge to the achievement of the goals for liquid biopsy.

CTC refers to tumor cell which disseminate from the primary tumor site to blood stream. Although CTC enumeration provides potential utility as a promising prognostic liquid biopsy marker, it has not been established yet due to its extreme rarity in comparison to other types of blood cells (1–10 CTCs/10^6 blood cells in 1 mL of blood). Representatively, CellSearch has been approved by the FDA about CTC enumeration system for breast, colorectal, and prostate cancer testing. And various microfluidic chips have been developed for CTC isolation based on physical and biochemical characteristics of CTCs. For example, some chips used epithelial cell adhesion molecule (EpCAM) antibody based capture and others used a size-selective manner. Many clinical papers were reported about the role of CTCs according to the remarkable improvement of the device. Notably, a high CTC count is associated with poor prognosis for cancer patients.

Despite the clinical importance and progress of CTC-based cancer diagnostics, most of the current methods of enriching CTCs are difficult to implement in general hospital settings due to complex and time-consuming protocols. Among existing technologies, size-based isolation methods provide antibody-independent, relatively simple, and high throughput protocols. However, the clogging issues and lower than desired recovery rates and purity are the key challenges.

In this thesis, fluid-assisted separation technology (FAST), which applied to centrifugal microfluidics with size-based membrane filtration, was suggested to solve clogging issues. FAST was inspired by antifouling membranes with liquid-filled pores in nature and it achieved high sensitivity (95.9 ± 3.1% recovery rate) and high selectivity (>2.5 log depletion of white blood cells) without clogging. Moreover, rapid (>3 mL/min) isolation of viable CTCs from whole blood without prior sample treatment enabled simple and ultrafast process which could be applied in clinical field. Numerical simulation and experiments demonstrated that FAST disc achieved uniform, clog-free, ultrafast cell enrichment with pressure drops much less than in conventional size-based filtration, at 1 kPa. We validated the clinical utility of the point-of-care detection of CTCs with 142 cancer patients' samples.

For the depth study, we selected lung cancer to apply molecular analysis based on CTCs. In particularly, lung cancer is the most common cause of worldwide cancer-related mortality with 1.8 million new cases reported every year in both men and women. NSCLC accounts for 85% of all lung cancers and epidermal growth factor receptor (EGFR) mutations are the representative mutation in 10-30% of patients. According to the mutant type of NSCLC patients, targeted therapies including EGFR tyrosine kinase inhibitor (TKI) drugs can induce improved clinical outcomes. For obtaining molecular information about their tumors, detection of EGFR mutation from patient-driven CTCs should be validated through the confirmation of concordance with tissue biopsy results.

Successive downstream analysis of single CTCs from each patient during treatment is needed for observing a change of characteristics related with therapeutic response. To make it possible, robust CTC isolation system with high efficiency is required. With the above needs in mind, we report the clinical validation and demonstration of a FAST disc capable of rapid CTC isolation and easy single cell picking for individual CTC characterization. We report here a proof-of-concept demonstration showing clinical meaning of CTCs included multigene expression as a monitoring marker in NSCLC.

Table of Contents

List of Figures

Figure 2.8. Numerical analysis comparing non-FAST and FAST disc methods. **(a)** Blood phase flows (left) and pressure contours (right) at 0.13 s, induced by centrifugal force generated by spinning the disc at 600 rpm in non-FAST (top) and FAST (bottom) modes. Pressure is developed due to centrifugal force in *O* (1 kPa), which is determined by the mass of the liquid phases and the angular velocity of rotation. In the non-FAST case, the pressure gradient in the upper chamber causes a non-uniform pressure drop across the membrane and, in consequence, the blood phase is filtered only through a small portion of the membrane. This significantly reduces the efficiency of the membrane. Meanwhile, in the FAST disc, the chamber under the membrane is filled with an aqueous phase during the entire filtration process. Therefore, when the blood phase reaches the membrane, the blood phase flows into the lower chamber uniformly and diffuses into and mixes with the liquid phase. The FAST disc uses the entire membrane area for filtration which significantly alleviates clogging. **(b)** Pressure plots in the radial direction above (1) and below (2) the membrane. **(c)** Pressure difference ($\Delta p = p_1 - p_2$) along radial direction. The broken lines correspond to the non-FAST cases (b,c) indicate those locations where liquid flow does not occur.

Figure 2.9. Electric circuit equivalent model for non-FAST and FAST methods. Electric circuit equivalent models for **(a)** non-FAST and **(b)** FAST methods. **(c)** Effect of outlet resistance (*R*2) in non-FAST method, which varies with the channel width. If the outlet resistance is too low (blue line), back flow may be possible, making system unstable. If the outlet resistance is too high (black line), the flow rate is significantly reduced. **(d)** Capacitance effect of lower chamber in non-FAST method. If the capacitance increases, the flow rate of the outlet stabilizes. If there is no air in the lower chamber (FAST method), the flow is almost incompressible and so can spontaneously respond to the flow rate while the system is running. These hydrodynamic behaviors should be considered to optimize the chamber configuration and fluid channels according to the operating conditions. .

Figure 2.10. Optimization of the FAST disc using cancer cells spiked into whole blood. The capture efficiency (red); defined as number of captured cancer cells/input number of cancer cells, and purity (blue); log depletion ratio defined as log (input number of white blood cells [WBCs]/number of remaining WBCs on the membrane), were evaluated with MCF-7 cells spiked into whole blood at various **(a)** rotational speeds and **(b)** numbers of washing steps. The

List of Tables

CHAPTER 1. Introduction

1.1 Liquid biopsy in non-small cell lung cancer

Lung cancer has been the most common cause of cancer-related mortality in both men and women worldwide, with 1.8 million new cases in a year [1, 2]. In contrast to the increase in survival rate for most other cancers, the 5-year relative survival still remains at 18% with an estimate of 158,040 deaths, which is about 26% of total cancer related death in 2017 for the USA alone. The highest mortality of lung cancer is partly because more than half of the cases are diagnosed at a distant stage, which the 5-year survival is only 4%. Therefore, there are critical needs to develop more sensitive technologies for early detection and to improve the survival rates of lung cancer.

Non-small cell lung cancer (NSCLC) represents 85% of lung cancer, in which epidermal growth factor receptor (EGFR) mutations occur in 10–30% of NSCLC patients. Recent advances in understanding molecular abnormalities in lung cancer and highly sensitive molecular analysis technologies revealed that targeted therapies such as EGFR tyrosine kinase inhibitor (TKI) drugs can deliver improved clinical outcomes for certain groups of patients with advanced NSCLC [3-7]. Currently, the tissue biopsy is conducted for most of the patients with NSCLC to obtain the molecular information of their tumors. However, the efficacy of the targeted therapy is limited because of the almost inevitable resistance development. The invasive nature of the tissue biopsy hinders frequent sampling to understand tumor dynamics and drug response. In addition, local sampling by tissue biopsy can be biased because of the heterogeneity of tumor and fail to detect the occurrence of metastasis at distant sites.

Less invasive “Liquid Biopsy” can provide real time dynamics of lung cancer via more frequent analysis of circulating biomarkers such as circulating tumor cells (CTCs) and circulating tumor DNA (ctDNA). Furthermore, the liquid biopsy is expected to offer a more comprehensive picture of the disease because blood circulating markers may contain cancer associated materials from multiple disease sites of the body (**Table 1.1)**. However, extreme rareness of tumor-associated biomarkers in blood has been a great challenge to achieve the desired goal. Recent innovations made in microfluidic chip-based ultrasensitive rare cell isolation technologies and affordable molecular detection technologies such as next generation sequencing (NGS) or droplet digital polymerase chain reaction

---

Table 1.1. Advantages of liquid biopsy compared to tissue biopsy

Tissue biopsy	Liquid biopsy
• Clinically validated • Invasive and risky • Difficult to repeat • Failure to reflect tumor heterogeneity • Failure to detect metastasis at distant sites • Impractical for periodic monitoring of treatment response	• Clinical practice rules are not yet established • Non-invasive • Easily repeated • Potential to reveal spatial and temporal tumor heterogeneity • Offers a more comprehensive picture of the disease • Real-time monitoring for drug response and resistance

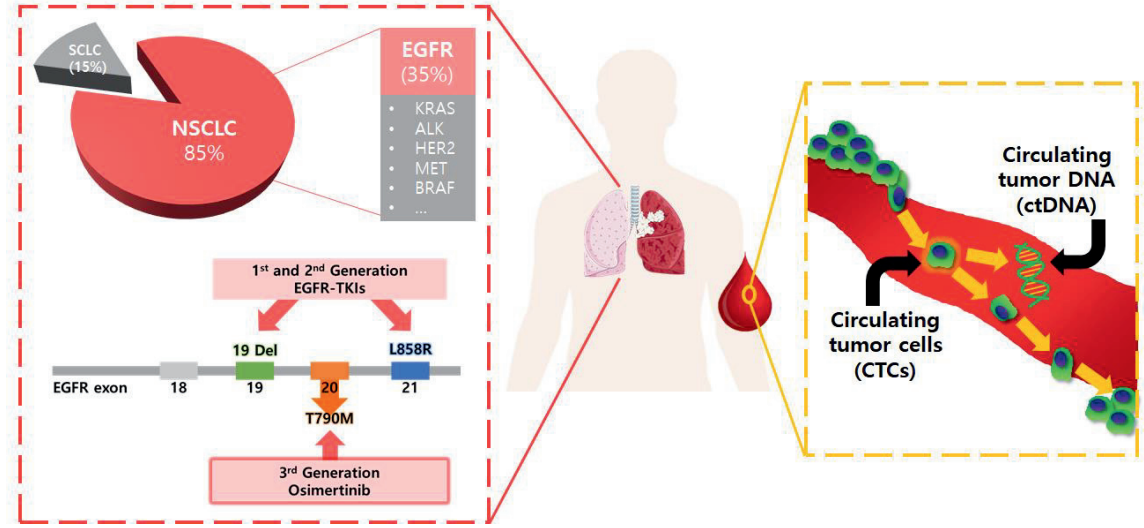

Figure 1.1. Schematic illustration of clinical utility of liquid biopsy for lung cancer. Circulating biomarkers (CTCs, and ctDNA) are used for the identification of actionable mutations such as sensitizing (exon 19 and 21) and resistant (T790M) EGFR mutations.

(ddPCR) offers promising clinical test results, which suggests the liquid biopsy based personalized medicine becomes a reality in near future.

While CTCs have still not been validated for the use in clinical settings for the disease management of the patients with NSCLC, ctDNA has been approved by the Food and Drug Administration (FDA) in 2016 as the first liquid biopsy test for patients with NSCLC, in which the ctDNA is analyzed for the presence of specific mutations to identify patients eligible for treatment with the EGFR-targeted therapy. Herein, we provide a brief overview of the clinical perspectives and opportunities of liquid biopsy in lung cancer specifically focusing on the identification of actionable mutations such as sensitizing (exon 19 and 21) and resistant (T790M) EGFR mutations, significance and uniqueness of the two most popular circulating biomarkers, i.e. CTCs, and ctDNA, and the detection methods of each biomarker and their current limitations. We further discuss the key areas of potential clinical applications of liquid biopsy using CTCs and ctDNA in early diagnosis, prognosis, monitoring response and resistance to treatment, and the remaining hurdles to overcome before the routine implementation in clinical settings.

EGFR mutations and resistance mechanisms

EGFR TKI drugs such as erlotinib, afatinib and gefitinib are used as the first line therapy for the patients with advanced NSCLCs [3-7]. As schematically shown in **Figure 1.1**, some groups with specific activating mutations, deletions in exon 19 (19 Del) and substitutions in exon 21 (L858R), in the tyrosine kinase domain of EGFR show dramatic response to gefitinib. It is also found that a large portion of the responding groups are Asian women with adenocarcinoma with or without a very little previous record of smoking. This offers a new paradigm of personalized medicine, in which patients can predict whether the targeted drug would be effective for them by the mutation analysis.

However, EGFR inhibitors often work only for several months or more, but eventually the drugs stop working because of the resistance development. One of the major resistance mechanisms is a secondary mutation in EGFR (T790M), which is found in 48 to 62% of EGFR TKI resistant patients. Recently, a third-generation EGFR TKI, osimertinib, was approved by FDA for T790M positive patients, which has shown significantly better efficacy than platinum-based therapy. Therefore, early detection of T790M mutation during the first line therapy and change the drug to osimertinib are extremely important in the disease management of NSCLC patients with EGFR mutations [8].

Significance and uniqueness of CTCs and ctDNA as a liquid biopsy biomarker

CTCs are the tumor cells, which are disseminated from primary tumor and/or metastatic lesions and circulate along the blood stream. CTCs are distinguished from other blood cells due to their positive expression of epithelial markers including epithelial cell adhesion molecule (EpCAM) and cytokeratins (CK), and negative expression of white blood cell specific marker, CD45 [9]. During intravasation into blood vessels, CTC undergoes epithelial-to-mesenchymal transition (EMT) and during extravasation into secondary organ, it undergoes mesenchymal-to-epithelial transition (MET). Thus, CTCs in blood stream have heterogeneous levels of biomarker expression related to EMT and MET [10]. Heterogeneous CTCs can be divided into various subgroups: intact single CTCs, apoptotic CTCs and CTC clusters. The size range of CTC is slightly bigger than other blood cells (8 – 20 μm) but the size is also heterogeneous depending on the cancer type [11].

As shown in **Table 2,** CTCs contain various cellular and subcellular components which can be used for further downstream analysis; e.g. intact DNA for well-known mutation analysis as well as novel marker discovery, RNA for gene expression profiling and various biomarkers for proteomic analysis. Direct visualization of cellular morphology for the identification of malignant phenotype is an important and unique aspect of CTCs compared to other circulating biomarkers. In addition, immunocytochemistry (ICC) [12] and Fluorescent in situ hybridization (FISH) [13] can be performed on CTCs to identify their phenotype and to detect some genomic alteration. CTCs are divided into various subgroups according to the cell diameter or nuclear fraction and each subgroup is analyzed for its characteristics [14]. Isolated CTCs are cultured in vitro to establish the permanent CTC cell line for further studies [15-17]. Furthermore, they can be applied to various in vivo, ex vivo and in vitro experiments for functional studies. CTC derived explants (CDXs), patient-derived xenograft models (PDXs), ex vivo cultured CTCs are applied to drug screening which would contribute for the personalized therapy.

However, CTCs are extremely rare compared to other types of blood cells (1 – 10 CTCs/10^6 blood cells in 1 mL blood). Furthermore, CTCs are heterogeneous both in surface protein markers and physical characteristics. Therefore, it has been a great challenge to isolate CTCs with high sensitivity and specificity. For example, the CTCs isolation technologies using the anti-EpCAM antibodies cannot isolate the cells which undergone EMT or with low EpCAM expression. Even if 99.9% of blood cells are purified, the purity of the isolated CTCs is below 1%, which is at the limit of the detection of the currently available molecular analysis techniques. Thus, the extremely sensitive and specific isolation and detection methods are required to improve their clinical utility in liquid biopsy. While the CellSearch technology was approved for breast, colorectal, and prostate cancer by the FDA, the CTCs in lung cancer are still under investigation.

Tumor-related genetic alterations can be detected in 'ctDNA', which is the fragmented DNA freely circulating in the blood stream shed from the tumor tissue by apoptosis, necrosis and secretion of the tumor cells [18]. The short length of DNA (~180 base pairs) is reminiscent of the ctDNA generated by apoptotic degradation of cellular DNA [19, 20]. Due to the short length of ctDNA, the clearance is very rapid with the half-life of less than 2 hours [21]. For ctDNA analysis, plasma samples are preferable to serum samples to avoid possible contamination of wild-type DNA released from other blood cells. The unfavorable stability of ctDNA is advantageous for real-time monitoring of the disease status though it adversely affects the sensitivity of the detection. Furthermore, ctDNA originates from any lesion of tumor in the body so that the sampling bias would be minimized. Thus, it has the advantage in the drug response monitoring to provide the crucial evidence whether the tumor newly developed resistance or not (**Table 1.2**). In this regard, the cobas EGFR Mutation Test v2, which is PCR-based liquid biopsy testing for NSCLC, has recently been FDA approved. However, the extremely low fraction of tumor-specific genetic alterations in 'sea' of normal cell-free genomic DNA requires further development of highly sensitive, advanced molecular detection technologies as well as ct-DNA specific isolation methods. Recent advances in cancer management by personalized medicine has been expedited together with the significant progress made in ultrasensitive molecular characterization methods such as the NGS and third generation PCR technology (e.g. ddPCR) [22-24].

Table 1.2. Unique advantages and limitations of circulating biomarkers; CTCs vs ctDNA

	CTC	ctDNA
Advantages	Morphological and functional analysis of cells (ICC[1], FISH[2]) Proteomics of both cellular and sub-cellular level Analysis of RNA expression In-vitro/in-vivo functional studies (PDX[3] model) Relevance for the metastasis	Potential for full representation of spatial and temporal tumor heterogeneity More sensitive to tumor burden, treatment monitoring, and development of resistance First FDA-approved liquid biopsy test for NSCLC Relatively simple isolation method
Limitations	Extreme rarity and fragility Heterogeneity of CTCs Lack of standard isolation method Require better sensitivity and specificity (EMT[4], WBC[5])	Rarity and fragility Difficult to isolate tumor specific DNA Contamination with DNA from normal cells No functional analysis

[1]ICC (Immunocytochemistry); [2]FISH (Fluorescent in situ hybridization); [3]PDX (Patient derived xenograft); [4]EMT(epithelial to mesenchymal transition); [5]WBC (white blood cells)

In summary, both CTC and ctDNA based liquid biopsy can contribute to cancer diagnosis, prognosis, and personalized treatment. EGFR mutation detection by ctDNA analysis is an exciting application of liquid biopsy as recently approved by the FDA. CTCs have their own advantages offering not only the mutation detection but also the analysis of multiple biomarkers (DNA, RNA, proteins) and morphological and functional analysis of intact cancer cells. Liquid biopsy using multiple kinds of biomarkers may minimize the sampling bias and provide more comprehensive picture of disease status. For example, ctDNA-based detection may be less vulnerable to the isolation methodology and better represent the cancer heterogeneity and longitudinal surveillance of cancer therapy while lack of materials and multiple choices of isolation technologies are unsolved issues for CTC analysis. On the other hand, the cytochemistry and morphological analysis of intact cancer cells gives valuable information relevant to the established cytological criteria in tissue biopsy. Furthermore, in-vivo functional assays using PDX model developed by CTCs can provide fundamental knowledge on the metastatic process and disease progression. However, both biomarkers are rare and fragile and require more sensitive isolation techniques from other blood components with the high-yield and high purity. Therefore, the improvement of the sensitivity specificity in the analysis of target biomarkers have been an active research area during last decades both in the chip-based rare cell isolation and advanced molecular characterization. Next session, we will review the representative commercialized products for liquid biopsy and related clinical reports on prognosis for NSCLC patients. Moreover, we introduce recent research papers studying molecular diagnosis based on the analysis of CTCs and ctDNA and give future perspectives about liquid biopsy for patients with NSCLC.

1.2 Technologies for CTCs analysis and clinical applications in NSCLC

1.2.1 Prognosis using commercially available CTCs isolation devices

CellSearch (J&J, Veridex) is the only FDA approved method to enumerate CTCs, in which the separation mechanism is based on the isolation of CTCs using magnetic beads conjugated with EpCAM antibody. Though it is approved for the prognosis of patients with metastatic breast cancer (2004), colorectal cancer (2007), and prostate cancer (2008), it shows limited detection sensitivity for low EpCAM expressed CTCs. For lung cancer case, there is no validation approved yet despite many studies conducted to establish CTCs counts as a diagnostic and prognostic tool for NSCLC patients.

As shown in **Table 1.3**, several studies indicate that the CTC counts might be useful as a prognostic marker for patients with advanced lung cancer even though the detection rate was relatively low. Most of the studies tried to identify the baseline CTC counts as a prognostic marker and reported significantly poor progression free survival (PFS) or overall survival (OS) in the patient group with high CTC counts [25-32].

The first and representative study in NSCLC patients was reported in 2011 on the clinical meaning of the baseline CTC counts measured by CellSearch. Among 101 patients with advanced NSCLC (stage IIIA-IV), patients were divided into 2 groups according to their base line CTC counts with a cut off of 5 CTCs / 7.5 mL. In this study, both PFS and OS were significantly poorer in CTC positive group than in CTC negative group (median PFS: 6.8 months vs. 2.4 months, median OS: 8.1 months vs. 4.3 months). Moreover, patients who had below 5 CTCs / 7.5 mL at two sequential time points achieved much longer PFS and OS (median PFS: 7.6 months vs. 2.4 months, median OS: 8.8 months vs. 4.3 months) [25].

Other papers reported the clinical importance of not only the baseline CTC counts but also the CTC counts during the time course of treatment [26]. Among 37 evaluable advanced NSCLC patients' samples, 75.7 % of patients had the positive CTC counts (≥ 1 CTCs / 7.5 mL) at baseline and they showed high association between baseline CTC counts and response to treatment by Response Evaluation Criteria in Solid Tumors (RECIST). More importantly, the change in CTC counts at 56 days after treatment had much stronger correlation with survival than change in CTC counts at 14 days or 28 days after treatment (P value at 56 days : 0.006 vs. at 14/28 days : 0.104) [26]. These data suggest a correlation between the decreases in CTC counts upon the treatment and longer PFS, which may indicate an early response to the therapy.

However, another study conducted with 59 advanced NSCLC patients showed that the CTC counts are poorly correlated with the treatment response while it was a good indicator for poor prognosis and the presence of distant metastasis [27]. The patients with CTC counts more than the cut off value of 2 CTCs / 7.5 mL showed significantly poor PFS and OS (median PFS: 6.2 months vs. 4.3 months, median OS: 11.2 months vs. 8.3 months). In addition, they noted that the CTC counts at 2 months after treatment were also well correlated with OS (P value of OS at baseline: 0.006 and at 2 months after: 0.008) [27].

In addition, the prognostic value of the CTC subgroups was analyzed based on the characterization of cell morphology or the expression levels of the specific biomarkers. Among 43 patients with advanced NSCLC, those who had more than 5 morphologically intact CTCs showed significantly poor PFS and OS (median PFS: 7.6 months vs. 4.1 months, median OS: 10.7 months vs. 4.6 months) [28]. Furthermore, the patients showing an increase of intact CTC after one cycle of chemotherapy showed

Table 1.3. Examples of studies on CTCs-based prognosis for patients with NSCLC

Methods	Therapeutics	Stage	# of patients	Cut off (CTCs / 7.5 mL)	Significance*	Detection rate	Reference
CellSearch	Platinum	IIIA - IV	101	5	PFS / OS (P < 0.001)	14.9%	25
	EGFR TKI	IIIB- IV	37[a] (41)[b]	1	PFS (P = 0.006)**	75.7%	26
	EGFR TKI	IIIA – IV	59	2	PFS / OS (P = 0.01 /P = 0.006)	40.7%	27
	QT treatment	IIIB - IV	43	5	PFS / OS (P = 0.034 /P = 0.008)	23.2%	28
	Platinum, EGFR TKI, ALK inhibitor	IIIB- IV	125	5	OS (P = 0.022)	19.2%	29
	Adjuvant chemotherapy	I - IIIA	27[a] (30)[b]	1	DFS / OS (P = 0.011 /P = 0.037)	22.2%	30
ISET	Neoadjuvant therapy	I – IV	208	50***	DFS / OS (P = 0.001 /P = 0.002)	30.8%	31
	Neoadjuvant therapy / Surgery	I – IV	210	1	DFS (P < 0.0001)	49.5%	32

*Progression free survival (PFS), overall survival (OS), disease free survival (DFS). P value in (27) and (29) are analyzed by multivariate Cox-proportional hazards regression analysis. P value in the other references are analyzed by Kaplan-Meier analysis. **Analyzed with CTC counts change at 56 days after treatment (baseline CTC: not available). ***This CTC count is not normalized with 7.5 mL. Instead, it is the number of CTCs from 6 mL of blood. [a]number of patients whose blood sample were analyzed, [b]number of patients who enrolled for the study.

poorer PFS. They also tested not only the intact CTCs which passed the calling criteria of the CellSearch system but also the CTC-like objects such as apoptotic CTCs or CK+ fragments. Interestingly, an apoptotic CTC positive group (≥ 2 apoptotic CTCs / 7.5 mL) also showed poor PFS and OS (median PFS: 7.6 months vs. 3.4 months, P = 0.017; median OS: 10.5 months vs. 3.6 months, P = 0.001) [28].

Furthermore, a recent study with 125 patients with advanced and metastatic NSCLC showed that that the total CTC counts (≥ 5 CTCs / 7.5 mL) can be used as a prognostic biomarker for OS (HR 0.55, 95% CI 0.33–0.92, P = 0.022) but not PFS (HR 0.68, 95% CI 0.42–1.1, P = 0.118). When they further analyzed the CTCs counts depending upon the Vimentin (Vim) expression and genetic subtypes (KRAS mutation, EGFR mutation, and ALK rearrangement), Vim expressed CTCs (≥ 1 Vim (+) CTCs) were significantly high in patients with EGFR-mutated cancer (total CTC (+) 57.1% vs. 30.1, P = 0.038; Vim expressed CTC positive 42.9% vs. 15.1%, P = 0.013), while no additional prognostic significance was obtained when the total CTC+ groups were subdivided into Vim(+) CTC and Vim(-) CTC groups. The Vim(+) CTCs were either reduced or not found in the subgroups of ALK-rearranged or KRAS-mutated subgroups, respectively. Because Vim is a protein marker related with the EMT, it was suggested that EMT characteristics can be different depending upon the genetic subtypes of NSCLC patients. However, the analysis has intrinsic limitation because the analysis of Vim, a mesenchymal marker, was done for the CTCs isolated by immunoaffinity capture using an epithelial marker, EpCAM antibody. Nonetheless, it suggests the importance of genetic subtypes for the clinical utility of the CTCs analysis [29].

Though majority of the CTCs analysis were conducted using the blood samples of the patients with advanced NSCLC, it would be certainly a ‘holy grail’ if the liquid biopsy can be used for the early screening of lung cancer. However, this application has not been successful yet though there have been a few reports worthy to note [30]. For example, 30 pulmonary vein samples and 27 peripheral blood samples from 30 NSCLC patients not in advanced stage but in early stage (Stage I - IIIA) were collected to test number of CTCs by CellSearch. Much more numbers of CTCs were detected in pulmonary samples (43% of patients show 1 – 3093 CTCs / 7.5 mL of pulmonary sample and 22% of patients have 1 – 4 CTCs / 7.5 mL of peripheral sample). However, the CTC counts from pulmonary sample had no significant correlation with the survival. Only the CTC counts from peripheral sample were strongly related with poor disease free survival (DFS) and OS (P = 0.011 and P = 0.037) [30].

To overcome the limitation of EpCAM-based isolation methods, separation techniques based on the differences in physical properties are also developed. For example, ISET (Rarecells) uses size difference between CTCs (8 ~ 20 μm) and other blood cells (6 ~ 10 μm). Compared to immunoaffinity-based methods, the size-based filtration is relatively simple and fast. Though the cell sizes are

heterogeneous as well, the number of CTCs isolated by using a track-etched polycarbonate membrane with pore diameter of 10 μm were higher than that of CellSearch methods [31, 32]. For example, the CTC positive group with the cut-off value of 50 CTCs/6mL, 30.8 % of 208 patients with NSCLC, had significantly poorer PFS and OS than the CTC negative group (P = 0.002 and 0.001, [31]). In a follow-up paper, 50% of patients had positive CTC detection with high correlation with DFS (P < 0.0001) when they used the cutoff value of 1 CTC / 7.5 mL. Interestingly, the patients who had positive CTC detection in both CellSearch and ISET had a stronger correlation with poor survival than patients who had positive CTC detection from only one method [32].

Taken together, the clinical meaning of CTCs counts still remains controversial although many studies indicate that the high CTCs count has strong correlation with poor survival. The number of CTCs is highly variable depending on the tumor types, patients groups, and the methods used for the isolation. It would require further validation to answer whether the CTC counts can be used for the prediction of the therapy response. The additional characterization of CTCs using molecular or protein markers are required to improve the clinical impact of CTCs. These limitations will be overcome by the development of more robust technologies with improved assay performance. Many new microfluidic chips based rare cell isolation technologies achieved higher yield and purity compared to the currently commercially available devices even though larger scale clinical tests with various patient groups are required before the validation of CTCs as a prognostic marker in clinical studies.

1.2.2 Molecular diagnosis using isolate CTC by microfluidic chips

In order to use CTCs for molecular diagnosis, the purity should be higher than the minimum requirements of the downstream molecular analysis techniques such as PCR and NGS. Therefore, many devices have been developed to improve the capture efficiency and purity. Here, we will review the most recent devices that have been used for the molecular analysis of CTCs isolated from patients with NSCLC as summarized in **Table 1.4**.

In order to improve the capture efficiency, ^{Hb}CTC-Chip which has herringbone pattern on the channel roof was developed **(Figure 1.2a).** The contact frequency between CTCs and EpCAM antibody coated on the chip surface could be highly enhanced by the microvortex formed due to its herringbone pattern. ^{Hb}CTC-Chip achieved higher capture efficiency than flat channel in PC3, a prostate cancer cell line, spiked experiment (Capture efficiency of ^{Hb}CTC-Chip: 79% ± 4.5% and Flat chip: 29% ± 4.3%). In clinical test with 15 metastatic prostate cancer patients, ^{Hb}CTC-Chip obtained detection rate of 93%

Table 1.4. Summary of reports on mutation detection in CTCs from patients with NSCLC.

Isolation method	Therapeutics	Stage	# of patients	Detection techniques	Mutation	Detection rate	Con-cordance
[Hb]CTC-Chip[34]	EGFR TKI Chemotherapy	III - IV	28[a] (40)[b]	DNA sequencing	T790M	50 % (14/28)	57% (12/21)
Nanovelcro[36]	EGFR TKI	III - IV	7	Sanger sequencing	L858R / T790M	85.7 % (6/7) 28.6 % (2/7)	100 % (7/7)
Single cell retrieval[37]	EGFR TKI	IV	6 [a] (7) [b]	Sanger sequencing	L858R / T790M	16.7 % (1/6) 66.7 % (4/6)	100 % (6/6)
MagSifter[39]	NA	I-IV	7 [a] (35) [b]	RT-PCR	19 del / L858R / T790M	42.9 % (3/7) 14.3 % (1/7) 42.9 % (3/7)	NA
OncoBean Chip[41]	NA	I-IV	4 [a] (36) [b]	RT-PCR	EGFR / KRAS	25.0 % (1/4) 50.0 % (2/4)	NA

[a]Number of patients whose CTCs were isolated and used for genotyping; [b]number of patients who enrolled in the study. Nanovelcro and Single cell retrieval required at least 3 repeated processes.
* Capture efficiency of MagSifter >95%, release efficiency 92.7 ± 6.1%, cells collected in eluted fraction 89.6 ± 12.1%; ** Purity was measured by spiked experiment except MagSifter (clinical sample experiment); *** After 2nd round of purification, number of WBCs decreased from 4350 WBCs/mL to 12 WBCs/mL.

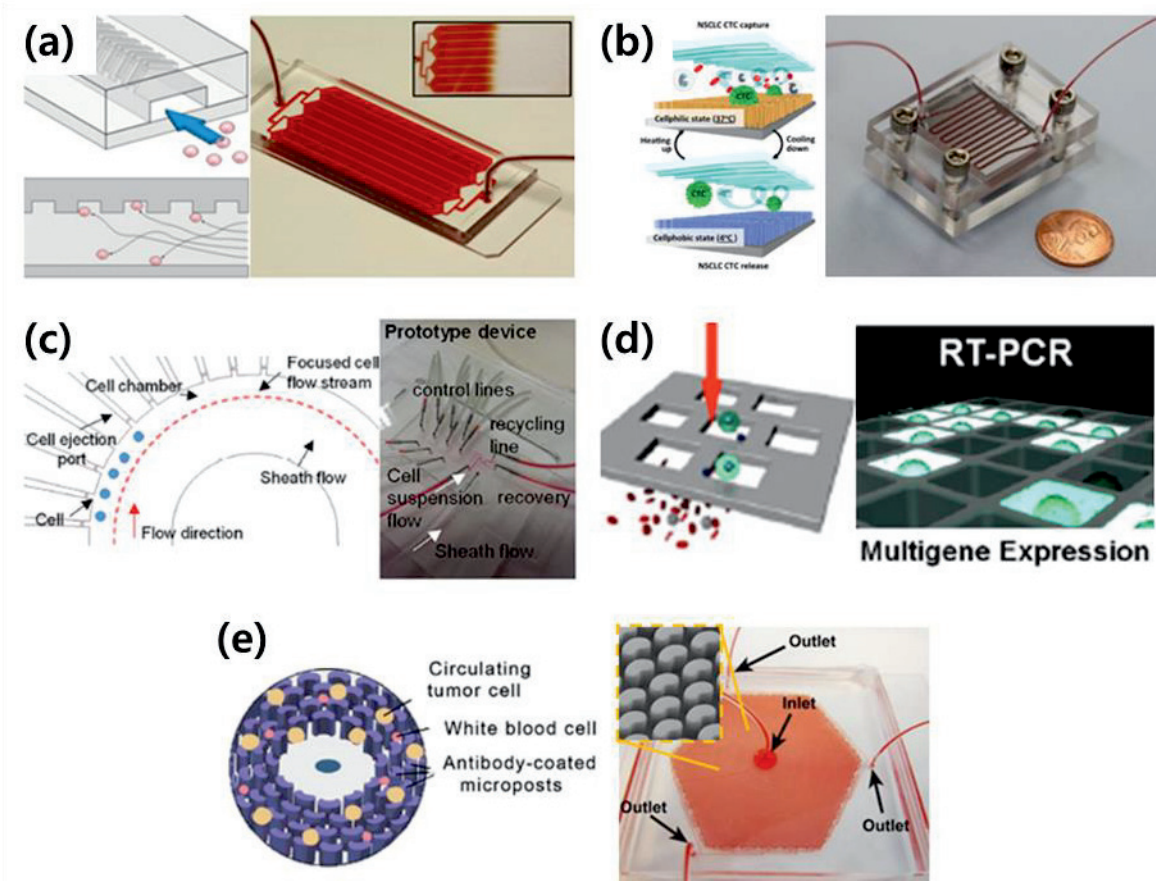

Figure 1.2. Examples of CTC isolation chips used for the mutation analysis of CTCs from patients with NSCLC. **(a)** HbCTC-Chip, which has a herringbone pattern on the channel roof, was developed to improve capture efficiency (Right : 1" × 3" glass slide)[33,34]; **(b)** The purity of the cells captured by NanoVelcro chip, which has silicon nanowires on its bottom substrate to maximize the surface bound antibody, were further improved by thermoresponsive purification step[36]; **(c)** A microfluidic device (3.5 cm × 2.5 cm PDMS chip) capable of single-cell isolation and retrieval was developed to improve purity[37]; **(d)** A nanowell array filled with CTCs magnetically captured by a dense array of magnetic pores (MagSifter) were used for multigene expression profiling from individual CTCs (Upper scale bar: 200 μm, lower scale bar: 50 μm)[38,39]; **(e)** OncoBean Chip, which has bean-shaped posts coated with antibodies were developed to improve the throughput (Right: 2" × 3" glass slide)[40,41]. Reproduced from ref. (33–41) with permission from the United States National Academy of Sciences, American States National Academy of Sciences, American Chemical Society, Nature Publishing Group, Royal Society of Chemistry, and Wiley-VCH.

(14/15 patients) [33]. In addition, [Hb]CTC-Chip was further utilized to detect T790M mutation in the EGFR mutant NSCLC patients to monitor the development of resistance to EGFR TKI therapy. From 40 patients with advanced NSCLC, genotyping was possible in 28 CTC samples (70%) and T790M could be detected from 14 (50%) patients, which was in 57% concordance with primary tissue biopsy result [34].

Another representative device in immunoaffinity based CTC isolation is 'NanoVelcro' which has silicon nanowires on the bottom substrate offering significantly enhanced surface area to contain larger amount of EpCAM antibody and micropattern on the roof for chaotic mixing to promote efficient mixing. In the performance comparison with CellSearch, NanoVelcro obtained much higher detection rate with 26 patients with prostate cancer; the detection rate of NanoVelcro was 76.9 % (20/26 patients) while CellSearch results were 30.8% (8/26) [35]. A follow-up study using additional thermoresponsive purification step reported a significantly improved purity from 35% to 98% when the tests were performed with blood samples spiked with H1975 NSCLC cell line **(Figure 1.2b).** From 7 advanced NSCLC patients, they could achieve 100% concordance in the detection of the EGFR L858R mutation from CTCs and tissue biopsy samples. Especially, two patients had EGFR T790M mutation in the relapse tissue samples and it was also detected in patient-derived CTC samples [36].

In order to improve the purity, a microfluidic device capable of single cell isolation and retrieval was developed. The cells are first hydrodynamically focused in a single stream in the main fluidic channel, and then guided into the single cell capture chamber due to the intrinsic pressure difference **(Figure 1.2c).** The trapped single CTC can be released on-demand to the main channel by positive pressure. The rare CTCs could be isolated with 100 % purity. This microfluidic single cell capture device was applied to detect EGFR L858R and T790M mutation from patient-derived CTCs by Sanger sequencing. A total of 26 CTCs were isolated from 6 of 7 patients, which is in 100% concordance with the corresponding tissue biopsy samples [37].

Furthermore, multigene expression profile from individual CTCs could be performed on a Nanowell array filled with CTCs magnetically captured by a dense array of magnetic pores, MagSifter [38]. The nanowell array can capture CTCs up to 25,600 cells and single cell level multigene RT-PCR could be performed for molecular characterization of single CTCs **(Figure 1.2d).** CTCs, defined as EpCAM+ cells with expression of both TERT and MET in a nanowell, were found in 31 of 35 (88.6%) patients with the cut-off of 7 CTCs in 2 mL. They also confirmed EGFR 19 del, L858R, and T790M mutations from 7 NSCLC patients [39].

In order to improve the throughput, OncoBean Chip which has bean-shaped posts coated with combination of multiple antibodies such as EpCAM, EGFR, and CD133 with a radial flow enabling increased cell capture under high flow rate conditions was developed **(Figure 1.2e).** Based on cell line spiked experiment, the OncoBean Chip achieved more than 80% of capture efficiency at 10 mL/hr flow rate [40]. CTCs were detected in 69.4 % and 83.3% of total 36 patients with NSCLC from intraoperative peripheral (Pe) and pulmonary vein (PV) blood samples, respectively. In this study, pulmonary vein cases achieved much higher CTC counts (0 – 10,278 per 3 mL, with a median of 7.5 CTCs per 3 mL), than peripheral vein cases (0 – 28.5 per 3 mL, with a median of 1.3 CTCs per 3 mL) [41]**.** In addition, CTC clusters were found in 50% of patients and interestingly, clusters found from PV were larger. Considering the fact that the CTCs found in PV are before going through the systemic circulation, it could be assumed that PV is an enriched source of CTCs with larger sized clusters. On the other hand, CTC clusters were either not found in Pe or smaller in size, which suggests that bigger clusters may not able to enter the systemic circulation or dissociated in the areas of smaller vasculature. It was found that the presence of the clusters in preoperative Pe was an indicative of poor prognosis. Furthermore, the mutations were found in 5 of 6 samples tested involving at least one of the genes CTNNB1, EGFR, KRAS, PIK3CA, and TP53. It is noteworthy that the gene expression analysis of CTCs recovered from PV and Pe were different, e.g. TP53 expression was higher in CTCs from Pe while ERCC1 was higher in PV samples, which may suggests the molecular heterogeneity of CTCs from two different sources.

In summary, there are evidences that the isolated CTCs can be used as a biomarker to determine poor prognosis and to predict recurrence. In order to improve the sensitivity and specificity as a biomarker for cancer management, various microfluidic chips are developed and used for molecular diagnostics for the selection of personalized medicine. Currently, rather limited numbers of studies were conducted for patients with NSCLC due to the rareness of CTCs in lung cancer, however, the results are promising and it is expected to have more advanced technologies because the mutation detection in subgroups of NSCLC patients is directly linked to the choice of actionable drugs and personalized cancer management.

1.3 Research motivations

For past few decades, liquid biopsy has been considered as the noninvasive alternative to tissue biopsy. Liquid biopsy is gaining enormous interest among clinics as it provides specific information to help doctors for decision of a proper treatment to patients at various stages of their disease. For this, several devices were developed for CTC isolation and validated clinical utility of CTCs as diagnostic, prognostic and treatment monitoring markers in cancer patients. Simultaneously, various methods of

molecular analysis such as sequencing or mutation analysis were also developed to study and understand their clinical implications.

Although many studies have demonstrated reliability of the liquid biopsy using CTC, until now there is no consensus on the criteria of CTCs as the prognostic markers in NSCLC due to the limitations such as lack of congruence; difficulties in standardization of the sample preparation and isolation method as well as selection of the sample type; heterogeneity of the samples; variations in marker expression such as EMT underwent CTCs with the lack of epithelial marker expression; reproducibility; selectivity and sensitivity etc. Furthermore, the selection of the blood collection tubes, blood volume, and type of downstream analysis, could affect the quality of the data and may induce inaccuracies and statistical errors. Related with the validation of liquid biopsy, Torga *et al.* recently report that independent tests at two different laboratories with identical sample showed only 7.5% of cases with completely matched mutations. This study emphasizes the necessity of standardization based on the development of the robust system and the importance of the prior validation of each technique with multicenter large-scale study for the real application of liquid biopsy in clinical routine. In addition, standardized protocols for blood collection and sampling are also accompanied to minimize the technical errors [42].

The above discussion clearly rationalizes that the development of a robust device for CTC isolation is necessary and analysis of isolated CTCs at single-cell level is essential to better understanding of cancer heterogeneity. Through this thesis, robust centrifugal microfluidic device will be demonstrated utilizing the new technique to prevent clogging issue. We expect this thesis can suggest the expansion of the ability to utilize CTC based liquid biopsy in clinical routine and longitudinal surveillance of cancer therapy.

1.4 Research aims

The research aim in this thesis is the development of robust device for CTC isolation and single cell analysis with isolated CTCs to find clinical meaning. Here, we demonstrate a clog-free CTC isolation device in label-free manner and mRNA profiling based CTC characterization.

Development of clog-free CTC isolation disc in label-free manner

In this thesis, the fast, simple and user friendly device for CTC enrichment with high performance was demonstrated. To take the advantages of lab-on-a-disc system and fluid-assisted separation technology(FAST), we developed the label-free and clog-free FAST disc. The FAST disc has high

capture efficiency regardless of the expression level of cell surface markers. The performance of disc was confirmed across the 142 cancer patients with 7 different cancer types including lung cancer, breast cancer, and pancreatic cancer. Moreover, the high robustness of the disc was confirmed with repeatability test during the 30 days. It is expected that this novel platform will possibly contribute toward liquid biopsy applications by providing a robust and practical solution for clinical field.

Single cell analysis of isolated CTCs to find clinical meaning

In second, clinical meaning of isolated CTCs related to prognosis was demonstrated. We confirmed the relationship of CTC counts and stage, survival, and drug response in NSCLC. We also compared the EGFR mutation which detected from CTCs and tumor tissues and achieved 100% concordance in 13 lung cancer patients. Moreover, T790M mutation, which related with the resistance about EGFR-TKI, is detected in two patients who had T790M mutation in tumor tissue from 2nd tissue biopsy result.

We analyzed the gene expression profiling with patient-driven CTCs in single cell level and found some clue to understand heterogeneity of CTCs and CTC evolution during drug treatment.

CHAPTER 2. Development of clog-free CTC isolation disc in label-free manner

2.1 Centrifugal microfluidics for size-based CTC isolation

2.1.1 Centrifugal microfluidics

In microfluidics field, lab-on-a-chip has been studied by many researchers in order to miniaturize and integrate several laboratory functions on microfluidic platforms [43-45]. One of the final goals is to develop a lab-on-a-chip in which all of the required analytical procedures are carried out on single chip. The user would simply add sample; then the chip would automatically process sequential steps of the assay and return the results. However, lab-on-a-chip requires multiplex operating system, including many pumps connected with several tubings, in contrast with the simple and small construction of the chip [46, 47] **(Figure 2.1a,b)**. To overcome the limitation, centrifugal microfluidic platform, also known as lab-on-a-disc, have emerged with simple operating system which composed with a rotor [48] **(Figure 2.1c)**. It uses centrifugal force as driving force and makes possible to perform various manipulations including valving, metering, mixing and pumping of reagents so it can be applied to point-of-care clinical diagnostics.

In centrifugal microfluidics, there are three intrinsic forces **(Figure 2.1d)** on a spinning system including centrifugal force (F_c), Coriolis force (F_{co}), and Euler force (F_E) [49]. These forces are represented as the following:

$$F_c = -\mathrm{m}\omega \times (\omega \times \mathrm{r})$$

$$F_{co} = -2\mathrm{m}\omega \times \frac{d}{dt} r$$

$$F_E = -\mathrm{m}\frac{d}{dt}\omega \times r$$

In the equations, m is the mass of point-like body where the forces exerted at position r from the center of the spinning system and ω is the angular velocity. F_c exerts radially outward, while the F_{co} force acts perpendicular to both of the fluid velocity and the angular velocity in the spinning system. Lastly, the F_E acts proportionally with angular velocity.

Because the spinning of a disc induces fluid transter, operating system of lab-on-a-disc, including a rotor, can be a table-top size equipment which is suitable for point-of-care test.

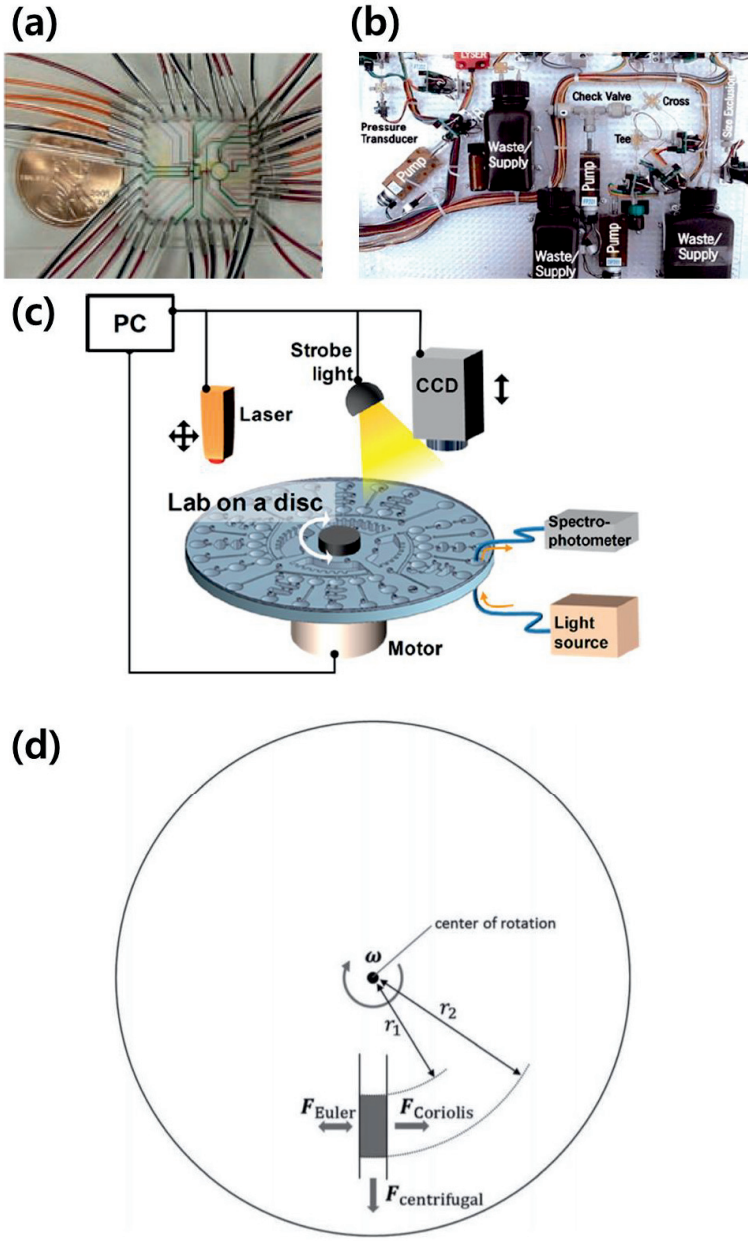

Figure 2.1. Microfluidic systems, lab-on-a-chip and lab-on-a-disc. (a) Image of miniaturized lab-on-a-chip [46]. **(b)** Image of operating system of lab-on-a-chip [47]. **(c)** Scheme of lab-on-a-disc and operation system [48]. **(d)** Forces acting in a spinning system [49].

2.1.2 Membrane filtration

Size based CTC isolation has strengths related with fast and simple operation in unbiased isolation of CTCs compared to immune-affinity based CTC enrichment. Membrane filtration, one of the size based CTC isolation, is used a porous membrane, which pore size is range of 5 – 8 μm, to isolate CTCs from other blood cells [11]. The most critical problem of membrane filtration is clogging issue due to the billions of blood cells, RBCs and WBCs. Because the flow direction of fluid is perpendicular to the membrane surface, the retained cells are collected on the membrane surface forming a filtration cake and occur clogging issue. Moreover, cake layer can increase the pressure drop which induces the damage to cells [50] **(Figure 2.2a)**.

To prevent clogging issue induced by cake layer, pretreatment of blood, such as blood dilution or RBC lysis, is applied to reduce the concentration of cells for increasing the efficiency of filtration [51]. However, each pretreatment has drawbacks; longer process is induced by blood dilution due to the increase in total volume of blood sample and RBC lysis can reduce the capture efficiency of intact CTCs because lysis buffer can affect to not only RBCs but also CTCs. The other case of membrane filtration, tangential-flow filtration, can be a good solution to prevent clogging issue. In tangential-flow filtration, the direction of feed flow is tangential to the membrane surface while the transferred permeate flow is perpendicular to the other side of the membrane [50] **(Figure 2.2b)**. Due to its perpendicular feed direction to the membrane, it prevents increases higher permeate rate and lower flux decline according to the decrease of the cell accumulation on the membrane surface.

To take the advantage of tangential-flow filtration, porous membrane is inserted into the lab-on-a-disc parallel to the direction of flow which induced by centrifugal force **(Figure 2.2c)**.

Although tangential-flow filtration enhances the filtration efficiency, high fluid velocity was required to limit the growth of cake layer on the membrane accompanying the high energy and large pressure drop. Further solution is required to maintain low pressure drop for intact CTC isolation.

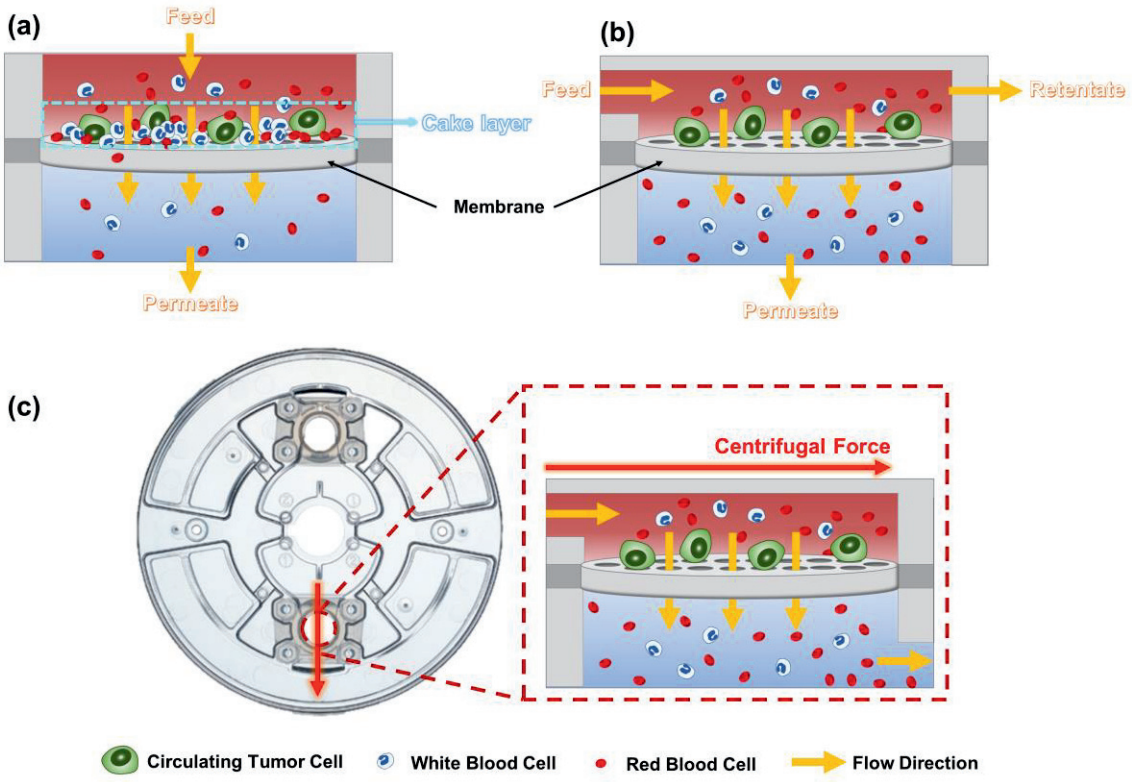

Figure 2.2. Scheme of membrane filtration. (a) Dead-end filtration (normal flow filtration) with cake layer. **(b)** Tangential-flow filtration (cross-flow filtration). **(c)** Insertion of memrane into the lab-on-a-disc for taking the advantage of tangential-flow filtration.

2.2 Fluid assisted separation technology (FAST) disc for CTC enrichment

2.2.1 Introduction

Circulating tumor cells (CTCs) shed into the peripheral blood from primary and metastatic tumors are important biomarkers for early detection of invasive cancer as well as for treatment monitoring in personalized cancer therapy.[52, 53] Since CTCs exist in extremely low concentrations (only a few CTCs out of a billion normal blood cells), the enrichment of CTCs with high recovery and purity has been a great challenge. Furthermore, CTCs are very fragile and thus it is highly recommended to do analysis within 6~8 hours after the blood collection from patients. Therefore, there is strong needs to develop rapid, efficient, robust, and affordable point-of-care CTC isolation technologies that could be broadly deployed in clinical settings.[54, 55]

Among previous efforts to selectively enrich CTCs from peripheral blood, the most common immunoaffinity-based capture strategy provides relatively high sensitivity and specificity, but the process time is long (> 1~4 hours).[9, 56] As a complementary method, the separation technologies based on the differences in physical properties such as size,[57-67] density,[68, 69] deformability,[70] and electrical properties[71-73] were also developed. Even though each strategy has its own advantages and limitations[56, 74-76], size-based isolation methods utilizing various kinds of microfilter structures offer high throughput as well as simple protocols facilitating automation and commercialization.[77-79]

Existing technologies for size-based isolation of CTCs have strived to improve the recovery rate and purity by developing expensive lithography-based microfilters with regular pore sizes and shapes.[59-61] Preferably, blood samples should have a prior dilution [61, 62] and/or fixation[79] and optimum transmembrane pressure should be maintained in order to achieve higher recovery rate and to avoid frequent clogging.[60, 67] Commercially available track-etched polycarbonate membranes are also utilized for CTC capture. Although this approach has some merits in terms of cost and mass production, it can attain only lower-than-desired recoveries with poor purity due to non-uniform and randomly distributed pores and low porosity.[60, 65-67]

We previously developed a lab-on-a-disc platform which allows rapid size-based isolation of CTCs with relatively high purity starting from whole blood.[66] Based on these advantages, we herein report

---

* *Chapter 2.2 is reproduced with the permission from "T.-H. Kim‡, M. Lim‡, J. Park‡, J.M. Oh‡, H. Kim; H. Jeong; S.J. Lee; H.C. Park; S. Jung; B.C. Kim; K. Lee; M.-H. Kim; D.Y. Park; G.H. Kim; and Y.-K. Cho, Analytical Chemistry 2017,* ***89****, 1155-1162." Copyright 2017 American Chemical Society*

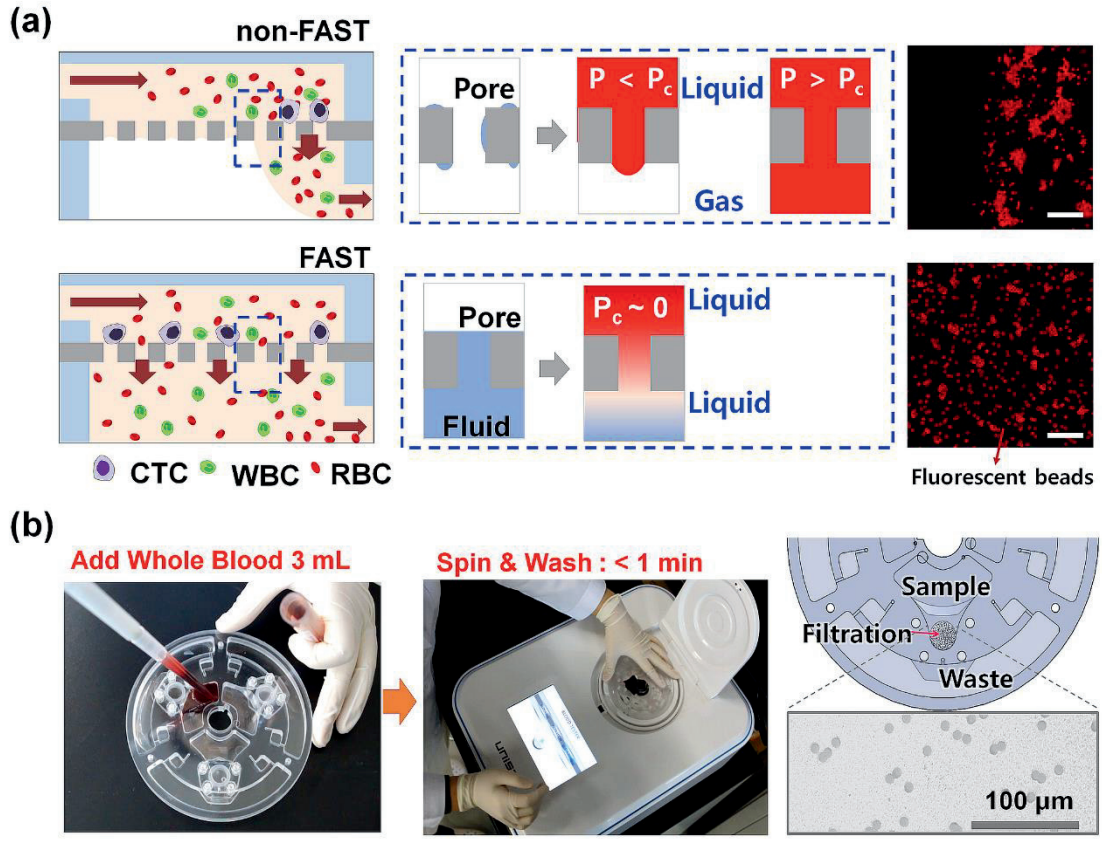

Figure 2.3. Design and function of the FAST disc. (a) Schematic illustration showing the mechanism of the Fluid-Assisted Separation Technology (FAST) disc. The pressure required to force a blood sample (red) through a membrane with liquid-filled pores (FAST) is expected to be much lower than that required to achieve transport through a bare membrane (non-FAST). The filtration occurs mainly in the outer rim of the filter with a disc spinning in non-FAST mode, whereas a more uniform transport of liquid takes place with the FAST disc, as demonstrated in the images showing 10 μm red fluorescent beads filtered with the conventional (top) and FAST (bottom) methods. **(**Scale bar: 100 μm) **(b)** Images of lab-on-a-disc and portable operation system. The track-etched polycarbonate membrane with 8 μm pores was employed for the CTC isolation.

a dramatic increase in recovery rate (from 54.0 ± 21.0% to 95.9 ± 3.1%) by utilizing the same track-etched polycarbonate membrane with 8 μm pores and unprocessed pheripheral blood but with a fluid-assisted separation technology (FAST), termed "FAST disc", for which size-selective CTC isolation is performed through the membrane pores filled with a stably-held liquid during the entire filtration process **(Figure 2.3a)**. As we show, the FAST disc approach enables a stand-alone, efficient, user-friendly, robust and cost-effective lab-on-a-disc system for point-of-care isolation of CTCs. We demonstrate its applicability to CTC capture and downstream molecular analysis with samples from patients with various types of cancer.

2.2.2 Experimental details

Disc fabrication process. The disc was designed with a 3D CAD program and milled with a CNC milling machine (3D modeling machine; M & I CNC Lab, Pyeongtaek, Korea). Polycarbonate sheets (PC: I-Components Co., Ltd, Pyeongtaek, Korea) were used for the body, which was milled from several layers. After milling, all of the layers were laminated using a pressure-sensitive double-sided adhesive (DFM 200 clear 150 POLY H-9V-95, FLEXcon, Spencer, MA). To form an easily detachable membrane, a supporting back plate equipped with a membrane holder and a gasket was assembled on the bottom of the disc body.

Samples. MCF-7, MDA-MB-231, MDA-MB-436 breast cancer cell lines, HCC78 lung cancer cell lines, and the AGS gastric cell line were purchased from ATCC (Manassas, VA). All of the cells were cultured in RPMI medium supplemented with 5% FBS and 1% antibiotics/antimycotics in incubators set to 37°C, under a 5% CO_2 atmosphere. For the spiking experiments, the cells were pre-labeled with a fluorescent dye CellTracker CMTMR (Life Technologies, Carlsbad, CA) according to the manufacturer's recommended protocol.

Blood samples. For blood sample preparation, peripheral blood samples from patients were obtained from the Pusan National University Hospital (Busan, Korea). This study was reviewed and approved by the Institutional Review Board (IRB) of PNUH and UNIST. Blood was collected in a K2-EDTA tube and inverted 10 times, immediately after the drawing of the blood. The blood samples were tested within 8 h of being collected to prevent cell damage. In the FAST disc experiments, the whole blood was used as is without dilution or red blood cell (RBC) lysis.

Isolation of CTCs from whole blood. Before the isolation of the CTCs, the surface of the disc was passivated with BSA. A 1% BSA solution was injected into the disc and then incubated for 30 min. The

BSA solution was then removed to the waste chamber by rotating the disc, after which the surface was washed with 1 mL of PBS solution. After the surface passivation, 3 mL of whole blood was introduced to the disc without any sample pretreatment steps. The CTCs were isolated on the filter by spinning the disc and then the filter was washed two times with 1 mL of PBS solution. The total filtration time required to isolate CTCs from 3 mL of whole blood was less than 1 min. To count the captured CTCs on the filter, immunostaining process was conducted on a disc.

Immunostaining process. The CTC isolation steps were followed by an immunostaining process to identify the cancer cells. The immunostaining process was also performed on the disc. First, the captured cells on the filter were fixed with 4% formaldehyde for 20 min at room temperature and then washed with PBS buffer. All of the pumping needed to generate the flow during the staining process was induced by the rotation of the disc at 600 RPM for 6 s. The fixed cells were permeabilized with 0.1% Triton X-100 in PBS for 5 min and then washed with PBS. After the permeabilization of the cells, the blocking step with 20 μg/mL of IgG was followed by staining with several antibodies. To stain the white blood cells, an anti-CD45 solution (H130, Life Technologies, Carlsbad, CA) was injected, incubated for 20 min, and then washed with 0.01% Tween 20 in PBS. Next, the CTCs were stained with a mixture of anti-cytokeratin conjugated FITC (CAM5.2, BD, San Jose, CA), anti-pan-cytokeratin conjugated Alexa 488 (AE1/AE3, eBioscience, San Diego, CA), and anti-EpCAM conjugated FITC (9C4, BioLegend, San Diego, CA). A mixture of these antibodies was introduced to the filter, incubated for 20 min, and then washed with 0.01% Tween 20 in PBS. Finally, the nuclei in the cells were stained with DAPI. Fluorescent images to confirm the CTCs were taken by using IX71 fluorescence microscopy (Olympus, Tokyo Japan) under 40× magnification. The captured cells were identified as CTCs if they exhibited the characteristic immunostaining feature of CK+ or EpCAM+, CD45- , DAPI+, and their diameter was in excess of 8 μm. The cells exhibiting EpCAM- and CK-, CD45+, and DAPI+ were identified as WBCs. Cells exhibiting EpCAM+ or CK+, CD45+, and DAPI+ were also found in several clinical samples (not in the healthy donor's blood) and they were defined as atypical cells.

Pressure drop measurement. A pressure sensor (MP3V5004DP, NXP Semiconductors, Eindhoven, Netherlands) with a measurement range of 0–3.92 kPa was employed with a data acquisition board (Arduino Pro Micro, Shenzhen Wonderwing Electronics Ltd., Shenzhen, China) combined with a Bluetooth module (HC-06 V1.4, Guangzhou HC Information Technology Co., Ltd., Guangzhou, China) in order to measure the pressure drop through the membrane during the spinning process. The pressure sensor, data acquisition board, Bluetooth module, and button cells were all integrated onto a disc and assembled onto a FAST disc for CTC isolation. The Coolterm software was utilized to acquire the data during the rotation.

Numerical simulations. The numerical simulation was performed by using open source code, OpenFOAM[1]. The domain of interest (DOI) was simplified into a membrane with a uniform pore size and distribution. The pore size and membrane thickness were set to 80 m and 100 m, respectively. The reservoir chamber was also simplified to reduce the computation cost. The generated mesh has 5,597,401 cells with 17,669,111 faces. The multiphase flow problem including blood, water, and air phases is discretized based on the volume of fluid with the continuous surface force (VOF-CSF) method. The two-equation eddy-viscosity model with the shear stress transport formulation (k- -SST turbulence model) was used to compensate for abrupt pressure fluctuations during high-speed spinning. The DOI rotates at 600 rpm, which is implemented by the moving reference frame (MRF) option in OpenFOAM. Its angular velocity increases linearly from t = 0–0.02 s, after which it is held constant until the end of the simulation time ($0 \leq t \leq 0.15$). The loading and filtration chambers were initially filled with the blood phase while the lower priming chamber was filled with air for the non-FAST case, and with water for the FAST case, respectively. All of the physical properties including the density, viscosity, and surface tension were set as constants at room temperature. All of the numerical visualizations were implemented in the Paraview open source software.

Flow rate calculation. The flow rate was calculated using the hydrodynamic resistance model proposed by van Rijn and Elwlenspoek[2].

$$\Delta P = RQ = \left[\frac{128L\mu}{\pi d^4} + \frac{24\mu}{d^3}\right]\frac{Q}{N} f_1(k)$$

where $f_1(k) = 1 - \sum_{i=1}^{\infty} a_i k^{(i+2)/2}$ and $a_1, a_2, a_{3,\ldots} = 0.344,\ 0.111,\ 0.066, \ldots$. Here, μ is the fluid viscosity, and $d, L,$ and k are the pore diameter, thickness, and porosity of the membrane, respectively. The number of pores (N) is determined by $d, k,$ and the membrane area.

Electric circuit equivalent model. The concept of a hydrodynamic resistance model can be extended to a general situation. Microfluidic networks are known to exhibit similarities to electric circuit networks. If we liken the flow rate and pressure difference in microfluidics to the electric current and potential difference in electric circuits, the microfluidic flow networks can be represented in terms of resistance, capacitance, inductance, etc., in the so-called electric circuit equivalent model. **Figure 2.9a** and **Figure 2.9b** show simplified schematics of the non-FAST and FAST modes together with corresponding electric circuit equivalent models. Here, $p_i, q_i, R_i, L,$ and C represent the pressure, flow rate, flow resistance, inductance, and capacitance, respectively. R_i and L for microfluidic

channels are well known and are described well in Oh et al.[3]. The capacitance C can be modeled as dV/dp. For the FAST case, the model equations can be represented by

$$q_1 = \frac{1}{R_1}(p_0 - p_1),$$

$$L\frac{dq_2}{dt} = (p_1 - p_2),$$

$$q_2 = \frac{1}{R_2}(p_2 - p_3),$$

$$\text{and } q_1 = q_2.$$

For this, there is the following analytical solution.

$$p_1 = p_{10} - \frac{Ap_{10} - B}{A}(1 - e^{-At})$$

where $A = \frac{R_1+R_2}{L}$ and $B = \frac{R_2p_0+R_1p_3}{L}$. Further, p_{10} is the initial pressure of p_1; p_1 converges to $B/A = \frac{R_2p_0+R_1p_3}{R_1+R_2}$. The convergence time depends on the inductance (L) of the outlet channel, while the characteristic time scale is 5.7×10^{-4} s in this case, which is much shorter than for the non-FAST case. The response in the FAST case is spontaneous and has no underdamped oscillation. This means that the FAST method is much more stable than the non-FAST method. For the non-FAST case, the model equations can be expressed as

$$\frac{dp_1}{dt} = \frac{1}{CR_1}(p_0 - p_1) - \frac{1}{CR_2}(p_2 - p_3),$$

$$\text{and } \frac{dp_2}{dt} = \frac{R_2}{L}(p_1 - p_2).$$

The stability of the non-FAST case is highly dependent on the outlet resistance as well as the membrane resistance, as shown in **Figure 2.9c** and **Figure 2.9d.** If there is an air phase in the waste chamber (e.g. in the non-FAST case), the flow rate can fluctuate unexpectedly, and backflow is even possible according to the outlet channel size. To enable the conservative design of microfluidic configurations, the microfluidic channel dimensions should also be optimized considering both cases.

Evaluation of capture efficiency. To confirm the capture efficiency and WBC depletion ratio of the FAST disc, 1 μL of cell suspension with a concentration ranging from 1–100 cell/μL was pre-counted and directly spiked into 1 mL of healthy donor's blood. In this case, the MCF-7 cells were used

after staining with CellTracker™ Green CMFDA dyes. After filtration, the membrane was released from the FAST disc and mounted on a slide glass with a DAPI mounting solution. The entire membrane was scanned and imaged with a fluorescence microscope, after which the CellTracker+/DAPI+ cells were counted to determine the capture efficiency, which was defined as the captured number of cells divided by the input number of cells (%).

Culture process for captured cancer cells. After isolating the cancer cells using the FAST disc, the membrane was released from the disc without performing the staining process and then introduced to the culture plate. The RPMI medium, supplemented with 5% FBS and 1% antibiotics/antimycotics, was added to re-suspend cells from the membrane surface. Then, the membrane was removed from the culture plate and the cells were incubated at 37°C in a 5% CO_2 atmosphere. To remove the remaining white blood cells, the RPMI medium was changed every other day. After 15 days, a live/dead assay (Life Technologies, Carlsbad, CA) was performed by following the manufacturer's recommended protocol.

Performance comparison with ScreenCell. To test the CTC isolation performance of the FAST disc, we divided the blood samples into two aliquots (~3 mL each) and tested them with the FAST disc and ScreenCell (Sarcelles, France), a commercially available size-based isolation kit, respectively. In the ScreenCell experiments, the manufacturer-recommended protocol was adopted. In summary, the FC2 buffer (pH 6.7, 4 mL), composed of an RBC lysis and fixation buffer, was mixed with 3 mL of whole blood. After being incubated for 7 min, the pretreated blood sample was introduced into the loading chamber. Blood filtration occurs as a result of the negative pressure produced by plugging the vacuum tube. After filtration, 1.4 mL of PBS buffer was introduced for washing. Finally, the system was disassembled to separate the membrane, followed by immunostaining and counting.

DNA isolation and detection of KRAS and EGFR mutation. To detect the mutation of isolated CTCs, DNA extraction from the H358, PC9 lung cancer cell lines, as well as from blood samples taken from patients with lung cancer was performed using an Amoy DNA prep kit (AmoyDx, Xiamen, China). The KRAS and EGFR mutations of gDNA was performed using an Amoy mutation kit based on real-time PCR, which has received the approval of the State Food and Drug Administration (SFDA) for clinical usage in mainland China. The EGFR mutation kit covers the 29 EGFR mutation hotspots from exon 18 to 21. The assay was carried out according to the manufacturer's protocol with a real-time PCR system (ViiA7, Life Technologies, Carlsbad, CA). A positive or negative result was obtained if it satisfied the criteria defined in the manufacturer's instructions.

2.2.3 Result and discussion

Design and function of the FAST disc. The rationale used to design the FAST disc was that membranes with liquid-filled pores can provide a reduced pressure drop for size-selective filtration[80] and thereby gentler yet more efficient filtration could be achieved (**Figure 2.3a**). In the case of conventional filtration, the transport of liquid occurs at a specific pressure that is higher than a critical value affected by interaction with solid surfaces, the pore size and geometry, and the surface tension. The wetting behavior and meniscus formation tends to be non-homogeneous through the membrane and the system is prone to fouling. With a FAST disc, however, the pores are primed with liquid stored in the fluid assistant chamber positioned underneath the membrane and the complete wetting remains during the entire filtration process, such that the liquid flow requires a minimal pressure difference and filtration occurs more uniformly throughout the entire membrane.

To realize a robust and user-friendly CTCs' isolation platform that can be readily adapted to clinical settings, we have developed a custom-designed portable spinning machine (**Figure 2.3b**). The FAST disc has a microfluidic layout composed of three independent filtration units; each unit consists of three chambers for sample loading, filtration, and waste storage. The membrane is detachable so that it can be easily mounted on a slide glass for follow-up image analysis and molecular characterization (**Figure 2.4**). In a centrifugal microfluidic device, the liquid is pumped radially outwards as the disc spins.[66, 81] Whole blood sample injected into the sample loading chamber is gently pushed into the filtration chamber and larger epithelial CTCs are captured by the membrane while smaller hematopoietic cells pass the membrane to be transferred to the waste chamber. The operation procedure is very simple; sequentially adding whole blood, washing buffer, and staining reagents is followed by pushing a button on the LCD panel of the custom-designed instrument which spins the disc (**Figure 2.5)**.

The dramatic difference between FAST and non-FAST mode operation was first highlighted with filtration experiments using fluorescent particles measuring 10 μm in diameter (**Figure 2.3a** and **Figure 2.6**). In non-FAST mode filtration on the spinning disc, the majority of the particles are located in the outer rim of the filter, suggesting that only small portions of the membranes are actually used for the filtration, whereas a more uniform distribution of particles was observed in FAST mode. This is achieved by simply having priming water under the membrane such that the membrane is fully wet before and during the entire filtration process. This makes sure that the liquid transport occurs at a pressure lower than the capillary pressure.

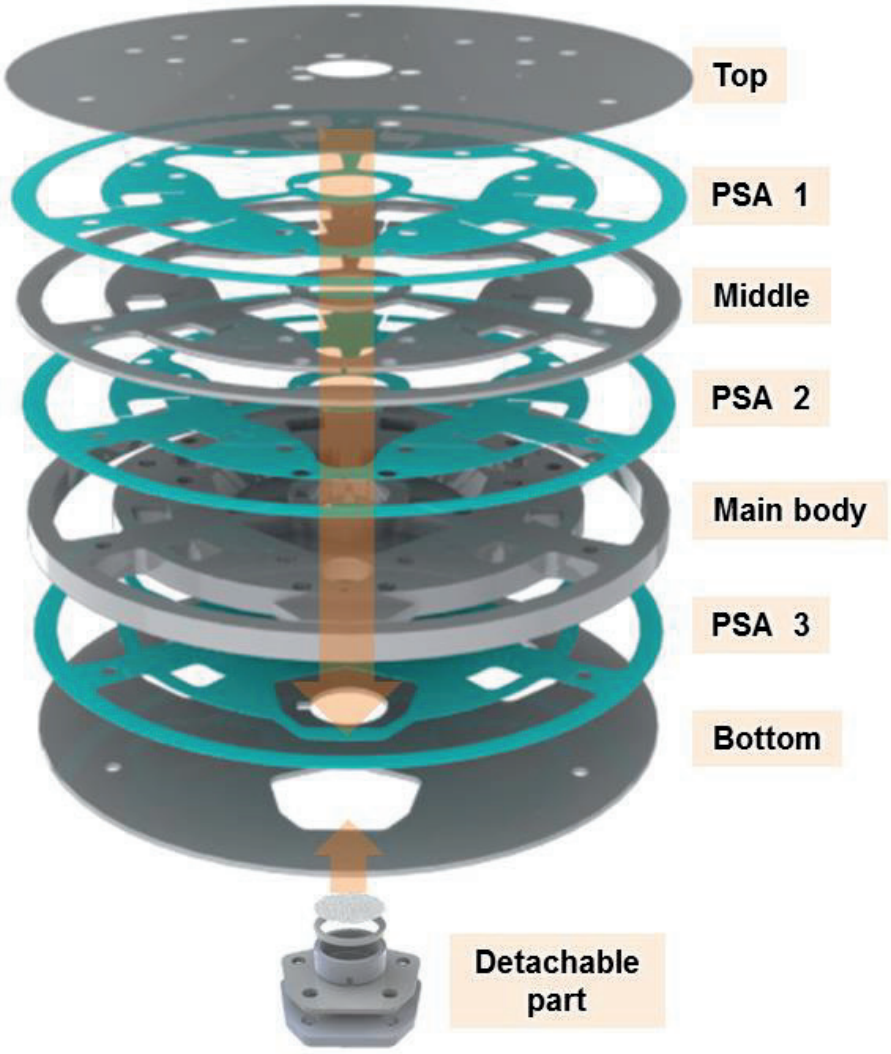

Figure 2.4. Expanded view of the FAST disc. A FAST disc is composed of 4 polycarbonate plates and 3 layers of pressure sensitive adhesive (PSA) tape sandwiched between the plates. The track-etched membrane is then assembled with detachable parts including o-rings, gaskets, holders, and a back plate using a bolt and nut.

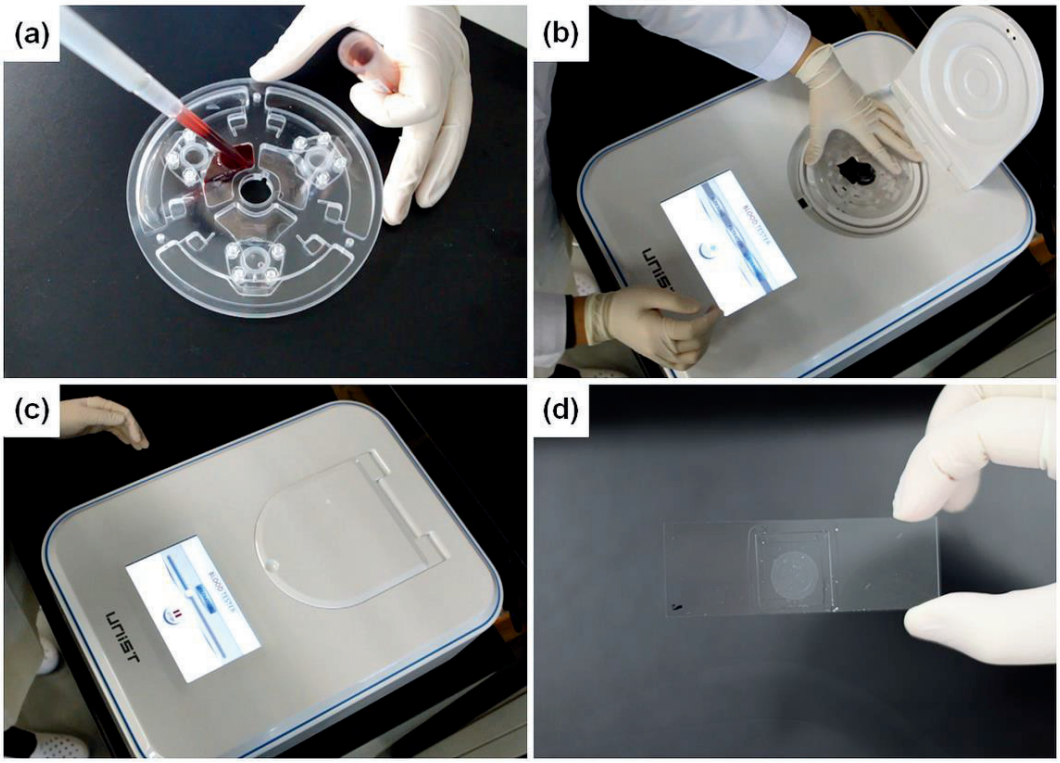

Figure 2.5. **Images showing the experimental procedure for CTC isolation from whole blood using the FAST disc system. (a)** 3 mL of whole blood was injected into the FAST disc without any prior sample treatment. **(b)** The disc was loaded into the custom-designed operation machine and **(c)** filtration was conducted by spinning the disc according to the preloaded spin program. **(d)** After CTC capture and immunostaining on the disc, the membrane was removed and mounted on a slide glass for imaging and storage.

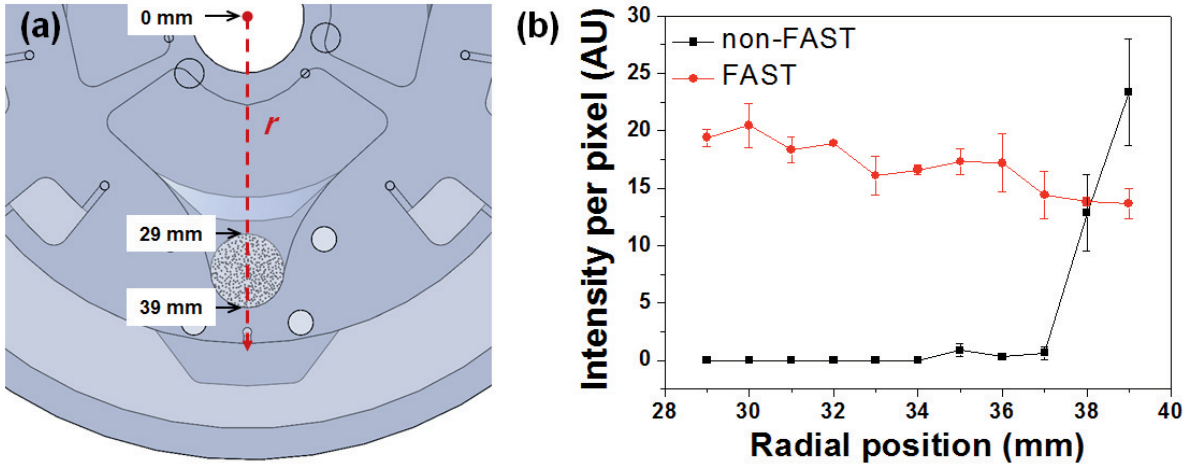

Figure 2.6. **Distribution of the particles on the membrane after filtration.** A suspension of fluorescent polystyrene particles with a diameter of 10 μm was filtered by spinning the disc at 600 rpm in conventional (non-FAST) and FAST mode. **(a)** The particle distribution was analyzed as a function of the radial position. **(b)** Image analysis shows that only part of the total area is used for filtration in non-FAST mode while more uniform filtration occurs in FAST mode.

The key advantages of the FAST disc, i.e., faster filtration and a reduced pressure drop, are further confirmed by means of whole-blood separation. The pressure drop measured by a wireless pressure-sensor system installed on the spinning disc (**Figure 2.7a**) showed a 50% reduction in the pressure drop for the FAST disc (**Figure 2.7b**). As shown in **Figure 2.7c**, it takes less than 20 s to filter 3 mL of whole blood using a FAST disc while about 100 s is necessary for non-FAST mode filtration. Compared to our previous report on CTC isolation using a non-FAST disc[66], the capture efficiency was greatly enhanced from 54.0 ± 21.0% to 95.9 ± 3.1% with the use of the FAST disc (**Figure 2.7d**). Taken together, it was validated that the FAST disc realizes faster filtration with high recovery despite there being a smaller pressure difference, which should be ideal for the size-selective filtration of live cells.

Simulation and theoretical analysis of FAST.

The flow field during the filtration process analyzed by means of numerical simulation also supports our argument from a fluid dynamics point of view. The volume of fluid method with continuous surface force is used to simulate multiphase flows in a complicated geometry.

With the rotation of the disc, the blood phase is pushed into the upper filtration chamber by centrifugal force, where it accumulates until the pressure difference between the upper and lower sides of the membrane reaches a threshold value which overcomes the capillary resistance in the non-FAST case (**Figure 2.8a**). The hydrodynamic pressure does not change much in the lower priming chamber and it induces a non-uniform pressure drop across the membrane surface, as shown in **Figure 2.8b** and **Figure 2.8c**. As a result, the blood phase mainly flows only through a small portion of the frontal area of the membrane, which significantly reduces the efficiency of the filtration. The filtered blood phase is not accumulated in the lower chamber but rather drains to the outlet immediately, which makes this inefficient process maintained during the filtration.

With the FAST disc, however, the lower chamber is initially filled with priming liquid. Therefore, as the disc rotates, the pressure in the lower chamber also increases until its magnitude is almost linearly proportional to the distance from the axis of rotation, in much the same way as in the upper part, as shown in **Figure 2.8b**. This constitutes the critical difference from the non-FAST case. The pressure gradient developed in the lower chamber is fairly well matched with that in the upper chamber, giving rise to a relatively uniform pressure drop, which induces a uniform flow across the membrane, as shown in **Figure 2.8c**.

The flow rate Q can be calculated from the pressure drop Δp and hydrodynamic resistance, R.

$$Q = \frac{1}{R}\Delta p$$

To maintain a stable and smooth flow during filtration with FAST, the dimensions of the disc geometry are an important factor. The effect of the outlet channel resistance and the capacity of the priming chamber under the membrane were investigated by using an electric circuit equivalent model (**Figure 2.9**). A low outlet resistance would make the system unstable while a high resistance would reduce the flow rate of the system. Furthermore, it was demonstrated that a larger priming chamber was more advantageous for attaining a stable flow.

Optimization of FAST disc using cells spiked into whole blood.

To evaluate the FAST disc, we first used a sample of unfixed MCF-7 human breast cancer cells, spiked into blood samples taken from healthy donors. As shown in **Figure 2.10a**, the capture efficiency was highest, >95.9 ± 3.1% (mean ± standard deviation [SD], n = 3), at 600 rpm, but fell significantly as the spin speed increased (49.9 ± 0.9% at 2400 rpm). Meanwhile, the purity increased marginally from 2.5-log depletion (mean: 6,420 WBCs/mL, range: 5,748–7,176 WBCs/mL) at 600 rpm to 2.9-log depletion (mean: 2,528 WBCs/mL, range: 1,533–3,392 WBCs/mL) at 2,400 rpm. At spin speeds of less than 600 rpm, the centrifugal force was not sufficient to achieve effective filtration. In our previous report on a CTCs' isolation disc operated in non-FAST mode[66], a spin speed of higher than 2,400 rpm was required to filter whole blood samples whereas 600 rpm proved sufficient in the current FAST disc.

Furthermore, the number of washing steps was further optimized to attain a higher degree of purity. When the number of washing steps was increased up to 6, we achieved 3.0-log depletion (mean: 1,636 WBCs/mL, range: 1,301–2,259 WBCs/mL) with a slightly reduced capture efficiency of 81.8% ± 5.0%, giving a degree of purity comparable to that attainable with the immunoaffinity-based positive enumeration method[82] (**Figure 2.10b**).

Tests with five cancer cell lines spanning a broad range of EpCAM expressions and sizes (**Figure 2.11**), spiked in whole blood demonstrated the efficient capture of viable cells (**Figure 2.10c**). In addition, the excellent reproducibility of the recovery rate, 96.2 ± 2.6%, was confirmed from repetitive tests performed over 15 different days with 30 different discs, which suggests that the FAST disc can provide a robust method of enumerating CTCs from whole blood (**Figure 2.10d**). A live/dead assay confirmed that the filtered cells are alive and can be applied to long-term culture (**Figure 2.10e and Figure 2.12**).

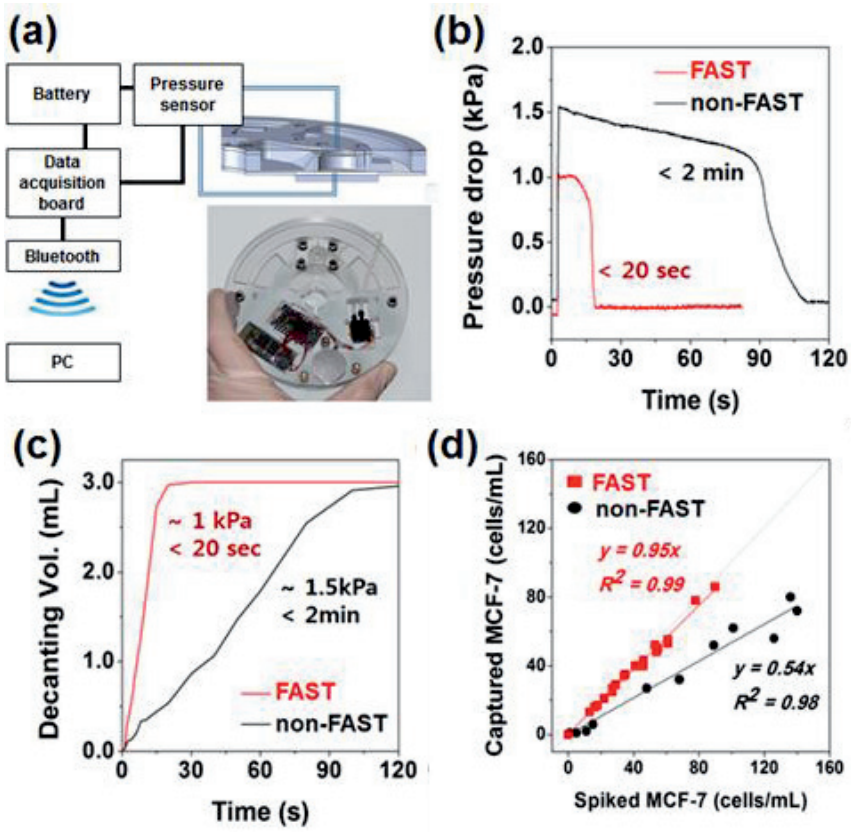

Figure 2.7. Effect of the FAST on the pressure drop, filtration time, and recovery of cancer cells from whole blood. (a) Schematic diagram and a photo image of a disc for the wireless measurement of the transmembrane pressure while the disc was being spun at 600 rpm to filter the whole blood. A pressure sensor was connected to a data acquisition board and the obtained data were transmitted to a computer by a Bluetooth module equipped with a data acquisition board. **(b)** Pressure drop and **(c)** Decanting volume measured during the filtration of whole blood as a function of time. Use of the FAST disc enables ultrafast (< 20 s for 3 mL of whole blood) CTC isolation with a reduced pressure drop (~1 kPa). **(d)** The recovery of MCF-7 cells spiked in whole blood showed a 95.9% efficiency with a good linearity for the FAST disc, compared to 54.0% in the non-FAST case

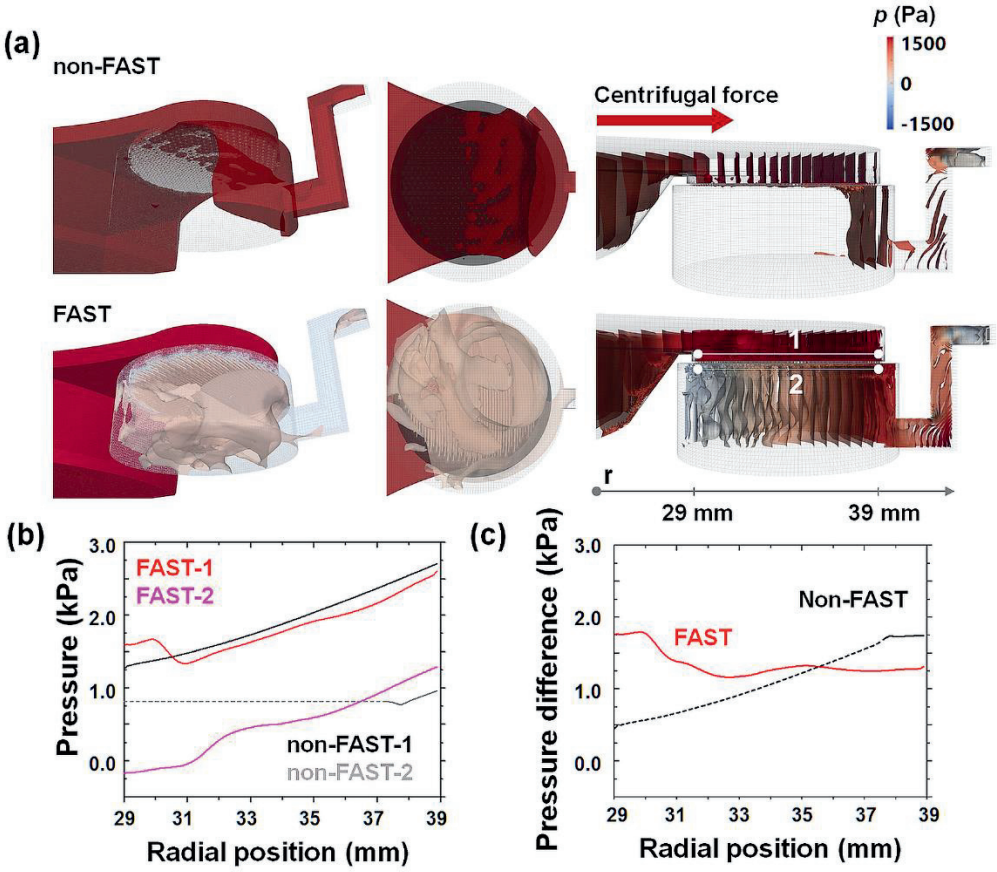

Figure 2.8. Numerical analysis comparing non-FAST and FAST disc methods. (a) Blood phase flows (left) and pressure contours (right) at 0.13 s, induced by centrifugal force generated by spinning the disc at 600 rpm in non-FAST (top) and FAST (bottom) modes. Pressure is developed due to centrifugal force in *O* (1 kPa), which is determined by the mass of the liquid phases and the angular velocity of rotation. In the non-FAST case, the pressure gradient in the upper chamber causes a non-uniform pressure drop across the membrane and, in consequence, the blood phase is filtered only through a small portion of the membrane. This significantly reduces the efficiency of the membrane. Meanwhile, in the FAST disc, the chamber under the membrane is filled with an aqueous phase during the entire filtration process. Therefore, when the blood phase reaches the membrane, the blood phase flows into the lower chamber uniformly and diffuses into and mixes with the liquid phase. The FAST disc uses the entire membrane area for filtration which significantly alleviates clogging. **(b)** Pressure plots in the radial direction above (1) and below (2) the membrane. **(c)** Pressure difference ($\Delta p = p_1 - p_2$) along radial direction. The broken lines correspond to the non-FAST cases (b,c) indicate those locations where liquid flow does not occur

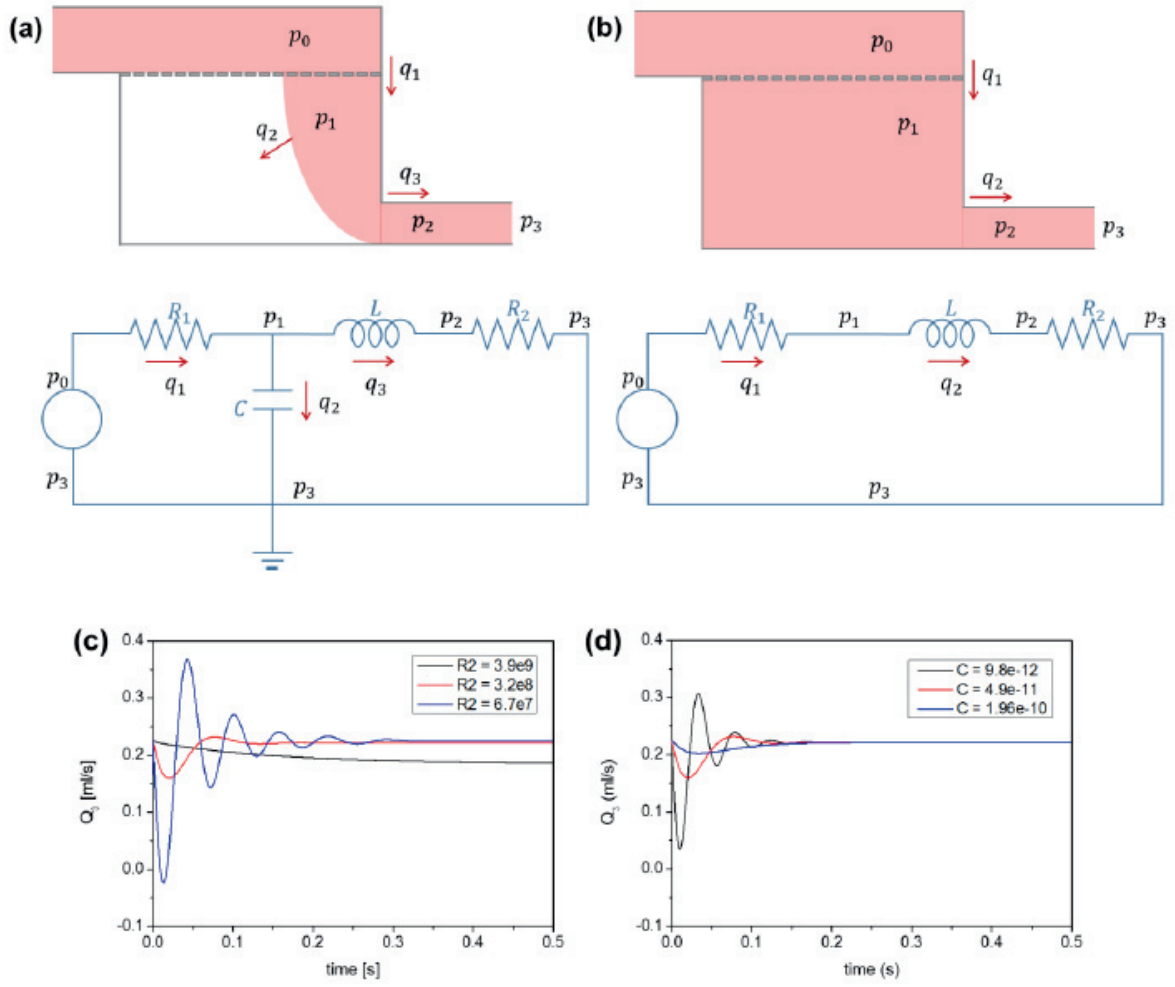

Figure 2.9. Electric circuit equivalent model for non-FAST and FAST methods. Electric circuit equivalent models for **(a)** non-FAST and **(b)** FAST methods. **(c)** Effect of outlet resistance (*R*2) in non-FAST method, which varies with the channel width. If the outlet resistance is too low (blue line), back flow may be possible, making system unstable. If the outlet resistance is too high (black line), the flow rate is significantly reduced. **(d)** Capacitance effect of lower chamber in non-FAST method. If the capacitance increases, the flow rate of the outlet stabilizes. If there is no air in the lower chamber (FAST method), the flow is almost incompressible and so can spontaneously respond to the flow rate while the system is running. These hydrodynamic behaviors should be considered to optimize the chamber configuration and fluid channels according to the operating conditions.

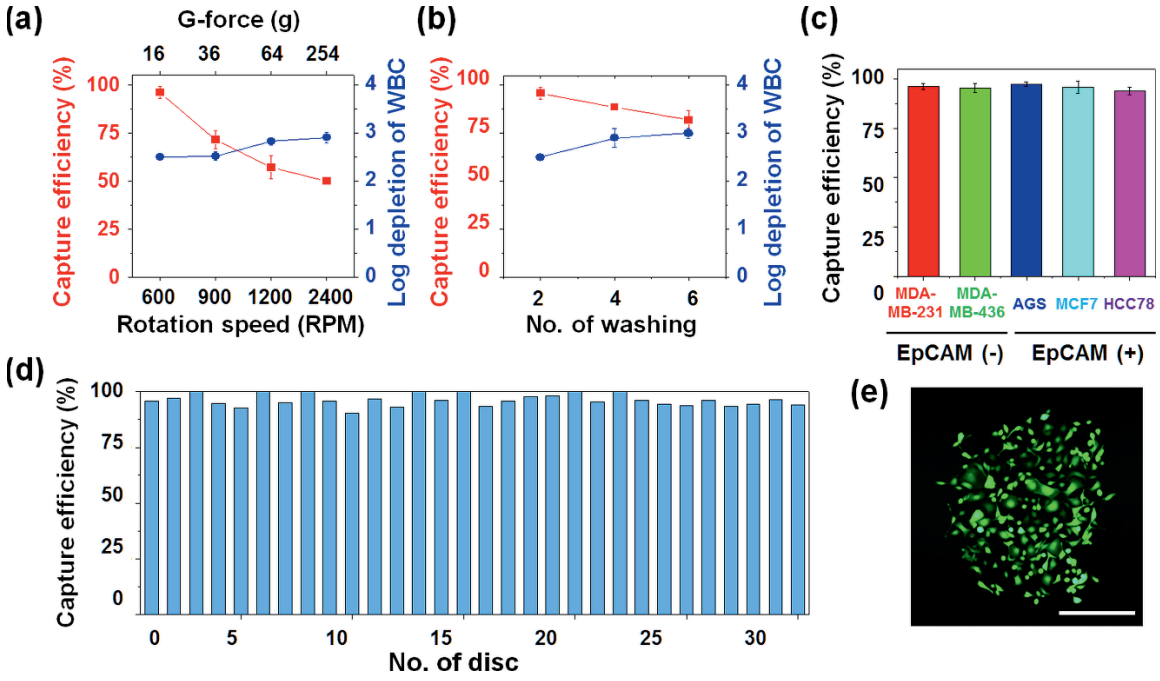

Figure 2.10. Optimization of the FAST disc using cancer cells spiked into whole blood. The capture efficiency (red); defined as number of captured cancer cells/input number of cancer cells, and purity (blue); log depletion ratio defined as log (input number of white blood cells [WBCs]/number of remaining WBCs on the membrane), were evaluated with MCF-7 cells spiked into whole blood at various **(a)** rotational speeds and **(b)** numbers of washing steps. The spin speed was held at 600 rpm and two washes were used for the follow-up experiments with cells spiked in whole blood. For the molecular analysis, six washes were used to achieve the >3.0-log depletion of WBCs. **(c)** Capture efficiency test with five cancer cell lines spanning a broad range of EpCAM expressions and sizes produced a > 96% capture efficiency with the FAST disc. **(d)** Reproducibility tests with spiked cells (10–100 MCF-7 cells) in whole blood conducted for fifteen days using 30 different discs showed 96.2 ± 2.6 % (mean ± SD) recovery. **(e)** Live/dead assay result for captured cells (AGS) on a FAST disc after being cultured for 15 days show good viability. Scale bar: 100 μm.

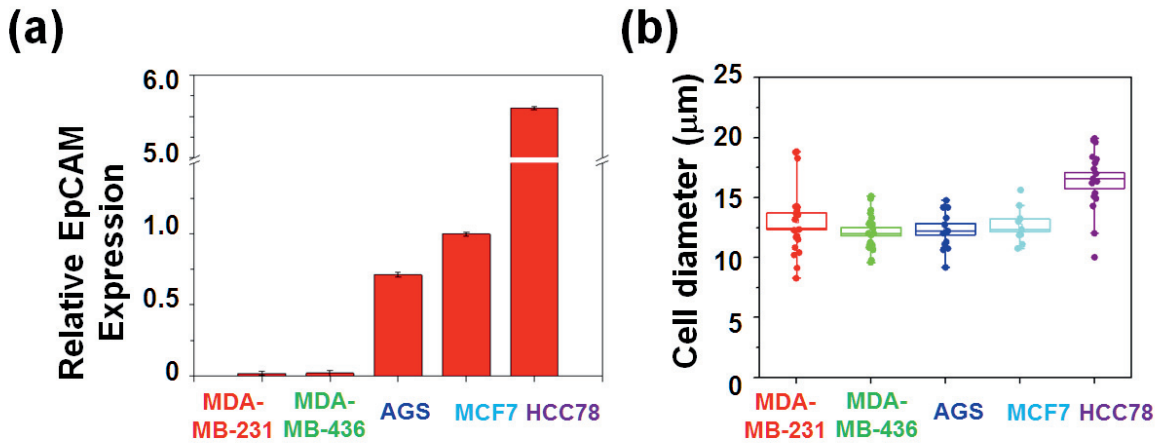

Figure 2.11. EpCAM expressions and sizes of five cancer cell lines. (a) EpCAM expression as confirmed by real-time PCR and normalized to GAPDH. MDA-MB-231, MDA-MB-436 breast cancer cells and AGS stomach cancer cells exhibited a low expression while HCC78 lung cancer cells exhibited a high expression compared to MCF-7 breast cancer cells. **(b)** Cell diameters of various cell lines were measured; MDA-MB-231 (13.4 ± 3.3 μm), MDA-MB-436 (12.2 ± 1.5 μm), AGS (12.4 ± 1.7 μm), MCF-7 (12.7 ± 1.6 μm), HCC78 (16.4 ± 2.7 μm). The data was the mean ± S.D (n = 3).

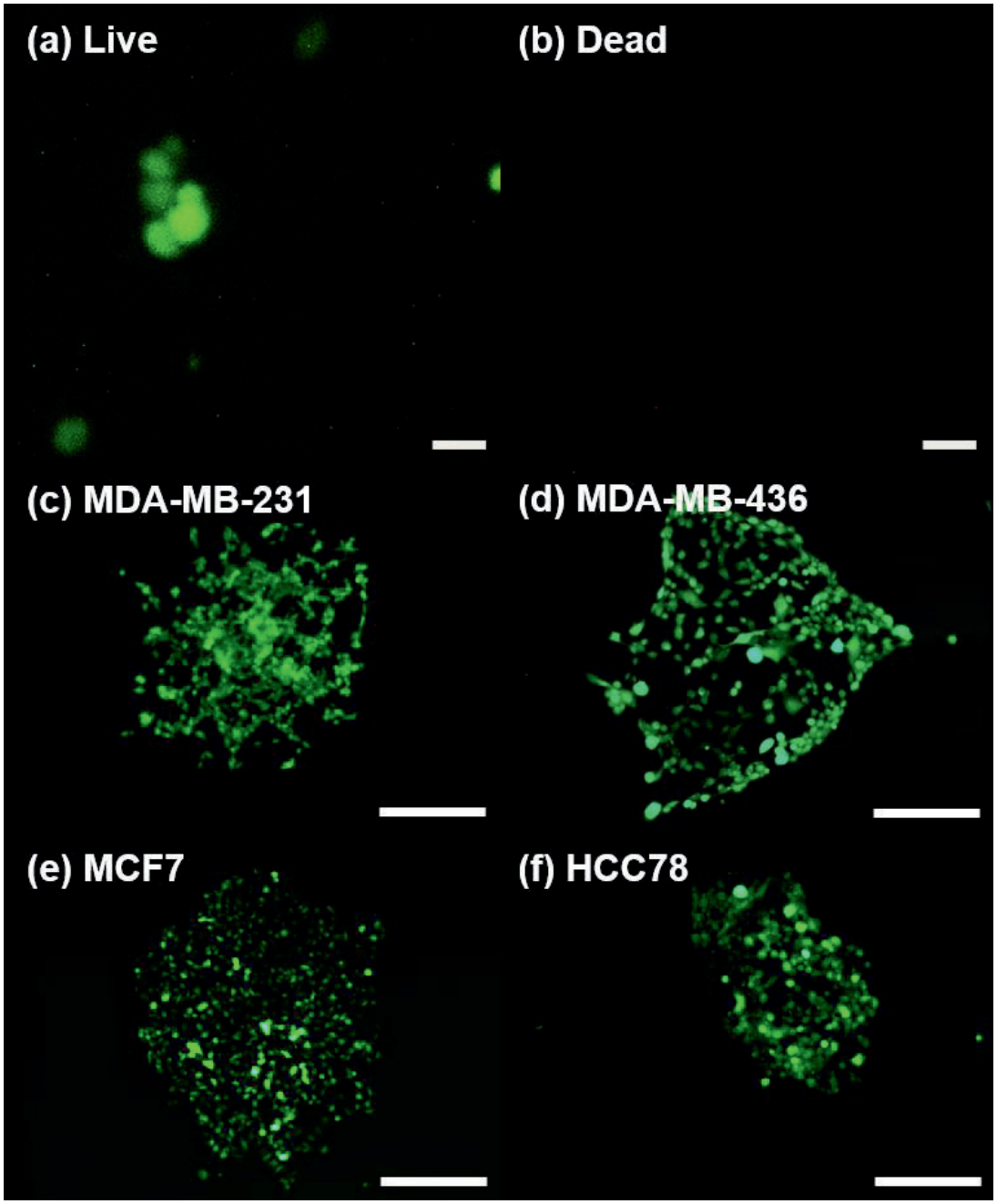

Figure 2.12. Results of live/dead assay after the filtration and 15 days culturing. The cell viability (97.6 ± 0.4%) was confirmed immediately after filtration by live/dead assay. Images show that there are only live cells **(a)** and no dead cells **(b)**. Scale bar: 20 μm. **(c-f)** Various kinds of cancer cells captured on the membrane by the FAST disc were incubated for 15 days. Images show the results of live/dead assay with the incubated cells of MDA-MB-231 **(c)**, MDA-MB-436 **(d)**, MCF-7 **(e)**, and HCC78 **(f)**. Scale bar: 100 μm.

Comparison with other size-based filtration methods.

The degree of CTC isolation with the FAST disc was first compared with a commercially available size-based filtration device, ScreenCell Cyto, using MCF-7 cells spiked in whole blood (**Figure 2.13a**). The capture efficiency was 95.9 ± 3.1% (n = 3, unfixed, whole blood) and 68.9 ± 10.0% (n = 3, diluted with a buffer for RBC lysis and fixation) for FAST discs and ScreenCell, respectively. FAST disc was found to provide a higher purity of 2.5-log (mean: 4,771 WBCs/mL, range: 4,330–5,483 WBCs/mL) compared to 1.7-log (mean: 32,950 WBCs/mL, range: 29,550–37,137 WBCs/mL) depletion.

In order to make direct performance comparisons of ScreenCell and FAST using clinical samples, two aliquots of the blood samples from each patient were tested with a FAST disc and a ScreenCell Cyto device under their corresponding recommended protocols. Using the conventional criteria for CTC identification, DAPI+, EpCAM/CK+, and CD45- (**Figure 2.13b and Figure 2.14**), FAST discs could detect at least one CTC from 14 out of the 16 patients with different cancer types (detection rate: 87.5%, mean: 18 CTCs/7.5 mL, median: 8 CTCs/7.5 mL, range: 0–90 CTCs/7.5 mL), while ScreenCell Cyto devices detected 8 out of the 16 samples (detection rate: 50.0%, mean: 12 CTCs/7.5 mL, median: 4 CTCs/7.5 mL, range: 0–90 CTCs/7.5 mL). Meanwhile, the number of WBCs remaining on the membrane identified by using the criteria of DAPI+, EpCAM/CK-, and CD45+ was 6.0 times higher with ScreenCell (mean: 30,339 WBCs/7.5 mL, median: 24,152 WBCs/7.5 mL, range: 13,407–58,312 WBCs/7.5 mL) than that with the FAST disc (mean: 5,075 WBCs/7.5 mL, median: 4,955 WBCs/7.5 mL, range: 1,923–9,249 WBCs/mL). Taken together, we were able to demonstrate that the FAST disc could provide CTCs with a higher recovery rate and higher level of purity from clinical samples (**Figure 2.13c and Table 2.1**).

Immunohistochemical and molecular analyses of CTCs from patients.

After the validation of the FAST disc platform, we analyzed blood samples from patients with different types of cancer (n = 142) as well as from healthy individuals (n = 50) as controls (**Figure 2.13d, Figure 2.15 and Table 2.2**). The clinical samples were collected from Pusan National University Hospital (PNUH) according to the approved IRB process. CTCs (mean: 58 CTCs/7.5 mL, median: 13 CTCs/7.5 mL, range: 0–540 CTCs/7.5 mL) were detected from 83.3% (15/18) of breast cancer patients with various stages while 50 healthy subjects had negligible CTC counts (mean, 0 CTCs/7.5 mL; median, 0 CTCs/7.5 mL; range, 0–5 CTCs/7.5 mL). Moreover, 63 of the 76 samples (82.9%) obtained from stomach cancer patients contained CTCs within a range of 2–485 CTCs/7.5 mL (mean: 21 CTCs/7.5 mL, median: 4 CTCs/7.5 mL). Due to the unique characteristics of the early diagnostics of stomach cancer by the National Cancer Screening Program in Korea, majority of the patients, 54 of the 76 patients (71.1%),

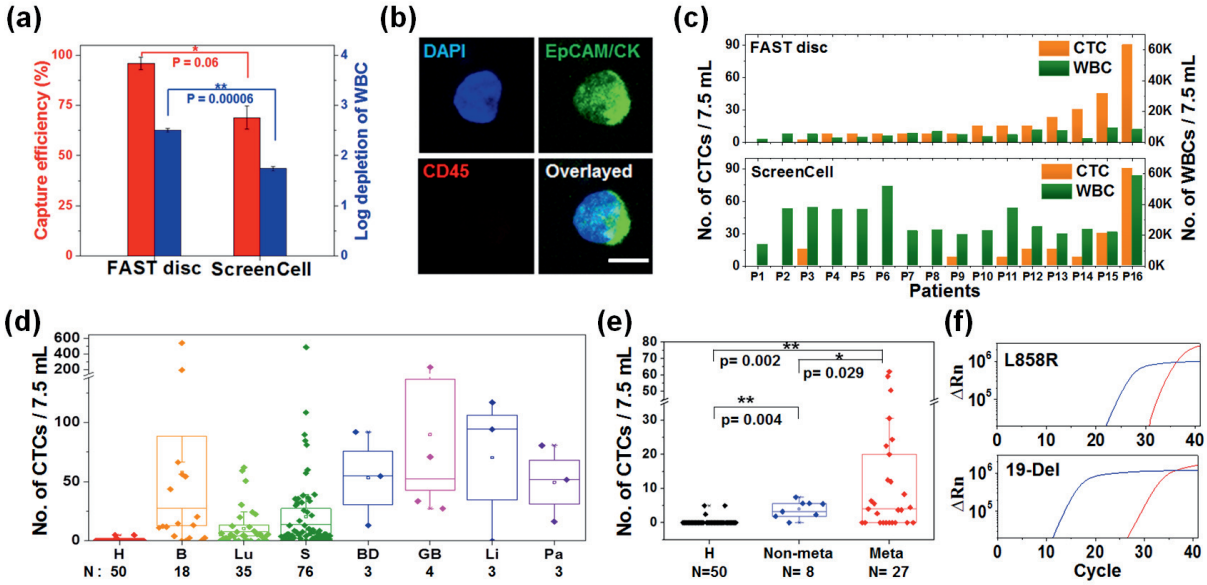

Figure 2.13. Performance comparison with the commercially available size-based filtration system and clinical test of FAST disc. (a) Capture efficiency and purity were compared for the results of the filtration experiments with MCF-7 cells spiked in blood samples. Whole blood was directly filtered through membranes with 8.0 μm pores with the FAST disc. The samples were diluted and prefixed according to the manufacturer's recommended protocol for the ScreenCell Cyto device, and were then filtered through membranes with 7.5 μm pores by the application of negative pressure provided by a vacuum tube. **(b)** Fluorescence images of isolated CTC obtained from a patient's blood sample (Scale bar: 8 μm). **(c)** Performance comparison with FAST disc and ScreenCell by using clinical samples obtained from patients with cancer of the breast (n = 3), stomach (n = 4), colon (n = 4), bile duct (n = 3), and lung (n = 2). All counts were normalized to 7.5 mL. **(d)** Number of CTCs isolated from blood samples of healthy donors (H, n = 50), patients with cancer of the breast (B, n = 18), lung (Lu, n = 35), stomach (S, n = 76), bile duct (BD, n = 3) gallbladder (GB, n = 4), liver (Li, n = 3), and pancreas (Pa, n = 3). **(e)** Number of CTCs from lung cancer patients with/without distant metastasis was compared with healthy donors. **(f)** EGFR real-time PCR assay was performed using the cells captured on membrane from blood samples of two lung cancer patients with the L858R and 19-Del mutations. Blue line is for internal control and red line is for the target sample. Negative controls did not show any amplification signal.

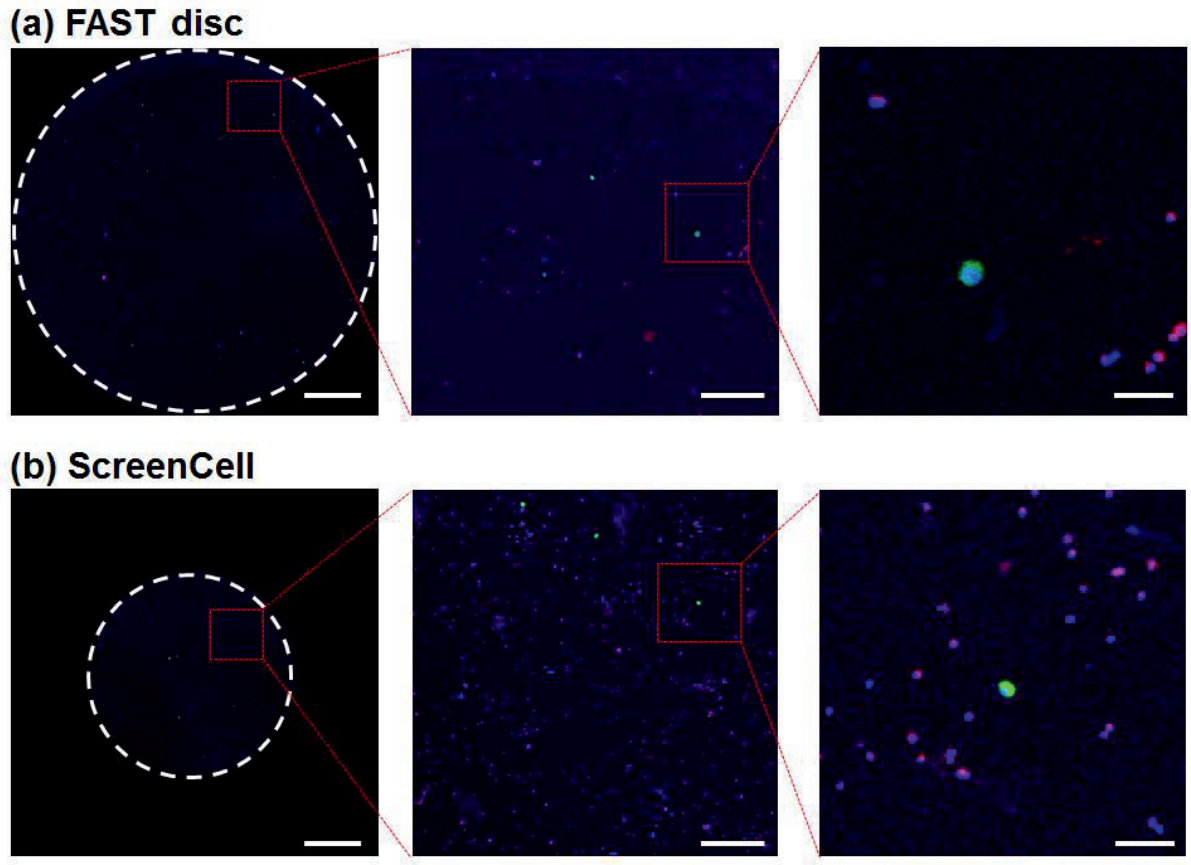

Figure 2.14. The fluorescence images of the membrane after the isolation of CTCs from the blood of a cancer patient. CTCs captured by size-based isolation using **(a)** FAST disc and **(b)** ScreenCell were immunostained. The blue, green, and red signals are from DAPI+, CK+ or EpCAM+, and CD45+ cells, respectively. The filter membranes were retrieved to acquire the fluorescence images. It is noted that the number of WBCs (DAPI+, EpCAM-, CK-, and CD45+) from a FAST disc is significantly smaller than that from ScreenCell. The circles in the left pictures show the whole area of the membrane with the diameter of 10 mm and 6 mm for a FAST disc and a ScreenCell, respectively. The red dot squares are zoomed to show an enlarged view of the corresponding area in the middle and right images. Scale bar is 2 mm, 300 μm and 100 μm from left to right, respectively.

Table 2.1. Comparison of CTC detection in cancer patient's blood using FAST disc and ScreenCell. CTCs were isolated from the blood of 16 cancer patients and the number of CTCs was normalized to 7.5 mL (standard volume used by CellSearch system).

Patient no.	Cancer type	Gender	Age	Blood Vol. processed (mL)	No. of CTCs / 7.5 mL		No. of WBCs / 7.5 mL	
					FAST disc	ScreenCell	FAST disc	ScreenCell
1	Breast	F	34	3.0	0	0	1924	13408
2	Stomach	M	66	3.0	0	0	5156	36863
3	Stomach	F	48	3.8	2	15	5009	37747
4	Colon	F	62	3.0	8	0	2788	36088
5	Stomach	M	72	3.0	8	0	2918	36270
6	Stomach	M	50	3.0	8	0	3752	51255
7	Colon	F	71	3.0	8	0	5674	22333
8	Lung	M	56	3.0	8	0	6789	23087
9	Bile duct	F	65	3.0	8	8	4901	19800
10	Bile duct	M	68	3.0	15	0	3561	22710
11	Breast	F	54	3.0	15	8	4633	37230
12	Breast	F	32	3.0	15	15	7543	25018
13	Lung	M	74	3.0	23	15	7260	20490
14	Colon	F	63	3.0	30	8	2021	23288
15	Colon	M	62	3.0	45	30	9249	21530
16	Bile duct	M	69	3.0	90	90	8029	58313

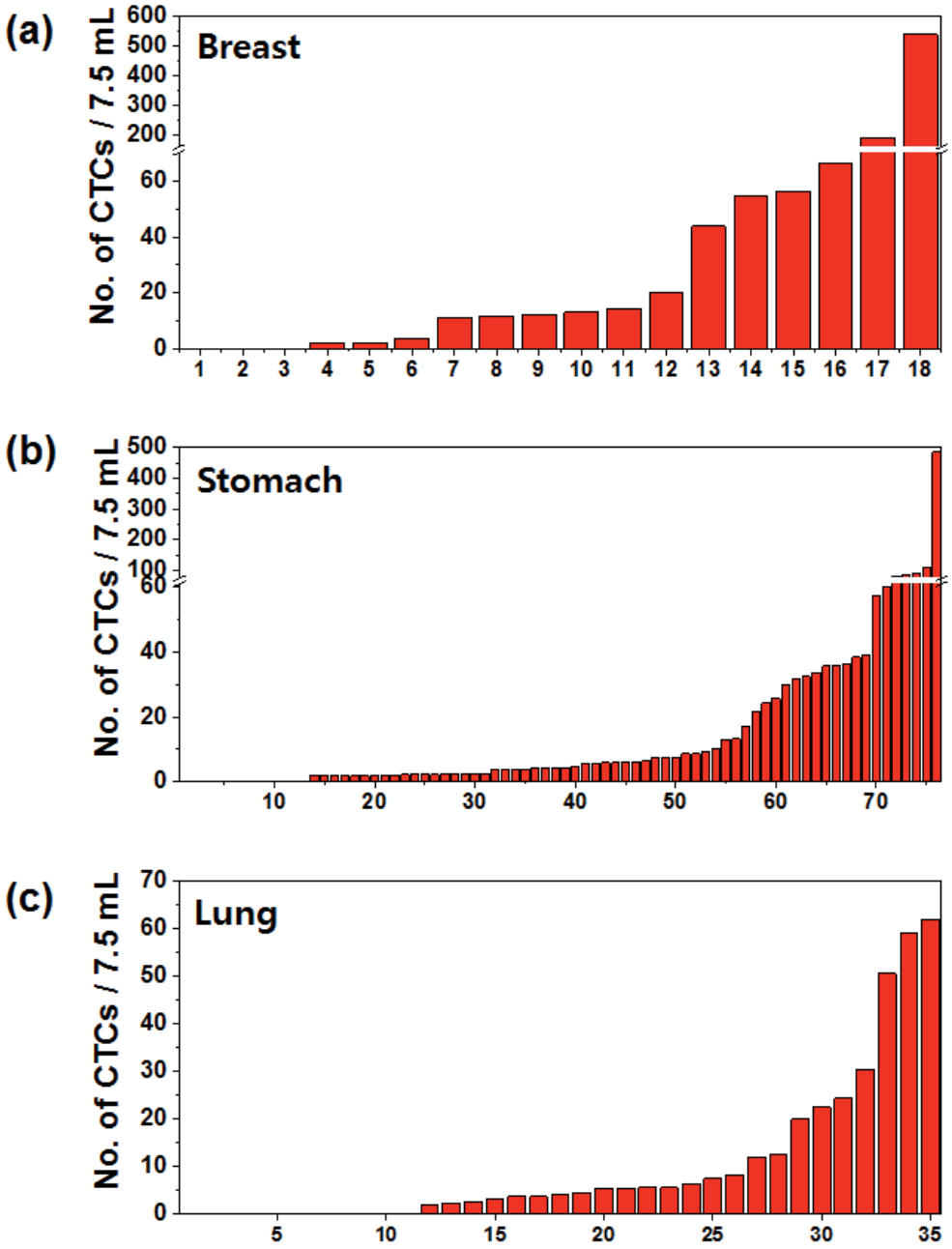

Figure 2.15. Prevalence of CTCs from patients with breast cancer (n = 18), stomach cancer (n = 76) and lung cancer (n = 35) (a) CTCs (mean: 58 CTCs/7.5 mL, median: 13 CTCs/7.5 mL, range: 0–540 CTCs/7.5 mL) were detected from 83.3% (15/18) of breast cancer patients. **(b)** In the case of stomach cancer patients, 63 of the 76 samples (82.9%) contained CTCs within a range of 2–485 CTCs/7.5 mL (mean: 21 CTCs/7.5 mL, median: 4 CTCs/7.5 mL). **(c)** CTCs (mean: 10 CTCs/7.5 mL, median: 4 CTCs/7.5 mL, range: 0–62 CTCs/7.5 mL) could be detected in 68.6% (24/35) of lung cancer patients.

Table 2.2. Number of CTCs isolated from blood samples of healthy donors and cancer patients. CTCs were isolated from blood samples of 50 healthy donors and 142 cancer patients and the number of CTCs was normalized to 7.5 mL (standard volume used by Cell Search system).

Subjects	Number of samples	CTC count per 7.5 mL of peripheral blood						
		0	≥1	≥2	≥3	≥5	≥10	≥50
		Frequency of samples (%)						
Healthy	50	47 (94)	0 (0)	0 (0)	1 (2)	2 (4)	0 (0)	0 (0)
Breast	18	3 (17)	0 (0)	2 (11)	1 (6)	0 (0)	7 (39)	5 (27)
Lung	35	11 (31)	1 (3)	2 (6)	5 (14)	7 (20)	6 (17)	3 (9)
Stomach	76	13 (17)	7 (9)	11 (15)	9 (12)	13 (17)	16 (21)	7 (9)
Bile duct	3	0 (0)	0 (0)	0 (0)	0 (0)	0 (0)	1 (33)	2 (67)
Gall bladder	4	0 (0)	0 (0)	0 (0)	0 (0)	0 (0)	2 (50)	2 (50)
Liver	3	1 (33)	0 (0)	0 (0)	0 (0)	0 (0)	0 (0)	2 (67)
Pancreas	3	0 (0)	0 (0)	0 (0)	0 (0)	0 (0)	1 (33)	2 (67)

		Merge	DAPI	EpCAM /CK	CD45
Breast F 61	1	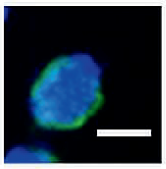		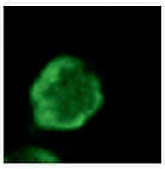	
	2	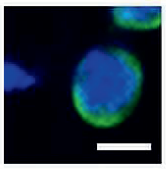	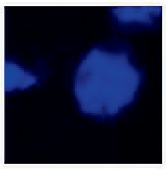	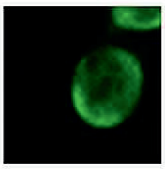	
	3	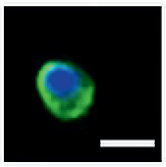	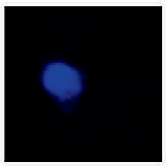	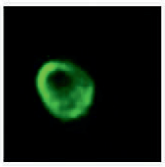	
	4	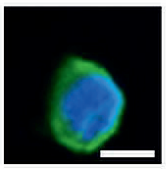	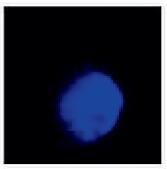	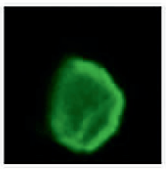	
	5	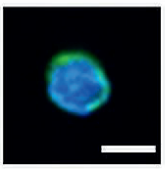			
Breast F 39	6	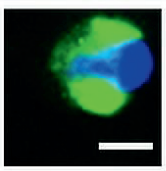	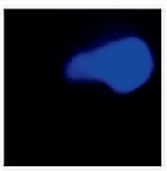	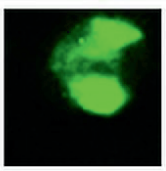	
	7	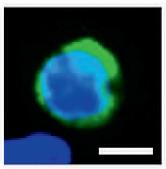		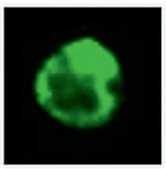	
	8	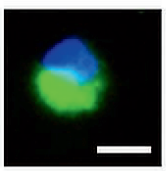	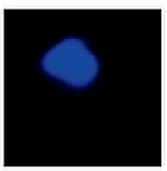	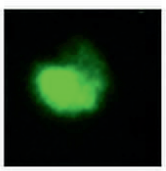	

		Merge	DAPI	EpCAM /CK	CD45
Stomach F 44	1	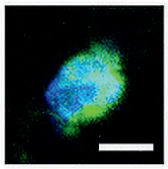	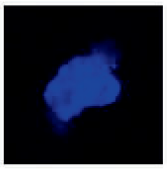	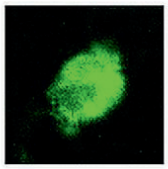	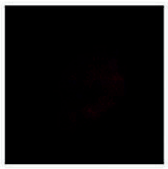
	2	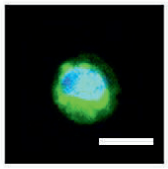	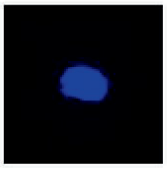	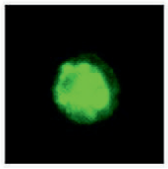	
	3	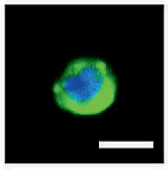	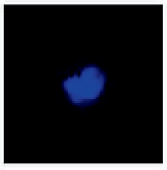	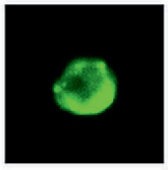	
	4	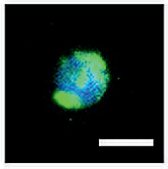	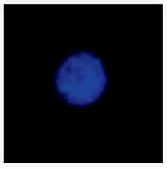	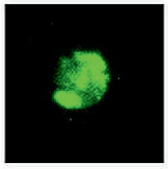	
	5	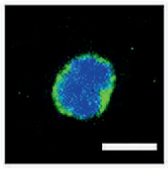		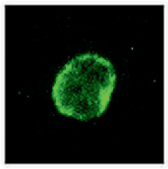	
	6	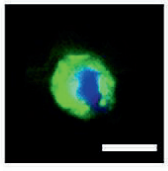	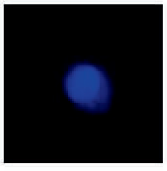	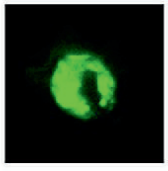	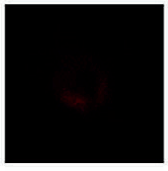
	7	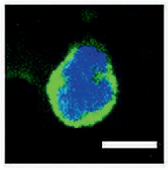	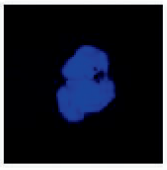	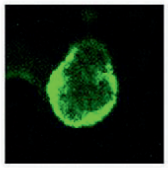	
	8	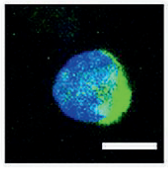	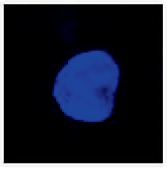	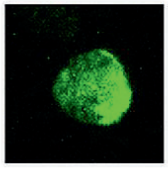	

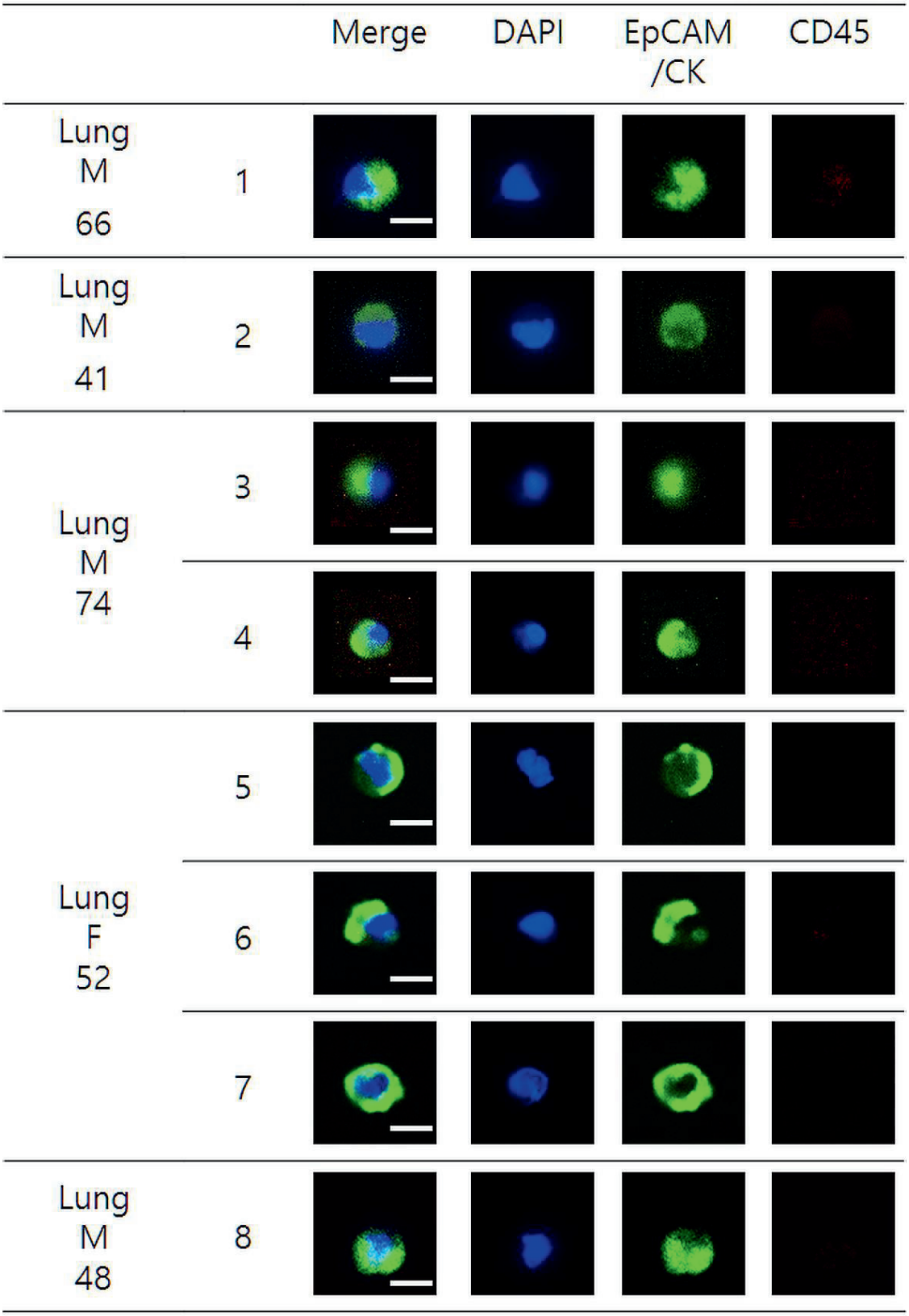

Figure 2.16. Examples of images of CTCs isolated from blood of patients with breast cancer, stomach cancer, and lung cancer. DAPI+, EpCAM/CK+, and CD45- cells are classified as CTCs. (Scale bar: 8 μm).

were in relatively early stages (I/II) and all patients were without distant metastasis, highlighting that our FAST disc might be potentially useful for the early detection of solid tumors.

In the case of lung cancer, the CTCs (mean: 10 CTCs/7.5 mL, median: 4 CTCs/7.5 mL, range: 0–62 CTCs/7.5 mL) could be detected in 68.6% (24/35) of the patents and the patients with long distance metastasis have significantly higher number of CTCs (**Figure 2.13e**). Example fluorescence images of the CTCs isolated from cancer patients are shown in **Figure 2.16.**

Beyond immunostaining and counting, molecular analyses are increasingly being practiced in CTC characterization, which is expected to improve personalized therapy.[54, 82] As a proof of concept experiment, a real-time polymerized chain reaction (PCR) was performed to detect somatic mutations in the epidermal growth factor receptor (EGFR) gene to select non-small-cell lung cancer (NSCLC) patients who are predicted to respond to targeted therapy such as EGFR tyrosine kinase inhibitors (e.g., gefitinib or erlotinib). The PC9 lung cancer cells spiked in whole blood were processed with a FAST disc and the lysate of the captured cells on the membrane was used as the subject for DNA preparation followed by real-time PCR. Mutation was detected with a success rate of 50.0% (3/6) and 100.0% (6/6) for 10 and 100 cells spiked in 3 mL of whole blood, respectively. The estimated purity is in the order of 0.1% and 1.0% for 10 and 100 cells spiked in 3 mL of whole blood, respectively since log depletion of WBC with FAST disc is demonstrated to be about 3.0.

Similarly, KRAS mutation analysis, which is often recommended to test the drug resistance of targeted medicines such as tyrosine kinase inhibitors, was conducted with H358 lung cancer cells spiked in whole blood. The use of the FAST disc followed by real time PCR could detect 10 and 100 cells spiked in 3 mL of whole blood with a 50.0% (3/6) and 100.0% (6/6) success rate, respectively. In addition, the mutation analysis was further confirmed with two clinical samples from lung cancer patients with L858R or 19-Del EGFR mutations (**Figure 2.13f**). It is important to note that the total process of CTC isolation from whole blood followed by the molecular analysis took less than 2 h, which can be potentially useful in clinical settings.

2.2.4 Conclusions

We introduce an ultrafast, user-friendly, and highly sensitive centrifugal microfluidic technology, the FAST disc, which can isolate live CTCs with good purity from the unprocessed whole blood of cancer patients. Existing size-based technologies exhibit lower sensitivity and specificity and often

require additional sample pretreatment steps and/or expensive lithographic microfilters to improve the capture efficiency of CTCs from blood samples.[57-63, 65] In conventional pressure-driven filtration, it is highly possible that only a small portion of the membrane might be actively used for the filtration. This decreases the overall efficiency of the filtering process and, furthermore, it will probably encounter clogging, which aggravates the filtering efficiency. If the clogging persists, a higher pressure difference is required to filter the blood cells over a long time, but it is not desirable for cells to be exposed to such high shear conditions. Meanwhile, with the FAST disc, the chamber under the membrane is filled with an aqueous phase prior and during the entire filtration process. Therefore, when the blood phase reaches the membrane, the blood phase flows down to the lower chamber uniformly and diffuses in the aqueous phase. The FAST disc uses the entire membrane area for filtration and greatly alleviates clogging issues.

Using the FAST disc, we could achieve a remarkable enhancement in the CTC capture yield and purity in size-based filtration, even when using a track-etched membrane. From the MCF-7 cells spiked in whole blood, we could detect CTCs with a 96.2 ± 2.6% recovery rate from repetitive tests conducted for more than 15 days with 30 different discs. A compact stand-alone instrument for user-friendly operation of the disc was custom-designed and used to test clinical samples taken from 50 healthy donors and 142 cancer patients. While the number of CTCs detected in the samples taken from the healthy subjects was negligible, the FAST disc was able to detect 0–540 CTCs/7.5 mL CTCs from 15 of the 18 (83.3%) samples taken from breast cancer patients and 2–485 CTCs/7.5 mL taken from 63 of 76 (82.9%) stomach cancer patients. It is important to note that all of the breast and stomach cancer patients in this study were without distant metastases. Although there are many reports on the importance of CTCs as a new biomarker for cancer metastasis,[83] few studies have so far been done to determine whether CTCs are also useful for the early detection of solid tumors.[84, 85] With highly sensitive, cost-effective and robust FAST disc technology, we could detect a significant number of CTCs not only from cancer patients with metastasis but also from patients in relatively early stages of cancer without distant metastases, which gives rise to the potential of CTCs being used as an early diagnostic marker. Furthermore, the CTCs isolated by the FAST disc are not fixed but instead are alive, allowing them to be readily used for standard analyses such as immunostaining, high-resolution imaging, and mutation analysis, which are particularly important for personalized therapy. Because the FAST disc mechanism can be applied to a variety of size-based filtration techniques, we expect it to prove useful in a wide range of applications.

Chapter 3. Single cell analysis of isolated CTCs by using FAST disc

3.1 Introduction

Lung cancer is the most common cause of cancer-related mortality in both men and women worldwide [86, 87]. Non-small cell lung cancer (NSCLC) accounts for 84% of all lung cancers, and despite improved diagnostic techniques, a great majority of patients with NSCLC present with advanced-stage tumors at diagnosis, and the 5-year relative survival rate is less than 20% [88]. Epidermal growth factor receptor (EGFR) mutations are found in 10–30% of patients with NSCLC, and targeted therapies, including EGFR-tyrosine kinase inhibitors (TKIs) can deliver significantly improved clinical outcomes, depending upon the type of mutation [4, 89]. As new-generation EGFR-TKIs (e.g. osimertinib) [90, 91] have been developed recently for patients who showed resistance to conventional EGFR-TKIs, frequent examination of the tumor susceptibility to EGFR-TKIs became very important. However, conventional tissue biopsy is invasive, and therefore, more facile and less invasive liquid biopsy methods, able to monitor the disease response to targeted therapy and track the emergence of drug resistance, could significantly aid in the clinical management of the disease.

Among various circulating biomarkers, circulating tumor cells (CTCs) offer a unique opportunity to obtain information on live tumor cells at the DNA, RNA, and protein levels. Despite significant challenges associated with the extremely rare and heterogeneous characteristics of CTCs, recent technological advancements have allowed studying the prognostic value of CTCs, as well as monitoring and predicting the efficacy of therapy. To date, various platforms have been developed to isolate CTCs based on their biochemical or physical properties, such as the expression of epithelial cell adhesion molecule (EpCAM) or their size. Nevertheless, only the CellSearch™ system (Menarini Silicon Biosystems) is currently approved by the US Food and Drug Administration for the enumeration of CTCs in patients with metastatic colorectal [92], breast [93], and prostate [94] cancer. However, the prognostic value of CTCs remains controversial in NSCLC. Although many previous studies have demonstrated that patients with a higher number of CTCs have a poor clinical outcome [28, 95-99], some studies have reported that baseline CTC counts had no significant correlation with the survival rate in patients with NSCLC [100, 101].

Previous immunoaffinity-based CTC enrichment methods using anti-EpCAM antibodies suffer from the limitation of missing clinically important CTCs with low EpCAM expression such as

---

* *Chapter 3 is reproduced with the permission from "M. Lim†, J. Park†, A.C. Lowe; H. Jeong; S. Lee; H.C. Park; K. Lee; G.H. Kim; M.-H. Kim; Y.-K. Cho, Theranostics 2020, **10**, 5181-5194." Copyright 2020 Ivyspring*

mesenchymal and stem cell-like tumor cells. Furthermore, immunoaffinity-based isolation methods require a relatively long processing time to achieve an efficient antigen–antibody interaction [102, 103]. Alternatively, marker-independent approaches, based on intrinsic physical properties of CTCs, have been developed [104, 105], but they tend to show lower capture yields and purity, and sample pretreatment requirements or clogging issues are often a problem. Size-based CTCs isolation methods using inertial microfluidics provide relatively high detection rates but require prior sample preparation steps such as removal of red blood cells and dilution [106, 107]. While most of the current CTC enumeration technologies rely on signal averaging across individual heterogeneous CTCs, facile analysis of CTCs at a single-cell resolution is highly desired to assess the cell heterogeneity and uncover its clinical consequences. Although much progress has been made and clinical significance of CTCs has been demonstrated, the remaining challenges include a high cost, low throughput, and complexity of the process, as well as false-positive/false-negative results, which hinder a wider adoption of CTC-based liquid biopsy as a routine practice in clinical settings.

In this report, we present the preclinical validation of a fluid-assisted separation technology (FAST) disc [108], which allows rapid (>3 mL/min), reproducible, and label-free isolation of CTCs directly from unprocessed whole blood of patients with NSCLC. We performed serial monitoring of CTC counts, mutation detection, and single-cell multiplex gene expression of CTCs from a prospective cohort of patients with NSCLC receiving EGFR-TKIs treatment. The study highlights the potential of a CTC-based liquid biopsy for assessing the efficacy of therapy and emergent drug resistance.

3.2 Prognostic values of CTCs through single cell analysis

3.2.1 Experimental details

Study design and blood sample collection

The biospecimens and data used in this study were provided by the Biobank of the Pusan National University Hospital (PNUH), a member of the Korea Biobank Network. The study protocol was reviewed and approved by the Institutional Review Board (IRB) of PNUH (H1612-019-049). This was a prospective, single-center study conducted at PNUH (Busan, Republic of Korea). Patients who met the following inclusion criteria were selected for the study: 1) a histologically or cytologically confirmed diagnosis of primary NSCLC; 2) a confirmed *EGFR* mutation in histological or cytological specimens; 3) previously untreated stage IIIB or IV according to the 7th edition of TNM staging system by the international association for the study of lung cancer [measurable disease according to Response Evaluation Criteria in Solid Tumors version 1.1 (RECIST 1.1)]; and 4) received at least one dose of EGFR-TKIs as the first-line therapy during the follow-up study. Blood samples were collected for

analysis within 3 days before/after EGFR-TKIs treatment. Written informed consent was obtained from all patients before blood sampling.

To monitor CTC counts during TKI therapy, blood samples were collected from 40 enrolled patients on a regular schedule. Peripheral blood (3 mL) was collected in a Vacutainer® (K2 EDTA, #367844; BD Medical) and CTC isolation was completed within 6 h [109-111]. For the detection of *EGFR* mutations and single-cell-level gene expression analysis, additional 3 mL blood samples were collected from 16 patients. For serial monitoring of single-cell RNA expression in CTCs, blood samples were collected from 75-year-old male (LP25) and 74-year-old female (LP38) patients diagnosed with 19del and L861Q EGFR mutant-positive lung cancer, respectively, who were receiving afatinib treatment.

Cell culture

Breast cancer (MCF7, MDA-MB-231, and SKBR3), prostate cancer (LNCaP and PC3), and lung cancer (H460, H2228, HCC78, and PC9) cell lines were purchased from the American Type Culture Collection. All cell lines were cultured in RPMI 1640 medium supplemented with 5% FBS and 1% antibiotics/antimycotics at 37°C, 5% CO_2. The *mycoplasma* test was confirmed by e-Myco™ Mycoplasma detection kit (Intron, Korea).

Immunofluorescent staining and analysis of CTCs

Immunofluorescent staining and detection were performed on the FAST disc membrane according to a previously reported protocol [108]. Briefly, CTCs captured on a FAST disc were fixed with 4% formaldehyde and permeabilized with 0.1% Triton X-100, followed by washing and blocking with 10 μg/mL IgG in PBS. Cells were identified using a three-color immunofluorescence method, including FITC-conjugated anti-cytokeratin (CK) and anti-EpCAM markers for epithelial cells, a PE-conjugated anti-CD45 marker for white blood cells (WBCs), and DAPI for nuclear staining. Cells that were CK^+ or $EpCAM^+$, $CD45^-$, $DAPI^+$, and morphologically intact were identified as CTCs, while cells that exhibited high CD45 expression levels were identified as WBCs. Fluorescently stained cells were automatically scanned on a slide using a BioView workstation (BioView, Inc.) for the FAST disc.

CTC isolation and analysis using CellSearch

CTC enumeration, immunofluorescent staining, and detection by the CellSearch epithelial cell test (Menarini Silicon Biosystems, Inc.) were performed using the CellSearch™ protocol (www.cellsearchctc.com) at the Brigham and Women's Hospital (BWH), Boston, MA (The BWH IRB number is 2016P001708). A FAST disc operation system was shipped to BWH and used for a direct comparison with CellSearch. Two blood samples were collected from 17 enrolled patients with cancer into two types of tubes: 7.5 mL of whole blood in CellSave tubes (Menarini Silicon Biosystems, Inc.) for CellSearch and 3 mL of whole blood in EDTA tubes for FAST disc detection. The enumeration of

CTCs was performed using the recommended protocols for each method, as described previously [108, 112, 113].

DNA mutation analysis

To detect mutations in isolated CTCs, genomic DNA was extracted using the QIAamp DNA blood mini kit (Qiagen). For the detection of L858R, 19del and T790M mutations in gDNA, PCR was performed using the following cycling conditions on a Master cycler pro S instrument (Eppendorf): 95 °C for 10 min, followed by 40 cycles of 95 °C for 30 s and 58 °C for 1 min, and 98 °C for 10min, then held at 4 °C. The PCR mixture (20 μL) contained 10 μL of ddPCR supermix for probes, no UTP (Bio-Rad), 1 μL of 20× primer/probe assay for mutant and wild type (Bio-Rad), and 8 μL of DNA. The copy number of mutants was quantified using the QuantaSoft software (QX-200, Bio-Rad).

Statistical analysis of CTC enumeration data

Overall survival (OS) and progression-free survival (PFS) were chosen as the endpoints to evaluate the prognostic value of CTC counts. The survival time was estimated using the Kaplan–Meier method, and the difference in survival between groups was assessed using a log-rank test. The SPSS 22.0 for Windows software was used for statistical analyses. To confirm the correlation between the CTC count change ratio; $\Delta\mathrm{CTC}\ (\%) = \frac{CTC_i - CTC_0}{CTC_0} \times 100\ \%$ where CTC_i is the CTC count at time point i and CTC_0 is the baseline CTC count and imaging response results, a two-tailed Student's *t*-test with a 95% confidence interval was performed using Origin 2015 (OriginLab Corp.). *P*-values < 0.05 were considered statistically significant.

Single-cell isolation and multiple gene expression analysis

Single cells were isolated using Kuiqpick™ (NeuroInDx). Cells captured on the membrane were stained for CD45, EpCAM, and DAPI to identify target cells. Single-cell cDNA was prepared using the Single Cell-to-Ct kit (Life Technologies), and a specific target was preamplified for gene expression analysis. qRT-PCR was performed using a BioMarkHD real-time PCR system and the software (Fluidigm). For analysis, quality thresholds of 0.65 and Ct ≤ 30 were considered.

Undetected genes were assigned a Ct-value of 999, which was imputed as the highest Ct-value observed for a given gene plus a value of 1 to provide balanced weights to missing data. All imputed Ct-values were converted to Z-scores to provide the same weights [114]. To assign equal weights to all measured mRNAs, the gene expression values were mean-centered and Z score-transformed by dividing the mean-centered expression value by the standard deviation. We conducted unsupervised hierarchical clustering and t-distributed stochastic neighbor embedding (t-SNE) to explore associations among sample groups. Unsupervised hierarchical clustering and its heatmap visualization were

performed using the *heatmap.2* function of the *gplots* package, and t-SNE analysis was performed using the *Rtsne* package in R (version 3.4.0).

Correlation matrix plots were constructed using the *corrplot* function in R. Correlation matrices were computed separately for patient-derived CTCs, cancer cell lines, and WBCs, with Spearman's rank correlations. Associated *P*-values were computed using the *cor.mtest* function in R. The Bonferroni correction of *P*-values was performed to adjust for multiple testing in the rank correlation matrix.

CTC classification

Based on the gene expression profiling data for individual cells, we calculated their epithelial (E) or mesenchymal (M) scores. Epithelial markers such as EpCAM and CK markers (KRT7, KRT18, and KRT19) were selected to measure scores related to epithelial characteristics of CTCs. The mesenchymal markers vimentin and CD44 were selected to calculate M-scores of CTCs. The mRNA expression values of the target markers, normalized to those of *GAPDH* using the $2^{-\Delta Ct}$ method, were added up for each E/M group, and the relative percentage was used to classify CTCs according to their epithelial-to-mesenchymal transition (EMT) characteristics.

3.2.2 Results and discussion

Label-free isolation of CTCs from whole blood using FAST disc

A FAST disc is a centrifugal microfluidic device, which enables clog-free, label-free CTC isolation from whole blood [108] (**Figure 3.1a**). In a FAST disc, the fluid flow by centrifugal force and that by filtration through the membrane are in perpendicular directions, similar to the tangential-flow filtration, which minimizes clogging (**Figure 3.1b**). The operation of the FAST disc is very simple and fast: 1) add 3 mL of whole blood to the sample-loading chamber; 2) spin the disc using a tabletop-sized, portable spinning machine; and 3) add 1 mL of washing buffer and spin. The total process of the isolation of CTCs from 3 mL of whole blood could be finished within 1 minute (**Figure 3.1c**). The CTC enumeration was performed using the conventional criteria for CTC identification, EpCAM/CK^+ and $CD45^-$, with immunofluorescence staining performed on the disc (**Figure 3.1d and Figure 3.2**).

Compared with a commercially available product, the CellSearch system (Menarini Silicon Biosystems, Inc.), the FAST disc showed a high capture efficiency, irrespective of the EpCAM expression levels in the cell lines, while CellSearch showed a high capture efficiency only for cell lines with high EpCAM expression (**Figure 3.1e)**. Further, clinical tests using blood samples from 17 patients with various cancer types demonstrated that size-selective CTC isolation using the FAST disc

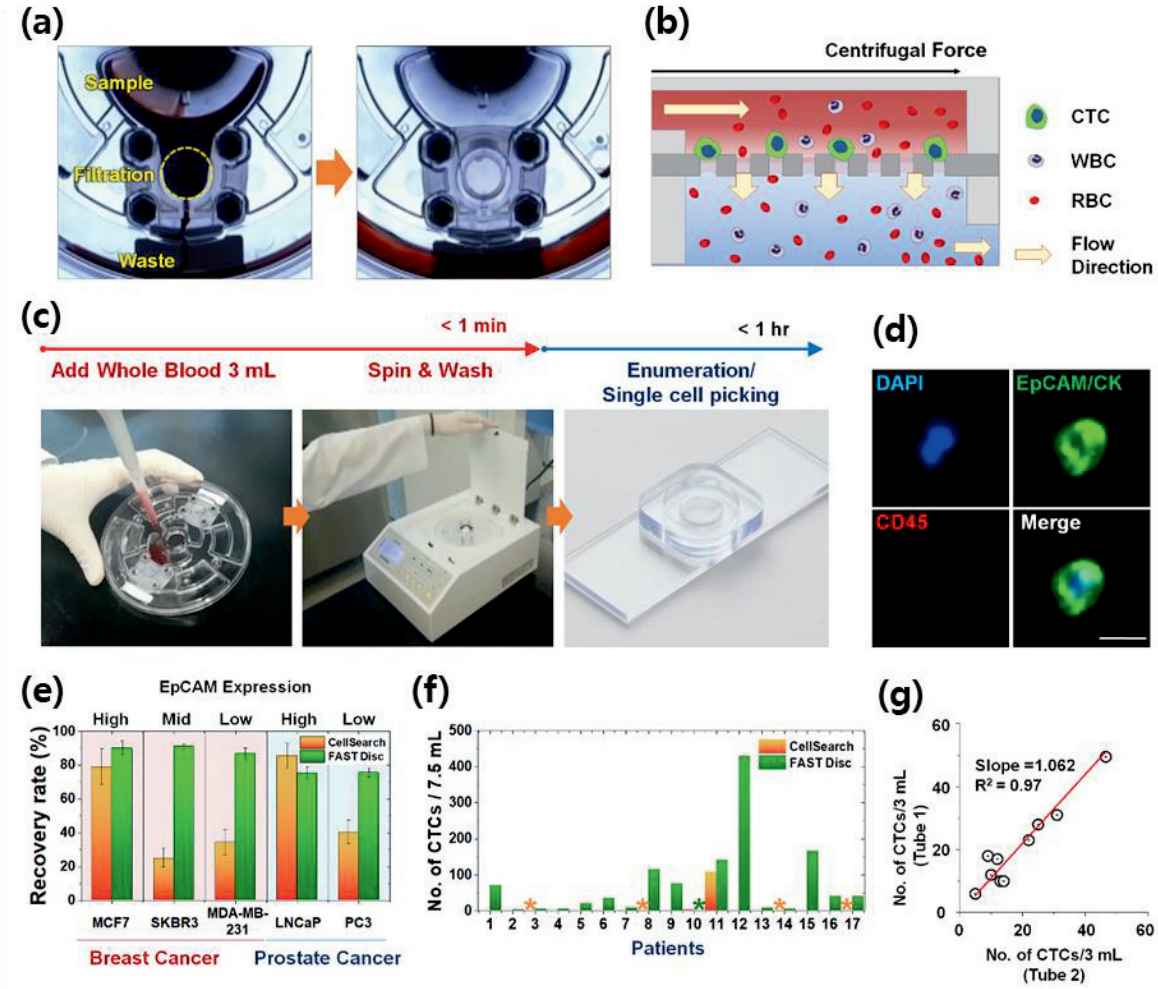

Figure 3.1. Workflow, mechanism, and performance of FAST disc. (a) Visualization of the FAST disc before and after the CTC enumeration process. **(b)** The centrifugal force pushes the liquid in a tangential direction to the flow filtering through the membrane. **(c)** Size-based isolation of CTCs from whole blood (3 mL) can be completed within 1 min, all in one disc. After washing and staining for enumeration, the filter can be removed and mounted on a slide glass for downstream analysis. **(d)** Representative images of CTCs ($DAPI^+$, $EpCAM/CK^+$, $CD45^-$) isolated from the blood of cancer patients. **(e)** Performance comparison between the CellSearch system and FAST disc using whole blood spiked with cancer cells (<100). Five cell lines with various EpCAM expression levels were used to quantify the recovery rates. **(f)** CTCs enumerated by the CellSearch system and FAST disc from the blood samples of 17 patients with different cancer types. **(g)** Reproducibility test using blood samples from one patient collected in two independent blood collection tubes showing similar CTC counts.

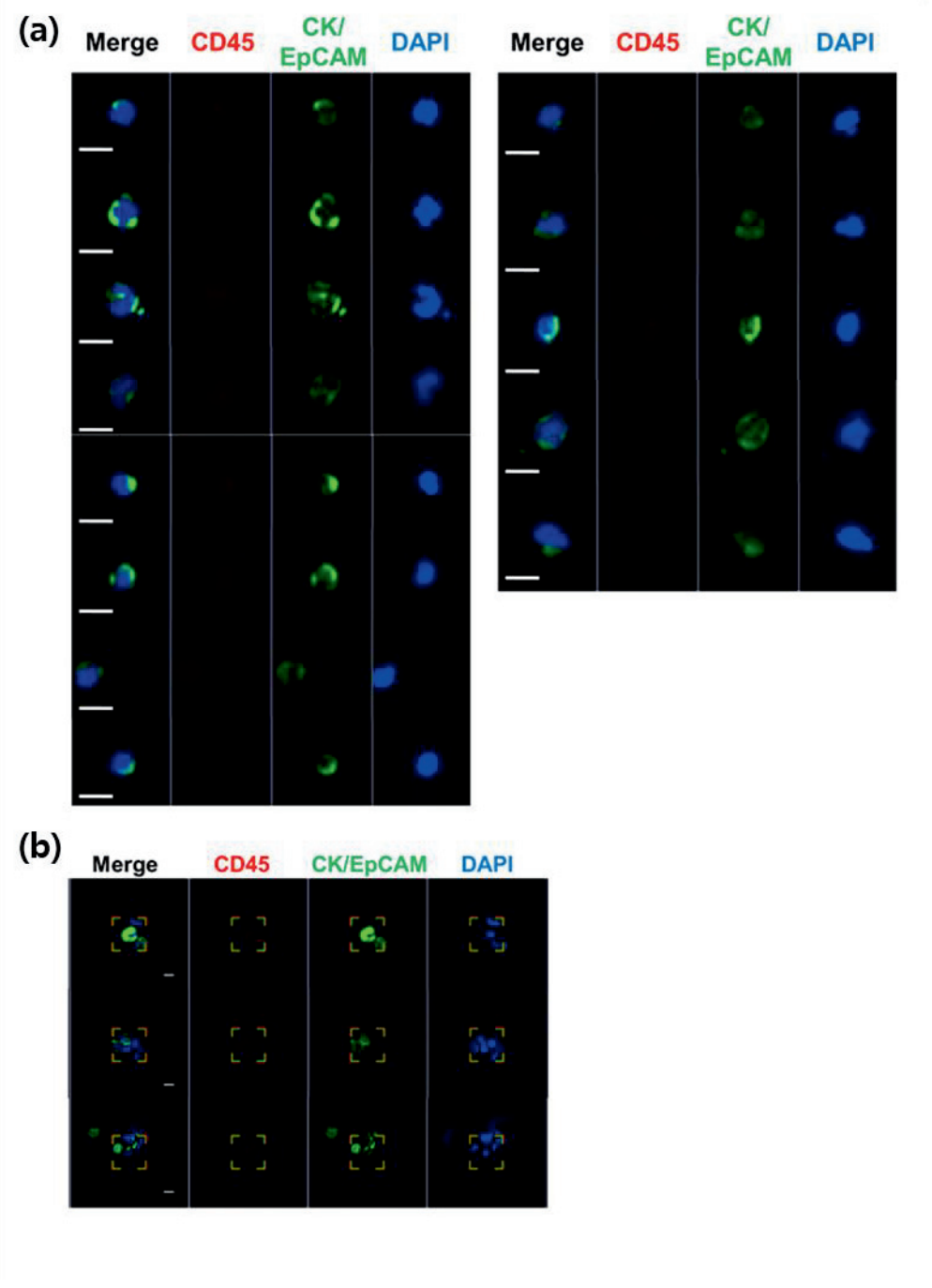

Figure 3.2. Fluorescence images of patient-derived CTCs. Representative examples of **(a)** patient-derived CTCs from two different NSCLC patients (Scale bar: 10 μm) and **(b)** CTC clusters from NSCLC patients (Scale bar: 8 μm). Merged images and three images from different fluorescent channels (DAPI, TRITC, and FITC) are shown. CTCs were defined as $DAPI^{+}/CD45^{-}/CK^{+}$ or $EpCAM^{+}$ cells.

outperformed the immunoaffinity-based enumeration by CellSearch; the detection rates were 94.1% and 11.8%, respectively. In addition, the failure rates were much lower for the FAST disc than for CellSearch, 5.9% and 23.5%, respectively (**Figure 3.1f)**. Measurement of CTCs in two blood samples collected from the same patient confirmed a good reproducibility of the FAST disc platform, which is a prerequisite for continuous monitoring of the disease status **(Figure 3.1g).**

Clinical characteristics of the prospective cohort of patients with NSCLC receiving EGFR-TKIs treatment

A total of 340 blood samples were obtained from 40 patients diagnosed with NSCLC with *EGFR* mutations at different treatment time points for CTC isolation using the FAST disc platform; a summary of the patients' baseline characteristics is shown in **Table 3.1**. At the time of analysis, 22 of the 40 patients (55.0%) experienced disease progression, and 12 patients (30.0%) died or were lost to follow-up, resulting in a median PFS of 13.1 months (95% CI: 11.7–16.3 months) and OS of 19.0 months (95% CI: 15.6–20.2 months). The average follow-up time for the 28 patients who were still alive was 19.6 months (range: 9.8–31.3 months).

Baseline CTC counts and survival

The median CTC_0 value among 38 tested patients was 37 CTCs/7.5 mL. With the cutoff value of 66 CTCs/7.5 mL, which minimized the p-value from the log-rank test, eight patients (21.1%) showed CTC counts higher than the cutoff (CTC^{High} group). Thirty patients (78.9%) showed CTC counts lower than the cutoff (CTC^{Low} group). As shown in **Figure 3.3a**, the CTC^{Low} group had a relatively longer OS than did the CTC^{High} group, but the difference was not statistically significant. Thus, no correlation was observed between CTC0 and OS. One possible reason is that the efficacy of the first-line therapy, rather than CTC_0 itself, might be more relevant to OS of the prospective cohort of patients tested in this study (**Figure 3.3b,c**).

Table.3.1 Patients demographics and clinical characteristics

Characteristics	No. (%)
Age at baseline, years	
Median	63
range	34-83
Sex	
Male	15 (37.5)
Female	25 (62.5)
M stage at diagnosis	
M0	3 (7.5)
M1a	6 (15)
M1b	31 (77.5)
EGFR mutation	
19del	19 (47.5)
L858R	16 (40)
Others	5 (12.5)
EGFR-TKI received	
Gefitinib	2 (5)
Erlotinib	9 (22.5)
Afatinib	29 (72.5)

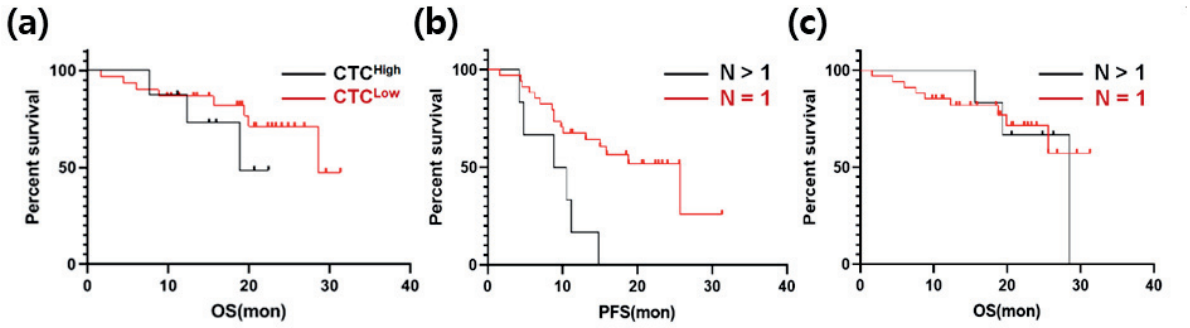

Figure 3.3. Correlation between CTC counts and treatment responses on CT scans. (a) Kaplan-Meier curves for OS between two patient groups according to the cutoff baseline CTC count (66 CTCs/7.5 mL). (CTCLow: n = 30, median OS: 18.04; CTCHigh: n = 8, median OS: 15.46, log-rank p = 0.3501; samples from two patients had a clogging issue.) **(b)** Six of 40 patients (15%) did not respond well to their first choice of therapy and had to change the treatment option more than once, resulting in a significantly poorer PFS than that of patients who responded well to the first-choice drug. Kaplan-Meier curves for PFS between two patient groups according to the number of treated drugs. (N = 1: n = 34, median PFS: 25.70, N > 1: n = 6, median PFS: 9.65, log-rank p = 0.0039). **(c)** Kaplan-Meier curves for OS between the two patient groups according to the number of treated drugs, demonstrating no significant difference. (N = 1: n = 34, median OS: undefined, N > 1: n = 6, median OS: 28.50, log-rank p = 0.7518).

Serial monitoring of CTC counts

We next focused on the trends of CTC counts to evaluate the correlation with patients' disease burden and treatment response, as shown in **Figure 3.4.** A cohort of 11 patients who had the 19del mutation and were enrolled for more than 19 months was used to evaluate the correlation of CTC counts with the treatment response. The RECIST criteria (version 1.1) were used to assess the treatment response via computed tomography (CT) scans acquired every two or three cycles, and responses were classified as a complete response (CR), partial response (PR), stable disease (SD), or progressive disease (PD) [115]. When we compared the change rate of the CTC counts as a function of the imaging response results, the PD group (average 70.1% increase, N=17) showed a significantly higher CTC count change rate than did the PR group (average 43.1% decrease, N=24).

Detection of *EGFR* mutations in tumor tissue and CTCs isolated using the FAST disc

We evaluated the concordance rate in detecting mutations in tumor tissue and CTCs isolated from blood samples. In 15 samples from 13 patients, the mutations identified in CTCs were 100% consistent with those found in the matching tumor tissues. Interestingly, the *EGFR* T790M mutation was detected in both relapsed tissue and CTCs isolated from blood samples of two patients, LP2 and LP49, who did not show this mutation during their first biopsy using both tumor tissue and blood samples, as summarized in **Table 3.2**.

Single-cell RNA expression analysis of patient-derived CTCs

To characterize the tumor heterogeneity, we applied a single-cell manipulation technique to isolate patient-derived live CTCs. After blood filtration and immunostaining for CD45 without a fixation step, live CTCs captured on the membrane were collected, and individual cells without a CD45 signal were subjected to single-cell RNA expression analysis **(Figure 3.5 and Figure 3.6)**.

We assessed mRNA expression in individual cells isolated from the four lung cancer cell lines, H2228, H460, HCC78, and PC9 (**Figure 3.7**), and from the blood samples withdrawn from three patients with NSCLC, LP25, LP38, and LP39, before starting their EGFR-TKIs therapy, using WBCs

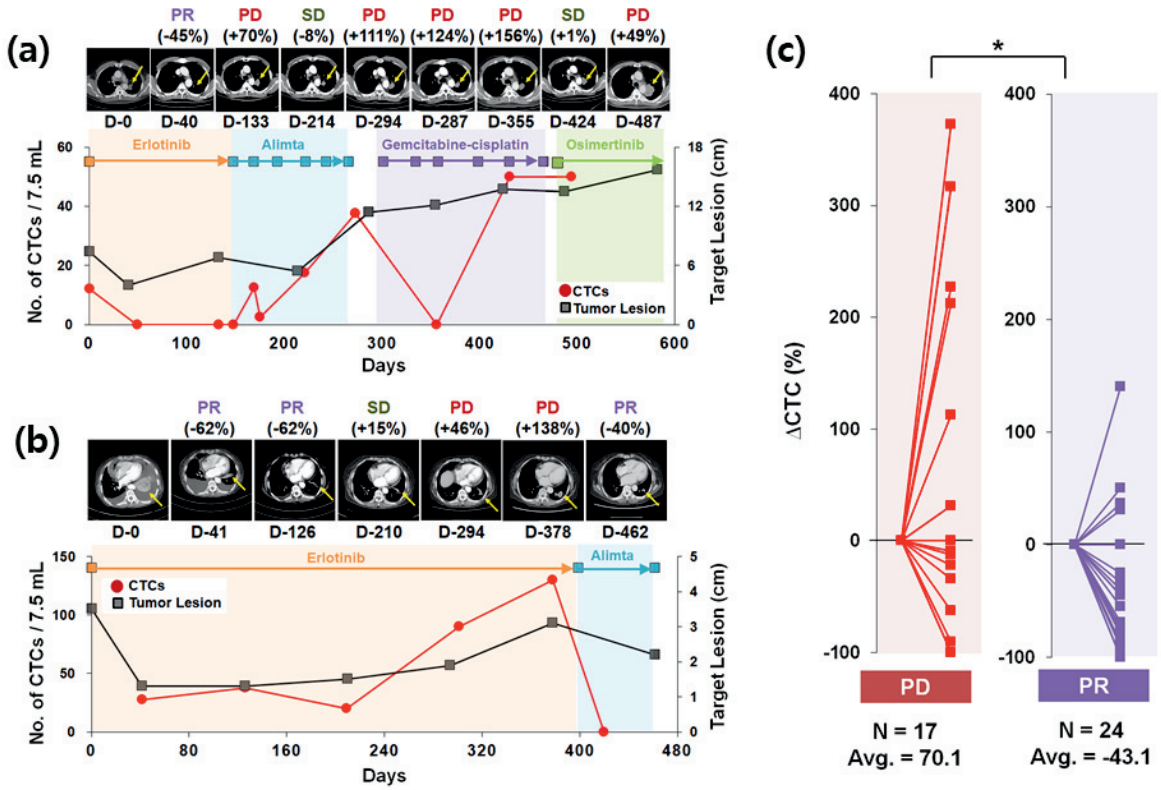

Figure 3.4. Representative examples of CTC counts and CT images obtained during the course of treatment and their correlations. (a) Tumor size and CTC counts show an increase in the tumor burden during 582 days of various EGFR-TKI treatments for patient LP2. **(b)** Patient LP11 continued to receive erlotinib initially. The CTC counts from the blood draw at 301 and 378 days were significantly increased with PD determined from CT images obtained on days 294 and 378. After the treatment was changed to alimta, both the CTC counts and tumor burden decreased dramatically and PR was determined at day 462. **(c)** Relationships with the change rate of CTC counts, △CTC (%); CTC counts change normalized by the baseline CTC, and CT scan image response results from patients with a 19 del mutation who enrolled in the follow-up monitoring study for more than 19 months. The CTC count change rate is sorted according to the imaging response results (PD or PR). The PD group showed a significantly greater CTC count change rate than the PR group (P = 0.011).

Table.3.2 Detection of EGFR mutation from CTCs. The mutation detection results from CTCs isolated from total 13 patients were in 100% concordance with the corresponding results obtained from tissue biopsy sample. Notably, T790M, the acquired resistance EGFR mutation, detected at relapse (AR) of samples, but not before the treatment (BT), from two patients (LP49 and LP2) both from noninvasive blood-based CTC analysis as well as tumor biopsy.

Patient	Sex	Age	Stage	L858R		T790M	
				Tissue	CTC	Tissue	CTC
LP1	F	52	IV	+	+	-	-
LP5	M	49	IV	+	+	-	-
LP6	M	58	IV	+	+	-	-
LP8	F	76	IV	+	+	-	-
LP10	M	63	IV	+	+	-	-
LP12	F	90	IV	+	+	-	-
LP13	F	53	IV	+	+	-	-
LP46	F	67	IV	+	+	-	-
LP47	F	83	IV	+	+	-	-
LP49 (BT)	F	65	IIIA	+	+	-	-
LP49 (AR)	F	65	IIIA	+	+	+	+
Patient	**Sex**	**Age**	**Stage**	**19 del**		**T790M**	
				Tissue	**CTC**	**Tissue**	**CTC**
LP2 (BT)	M	53	IV	+	+	-	-
LP2 (AR)	M	53	IV	+	+	+	+
LP25	M	74	IV	+	+	-	-
LP43	F	59	IV	+	+	-	-
				100%		***100%***	

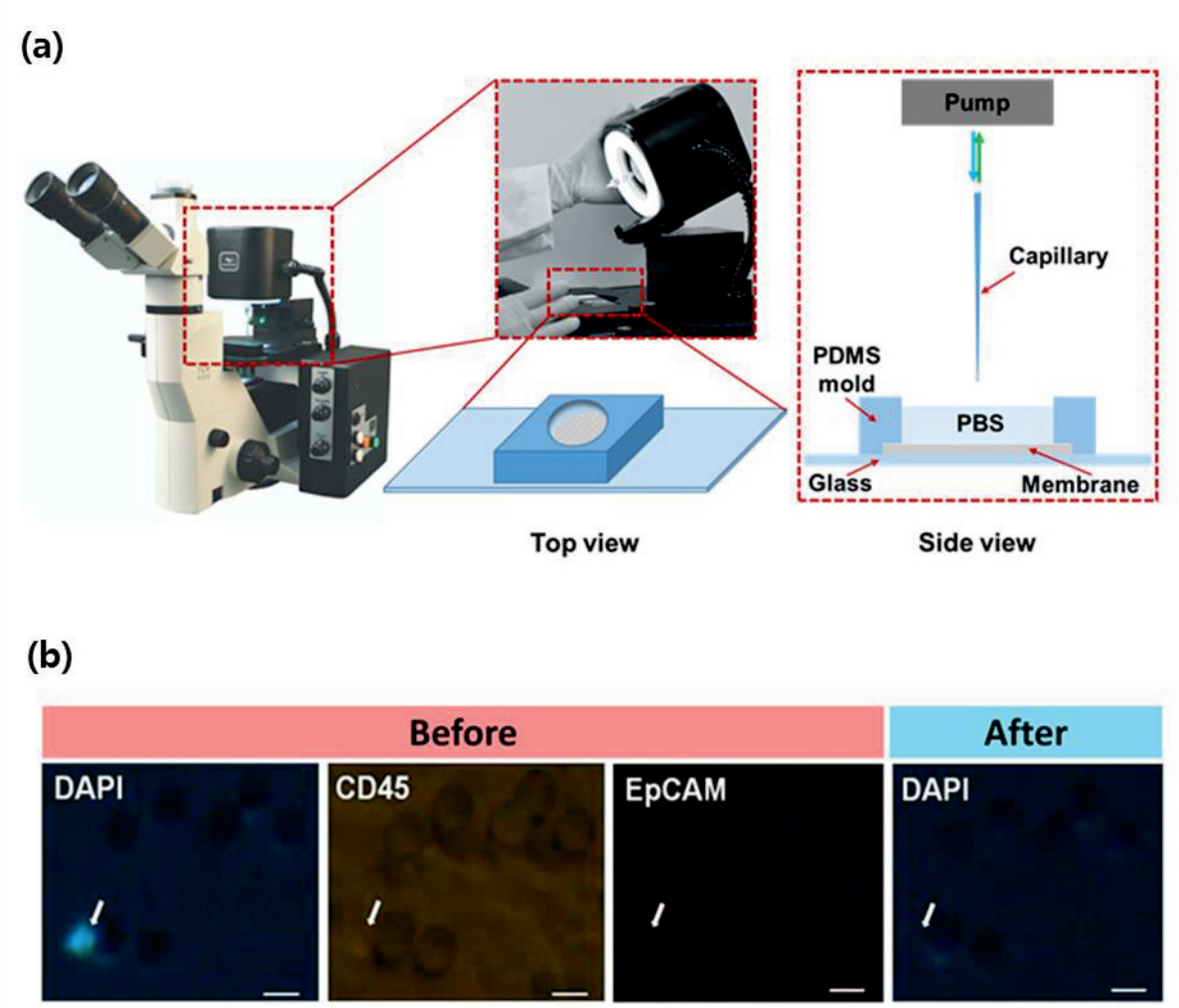

Figure 3.5. Procedures for single cell picking. (a) Schematic image of single cell picking. The membrane was separated from the disc and mounted onto the glass with the PDMS reservoir containing PBS. Using a capillary connected with a pump, a single cell was picked by the vacuum-assisted method. **(b)** Fluorescence images of a cell before and after picking from the membrane. DAPI+/CD45- stained cells are candidates for analysis. Image set of DAPI, CD45, and EpCAM before picking showing the target cells, and the other DAPI image shows the same spot after picking. (Scale bar: 10 μm).

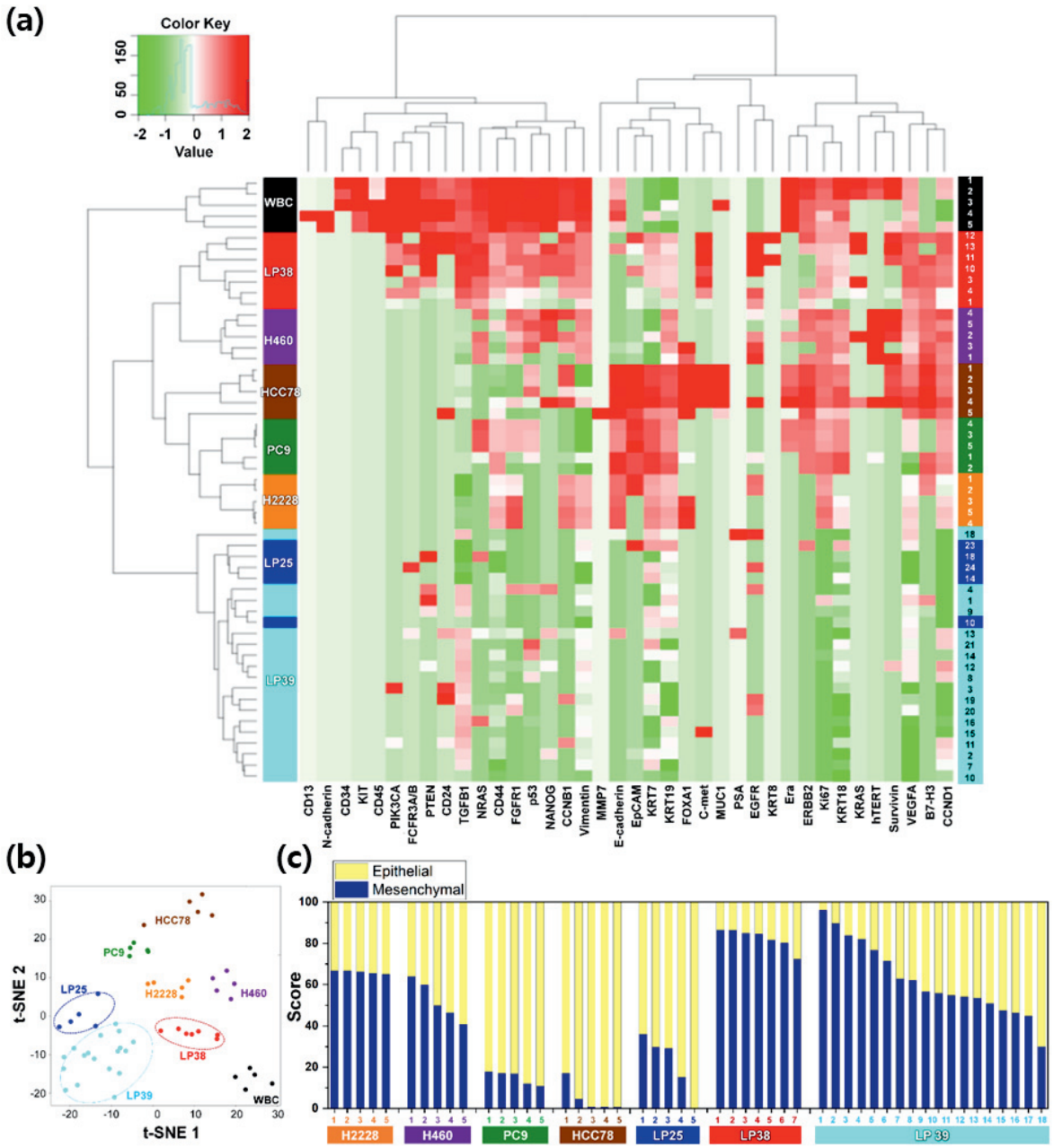

Figure 3.6. Gene expression profiles of single CTCs isolated from three patients with lung cancer and from lung cancer cell lines. (a) Heat map for the hierarchical clustering of the differentially expressed genes of single cells from four different NSCLC cell lines [H2228 (orange), H460 (purple), HCC78 (brown), and PC9 (green)], WBCs (black), and CTCs from three patients [LP25 (red), LP38 (blue), and LP39 (cyan)]. Each row represents a single-cell sample. The scale bar indicates the Z-scores of gene expression values, with highly expressed genes depicted in red and low-expressed genes depicted in green. **(b)** Two-dimensional t-SNE analysis based on hierarchical clustering. Cells clearly grouped according to the sample source. **(c)** Gene expression data of individual cells were further characterized to show an epithelial or mesenchymal cell signature. Intra- and intercellular heterogeneity is demonstrated using four different NSCLC cell lines, and profiling of individual CTCs isolated from three patients with NSCLC patients before chemotherapy. Patients LP25 and LP39 carried an 19del mutation, and patient LP38 had the L861Q mutation.

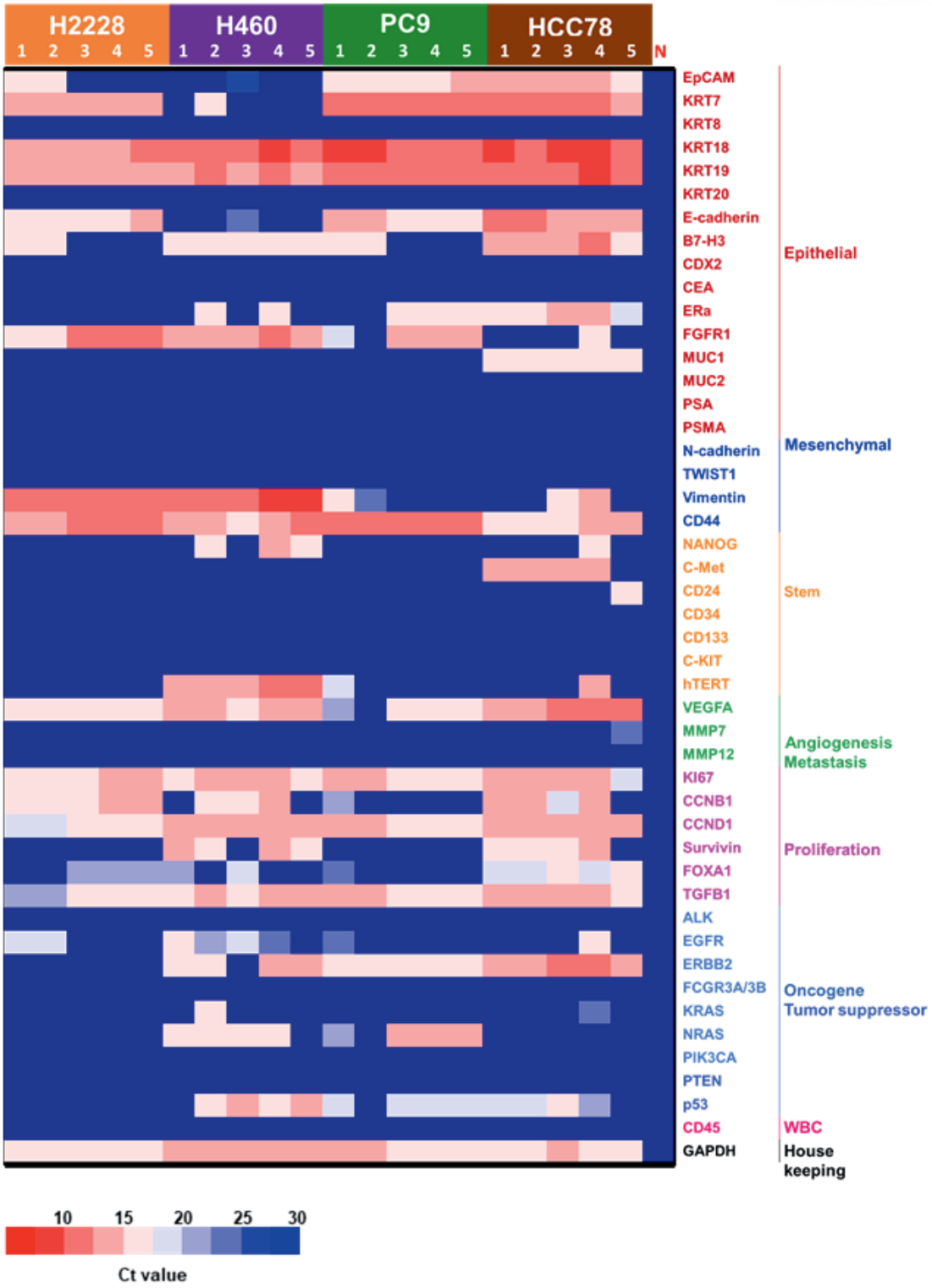

Figure 3.7. Single-cell real-time PCR using various lung cancer cell lines. Single-cell mRNA expression of four lung cancer cell lines, H2228, H460, PC9, and HCC78, determined using BiomarkHD qRT-PCR. After picking individual cells captured on the membrane by a cell-picker, RNA was extracted and preamplified for single-cell mRNA expression analysis. Ct ≤ 30 with a Fluidigm real-time PCR analysis software quality threshold of 0.65 was considered for the analysis. Columns and rows show individual cells and the target genes assayed, respectively. N means no template control.

as a control (**Figure 3.8**). Differences in the gene expression were confirmed between the cell lines, and CD45 was only detected in WBCs. The list of genes used in the single-cell qRT-PCR experiment is presented in **Table 3.3**. To explore associations among different cell groups, the data were analyzed using unsupervised hierarchical clustering (**Figure 3.6a**). It is obvious that individual cells show heterogeneous gene expression profiles, while single cells from the same group are clustered together, which implies a higher degree of interpatient heterogeneity of CTCs. In addition, the t-SNE analysis, shown in **Figure 3.6b**, clearly presents the inter-cell line and interpatient heterogeneity of CTCs. A correlation matrix plot showing Spearman's correlation coefficient among 30 baseline CTCs isolated from three patients, five WBCs, and 20 cells from the four different NSCLC cell lines (H2228, H460, HCC78, and PC9) is shown in **Figure 3.9.**

We further characterized an epithelial or mesenchymal signature of individual CTCs, based on previous reports [116-118]. Epithelial CTCs showed high levels of the epithelial marker EpCAM and CK markers, KRT7, KRT18, and KRT19, and low levels of mesenchymal markers, vimentin and CD44, whereas mesenchymal CTCs expressed the opposite trend. Individual cells from the four different NSCLC cell lines and three different patients with NSCLC showed different E/M hybrid signatures **(Figure 3.6c** and **Figure 3.10a)**. Based on the classification criteria, the H2228 cell line had an M-score of 66.0% ± 0.7%, which was consistent with its reported EMT properties [119]. The HCC78 and PC9 cell lines had the highest expression ratios of the epithelial markers, 95.2% ± 6.3% and 85.0% ± 2.9%, respectively. The H460 cell line had an intermediate expression ratio, with an M-score of 52.2% ± 8.5%. Despite their heterogeneity, single cells from the same cell lines were clustered together when we plotted the gene expression of the mesenchymal markers, vimentin and CD44, against that of the epithelial markers, EpCAM, KRT7, KRT18, and KRT19 (**Figure 3.11**).

Further, distinct differences in gene expression patterns among single CTCs from the three patients were clearly more significant than the heterogeneity found among individual CTCs isolated from each patient. Five CTCs from patient LP25 mainly exhibited the epithelial signature, whereas seven CTCs from patient LP38 were mesenchymal. On the other hand, 18 CTCs from patient LP39 were more heterogeneous, with the intermediate expression of mesenchymal markers **(Figure 3.6c** and **Figure 10a)**. High expression of EMT markers is known to be characteristic of more aggressive CTCs [120]. Although the number of samples was very limited in this exploratory study, patient LP38, whose CTCs showed the highest mesenchymal gene expression, had the shortest survival, whereas patient LP25, whose CTCs mainly showed epithelial characteristics, had the longest survival. The survival periods of patients LP25, LP38, and LP39 were 624, 212, and 468 days, respectively.

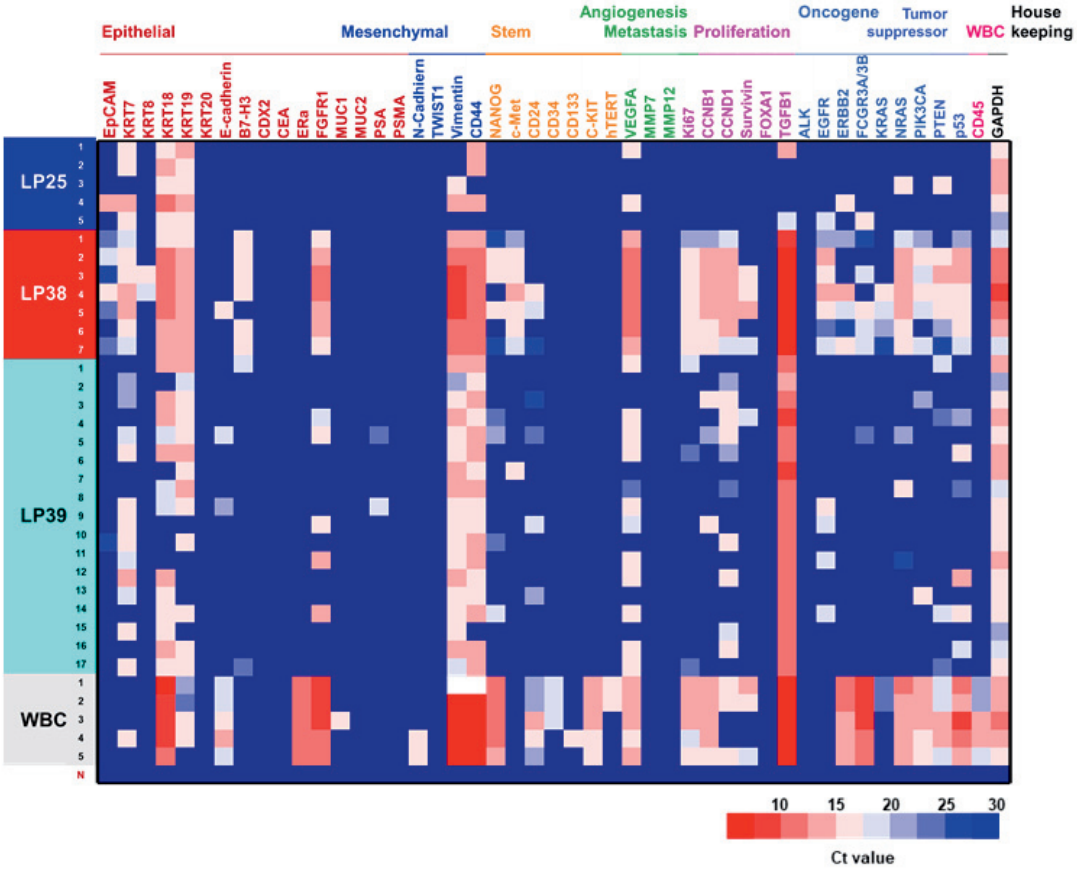

Figure 3.8. Single-cell real-time PCR using patient-driven CTCs from baseline samples and white blood cells. Single-cell mRNA expression of CTCs from three different patients at baseline (LP25, LP38, and LP39) determined using BiomarkHD qRT-PCR with five WBCs. Columns and rows show individual cells and the target genes assayed, respectively. N means no template control.

Table 3.3. Genes used to profile single CTCs. 48.48 dynamic array microfluidic qRT-PCR chips (Fluidigm) used to confirm the expression of genes in all captured single cells.

ALK	Anaplastic lymphoma kinase, CD246
B7-H3	CD276
CCNB1	Cyclin B1
CCND1	Cyclin D1
CD133	CD133 antigen, prominin-1
CD24	CD24 antigen
CD34	CD34 molecule
CD44	CD44 antigen
CD45	PTPRC; protein-tryosine phosphatase, receptor-type, C; leukocyte-common antigen
CDX2	Homeobox protein
CEACAM5	Carcinoembryonic antigen-related cell adhesion molecule 5; carcinoembryonic antigen (CEA)
c-MET	MET protooncogene; hepatocyte growth factor receptor (HGFR)
E-cadherin	CDH1; E-cadherin; liver cell adhesion molecule (LCAM)
EGFR	Epidermal growth factor receptor; HER1; ERBB1
EpCAM	Epithelial cellular adhesion molecule; tumor-associated calcium signal transducer (TACSTD1)
ERa	Estrogen receptor 1; estrogen receptor, alpha (ER-a), ESR1
ERBB2	HER2; V-ERB-B2 avian erythroblastic leukemia viral oncogene homolog 2; NEU
FCGR3A/B	Low affinity immunoglobulin gamma Fc region receptor III, CD16a/b
FGFR1	Fibroblast growth factor receptor 1
FOXA1	Forkhead box A1; hepatocyte nuclear factor 3-alpha (HNF3A)
GAPDH	Glyceraldehyde-3-phosphate dehydrogenase
hTERT	Telomerase reverse transcriptase
Ki67	MKI67, marker of proliferation Ki-67
KIT	Proto-oncogene c-Kit, CD117
KRAS	K-ras, KRAS proto-oncogne
KRT18	Kerain 18; cytokeratin 18
KRT19	Keratin 19

KRT20	Keratin 20
KRT7	Keratin 7
KRT8	Keratin 8; cytokeratin 8
MMP12	matrix metalloproteinase-12
MMP7	matrix metalloproteinase-7
MUC1	Mucin 1, transmembrane
MUC2	Mucin 2
NANOG	Nanog homeobox
N-cadherin	CDH2; neural cadherin (NCAD)
NRAS	Neuroblastoma RAS viral oncogene homolog
p53	Tumor protein p53, transformation-related protein 53(TRP53)
PIK3CA	phosphatidylinositol-4,5-bisphosphate 3-kinase, catalytic subunit alpha
PSA	Prostate-specific antigen
PSMA	prostate-specific membrane antigen, folate hydrolase 1(FOLH1)
PTEN	Phosphatase and tensin homolog
Survivin	Baculoviral IAP repeat-containing protein 5; apoptosis inhibitor 4 (API4); BIRC5
TGFB1	Transforming growth factor, beta-1
TWIST1	Twist, drosophila, homolog of 1
VEGFA	Vascular endothelial growth factor A
Vimentin	VIM

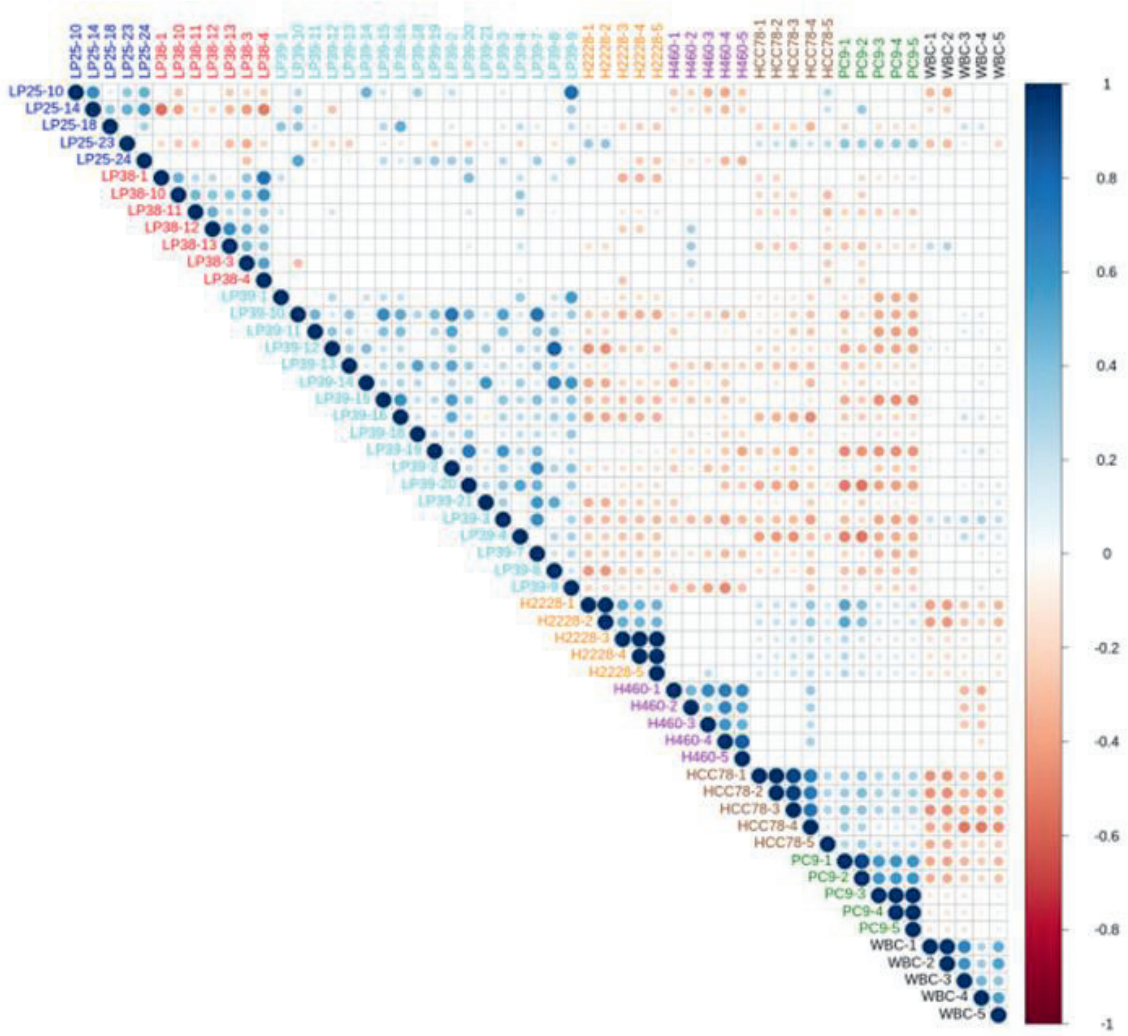

Figure 3.9. **Correlation matrix plots of correlations among 20 cells from four different cancer cell lines, five WBCs, and 30 patient-derived baseline CTCs isolated from three different patients.** Spearman correlation coefficients for sample characteristics. High and low similarity is indicated with blue and red color based on the scale bar, respectively. The circle size represents the magnitude of the correlation. P-values in this correlation analysis were derived using the *Cor.mtest* function in R. Bonferonni correction was applied to P-values to account for multiple testing in the rank correlation matrix.

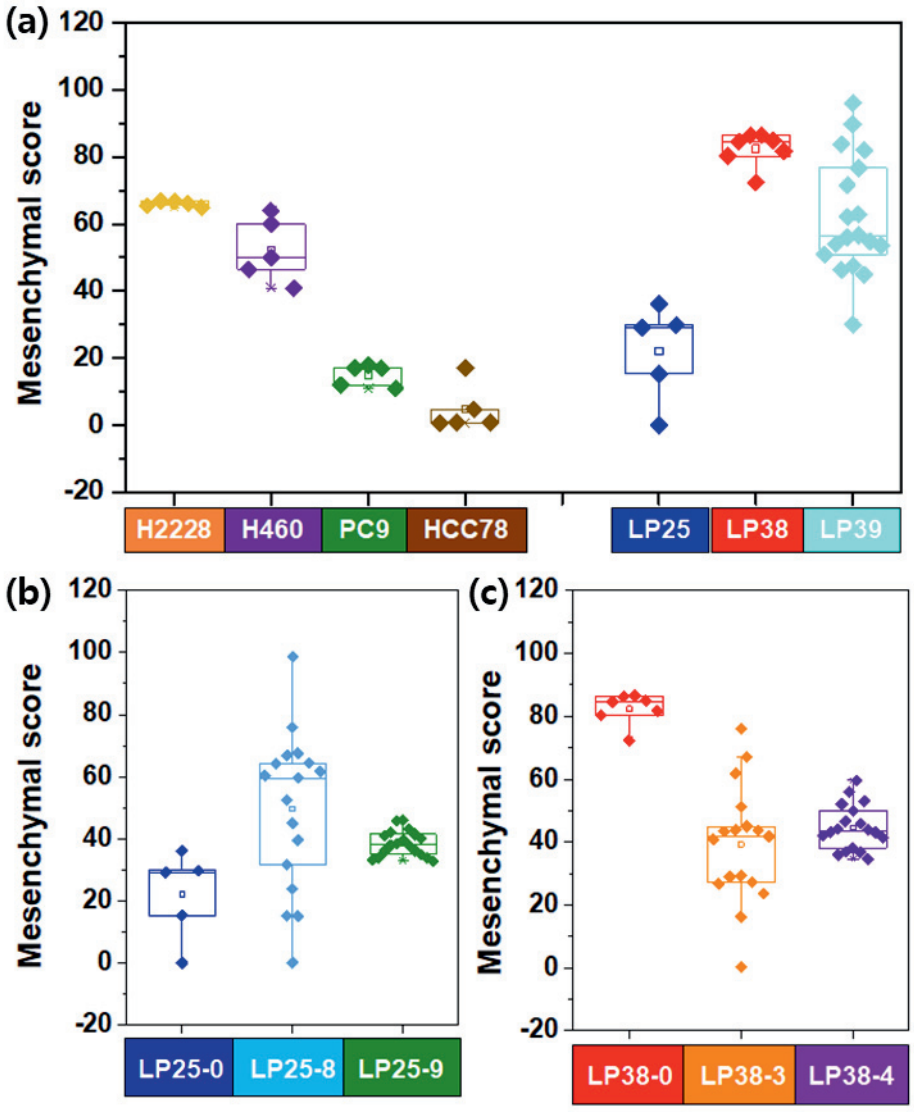

Figure 3.10. Summary of mesenchymal scores. (a) Distribution of mesenchymal scores from each sample according to the EMT characterization among four NSCLC cell lines and three NSCLC patients. Mesenchymal scores of single CTCs from patients **(b)** LP25 and **(c)** LP38 during TKI treatment.

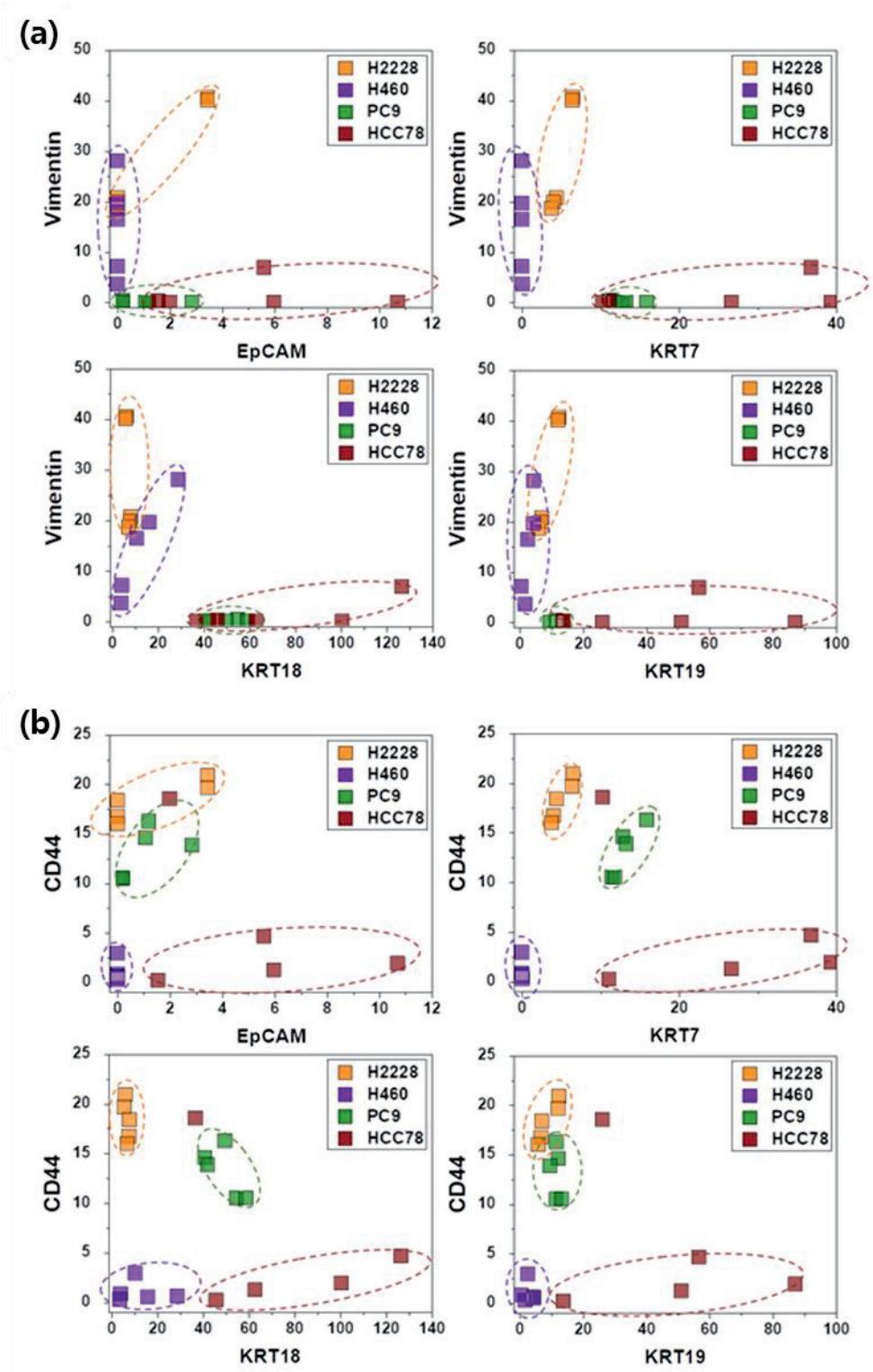

Figure 3.11. Correlation of marker expression among four NSCLC cell lines. (a) Vimentin expression of five cells from each cell line according to the expression of epithelial markers EpCAM, KRT7, 18, and 19, respectively. **(b)** CD44 expression of five cells from each cell line according to the expression of epithelial markers EpCAM, KRT7, 18, and 19, respectively.

Serial monitoring of single-cell RNA expression in CTCs from patients with NSCLC during EGFR-TKI treatment

For treatment response monitoring using CTCs, we performed a single-cell-level mRNA gene expression analysis using individual CTCs isolated at three time points during chemotherapy, in addition to regular measurements of CTC counts and CT image responses. For this proof of concept study, we enrolled two prospective patients, LP25 (**Figure 3.12**) and LP38 (**Figure 3.13**), during the period of EGFR-TKI (afatinib) treatment.

In the case of patient LP25, the initial treatment response was relatively good, and the number of CTCs/7.5 mL of blood decreased from 57.5 at baseline to 2.5 after 159 days of treatment, which was consistent with the CT scan-based SD and PR statuses after 30, 90, and 180 days of treatment, as shown in **Figure 3.12a**. However, the CTC counts increased to 15.0, 67.5, and 195.0 per 7.5 mL after 187, 250, and 281 days of treatment, which was in good agreement with radiographic data, indicating PD, at 282 days of treatment.

In contrast, patient LP38 showed 67.5 CTCs/7.5 mL at baseline, but the counts decreased to 12.5, 25.0, 5.0, and 15.0 at 71, 120, 155, and 196 days of treatment, respectively. Although the patient initially showed an SD response, until 120 days of treatment, the tumor size increased again, scoring PD, at 196 days, and the patient died 211 days after entering the study.

Although the dynamic changes in the numbers of CTCs were overall consistent with the CT data and clinical outcomes, the CTC counts were not sufficient to predict clinical outcomes. We hypothesized that, in addition to the total number of CTCs, the heterogeneity of individual CTCs and their characteristics might affect the patient outcome. Therefore, we tracked the gene expression characteristics of individual CTCs during the time course of TKI therapy.

For patient LP25, the single-cell-level gene expression profiling was performed using 5, 17, and 20 CTCs isolated before (LP25-0), after 250 days (LP25-8), and after 281 days (LP25-9) of treatment, respectively **(Figure 3.12** and **Figure 3.14**). From patient LP38, 7, 17, and 22 CTCs were isolated before (LP38-0), after 120 days (LP38-3), and after 155 days (LP38-4) of treatment, respectively **(Figure 3.13** and **Figure 3.15**). The numbers of CTCs used for the gene expression analysis **(Figure 3.12b–d** and **Figure 3.13b–d)** did not reflect the total numbers of CTCs, which were more carefully enumerated using an additional blood sample, as shown in **Figure 3.12a** and **Figure 3.13a**. As shown in the 3D t-SNE plots in **Figure 3.12c** and **Figure 3.13c**, each individual CTC showed a different gene expression pattern in hierarchical clustering, but CTCs from the same time point were well clustered together for both patients.

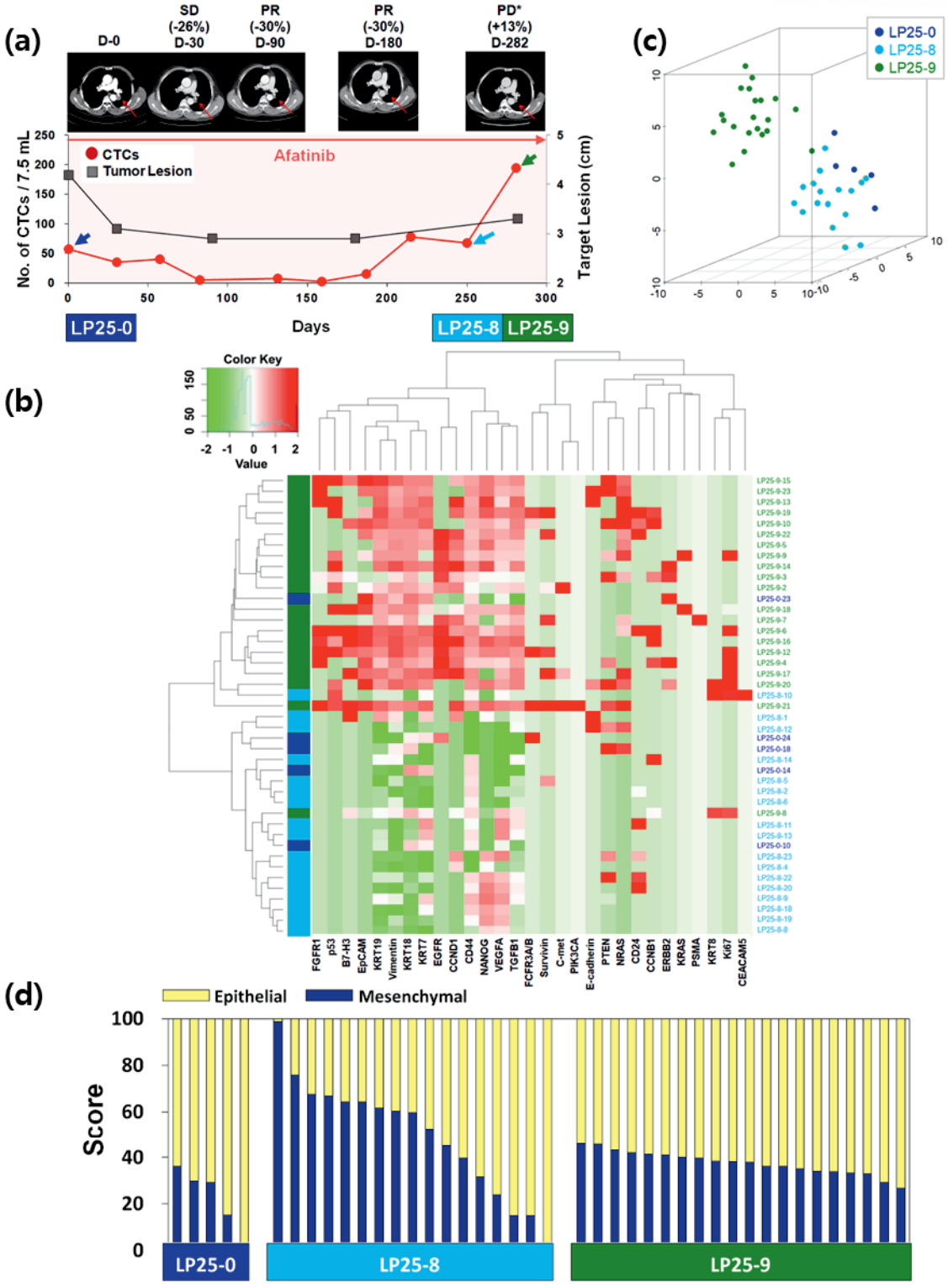

Figure 3.12. Longitudinal study of LP25 with CTC counts, individual CTC profile, and CT image response during TKI therapy. (a) Correlation between the number of CTCs and tumor size from CT images in patient LP25 with EGFR-mutant NSCLC during the course of TKI therapy. **(b)** Heatmap of the hierarchical clustering of gene expression profiles of single CTCs. **(c)** Three-dimensional t-SNE plots for CTCs isolated at three time points during the therapy of patient LP25. Despite the inter-sample heterogeneity of CTCs, cells clustered according to the same time point during the treatment. **(d)** EMT characterization of single CTCs from patient LP25 during TKI treatment.

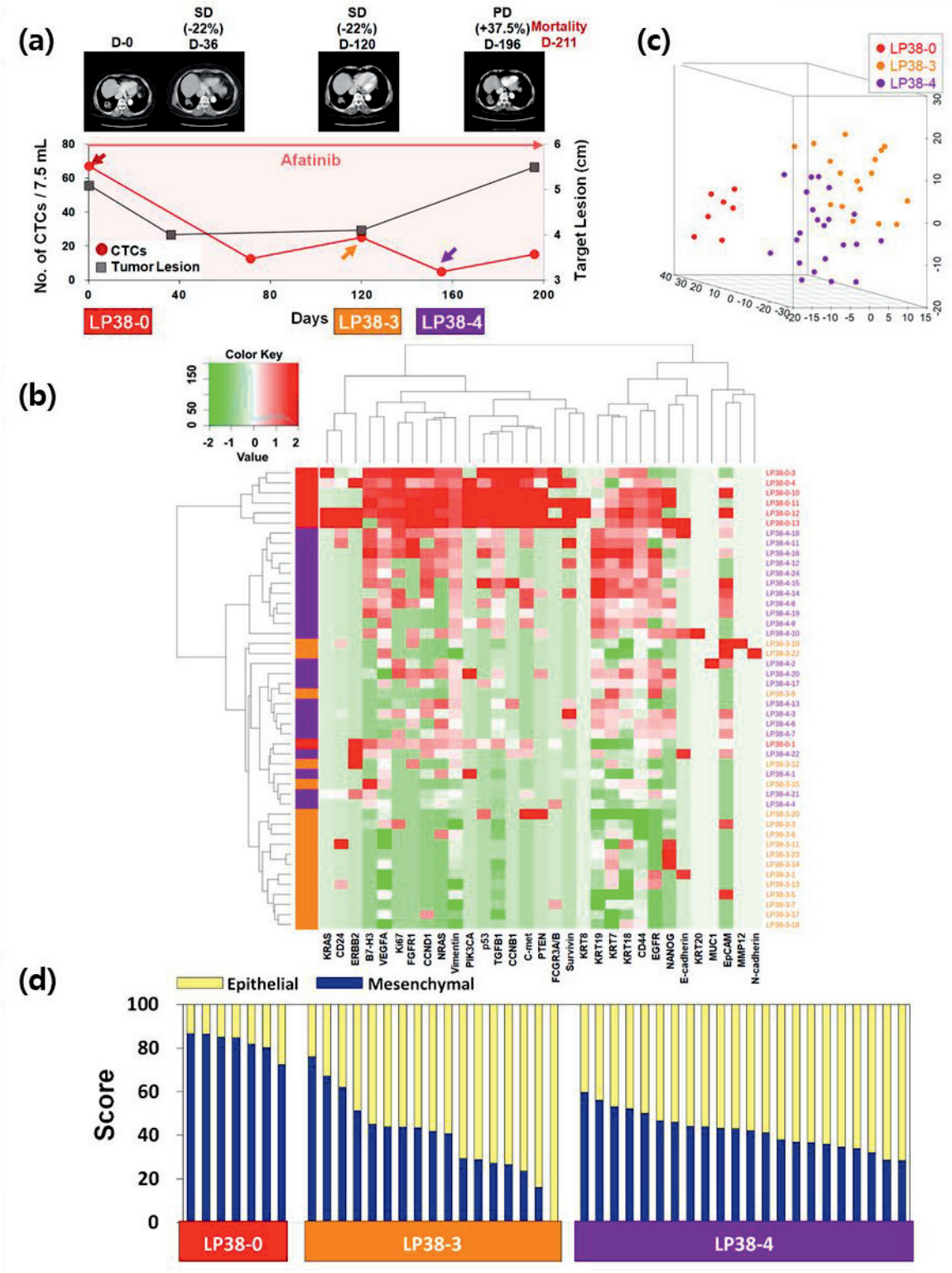

Figure 3.13. Longitudinal study of patient LP38 with CTC counts, individual CTC profile, and CT image response during TKI therapy. (a) Correlation between the number of CTCs and tumor size from CT images in patient LP38 with EGFR-mutant NSCLC during the course of TKI therapy. **(b)** Heatmap of the hierarchical clustering of gene expression profiles of single CTCs. **(c)** Three-dimensional t-SNE plots for CTCs isolated at three time points during the therapy of patient LP38. Despite the inter-sample heterogeneity of CTCs, the cells clustered according to the same time point during the treatment. **(d)** EMT characterization of single CTCs from patient LP38 during TKI treatment.

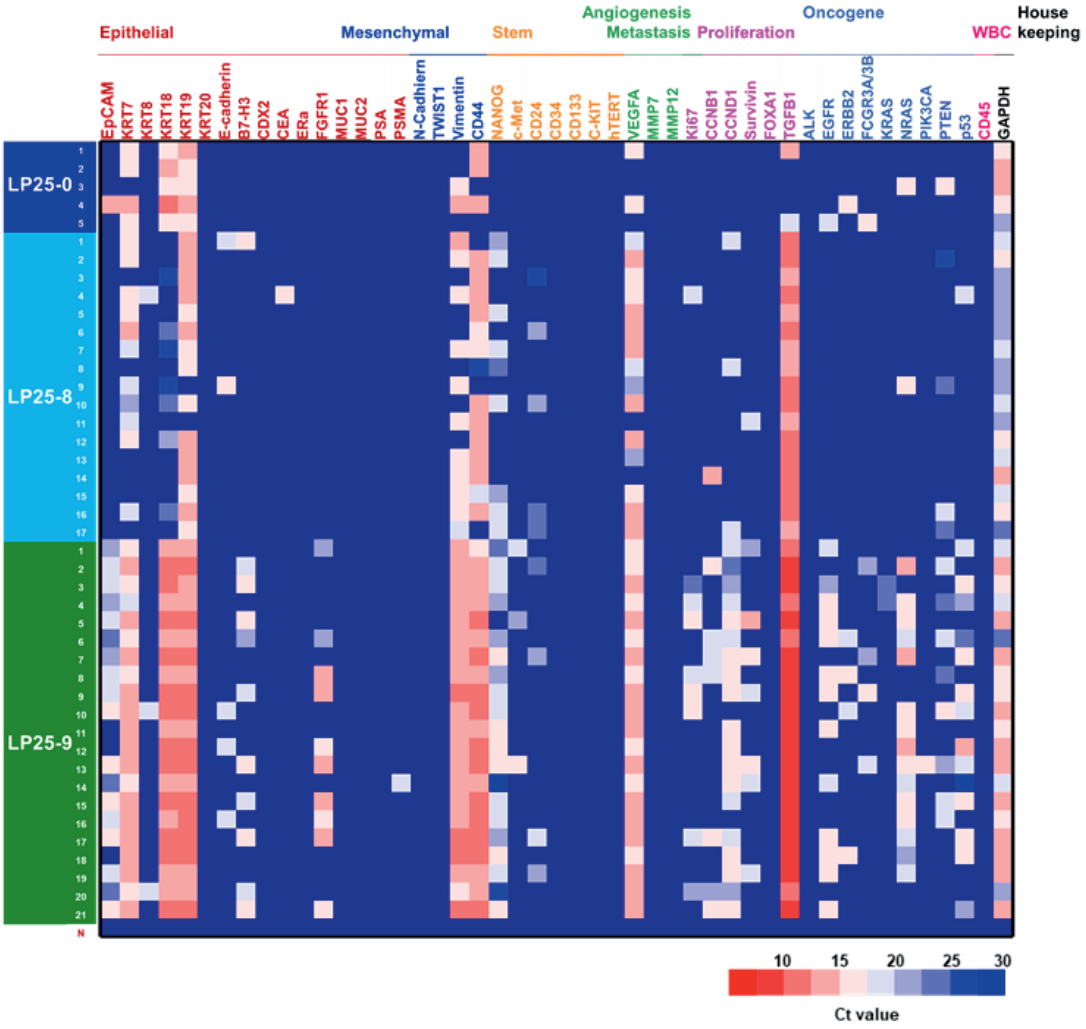

Figure 3.14. Single-cell real-time PCR using CTCs from patient LP25 at various time points. Single-cell mRNA expression was determined using BiomarkHD qRT-PCR. Columns and rows show individual cells and the target genes assayed, respectively. N means no template control.

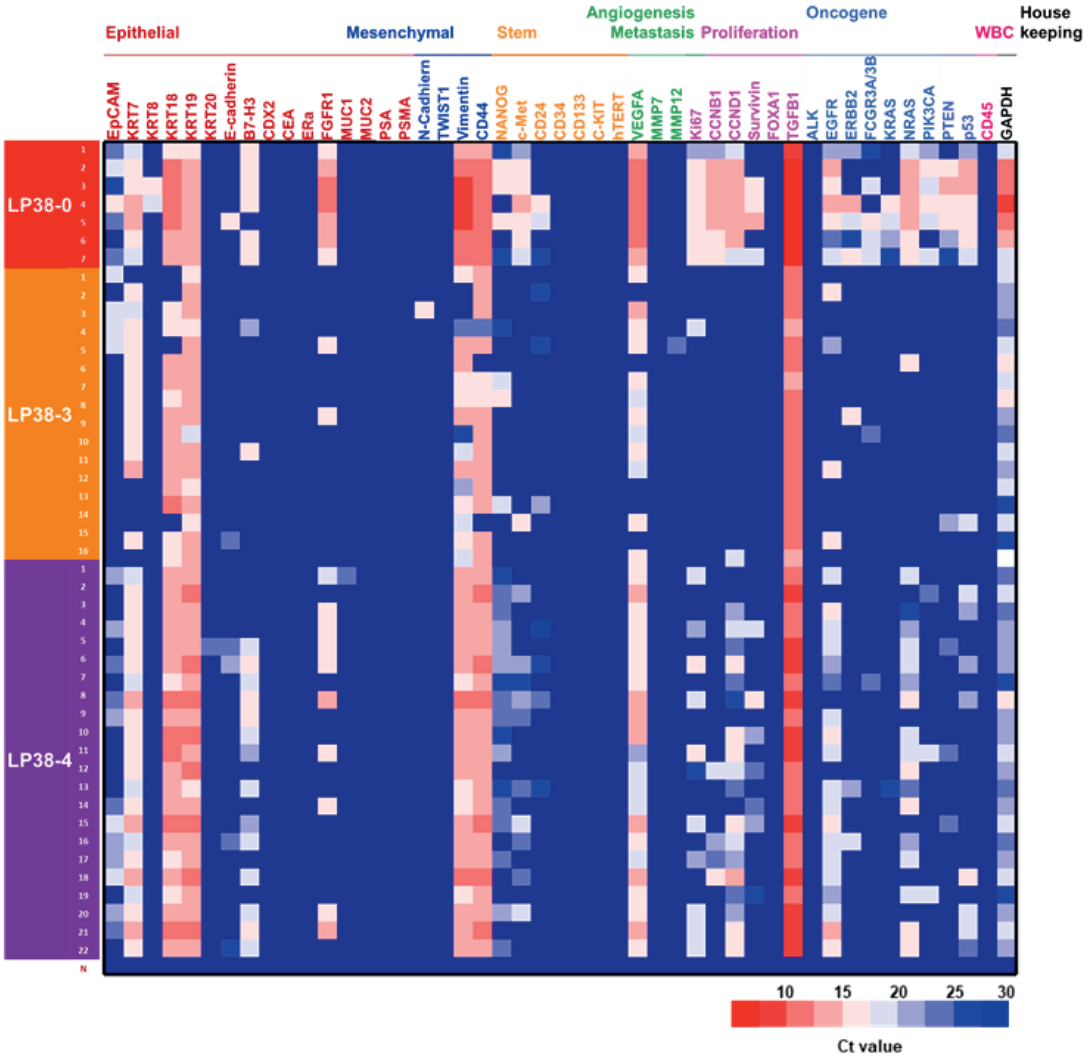

Figure 3.15. Single-cell real-time PCR using CTCs from patient LP38 at various time points. Single-cell mRNA expression was determined using BiomarkHD qRT-PCR. Columns and rows show individual cells and the target genes assayed, respectively. N means no template control.

In addition, the gene expression profiles of CTCs isolated at different time points were distinctly different, which was also demonstrated by the correlation matrix analysis (**Figure 3.16** and **Figure 3.17**).

We further characterized the EMT signatures of individual CTCs isolated during the time course of therapy. As shown in **Figure 3.12a**, patient LP25 showed SD and PR based on the CT scan results until 180 days, but the status changed to PD because of a new brain lesion at 282 days (LP25-9). Interestingly, the LP25-9 CTCs showed much higher expression of many more genes than did the LP25-0 or LP25-8 CTCs. When we classified individual CTCs based on the epithelial or mesenchymal gene expression signature, the heterogeneity of individual CTCs, as well as the dynamic change of the M-score, was obvious, as shown in **Figure 3.12d**. The M-score of CTCs at baseline (LP25-0) was relatively low (22.06% ± 12.96%) but increased, with a large standard deviation (49.53% ± 24.80%), for CTCs isolated after 250 days (LP25-8), which was approximately 1 month before PD was scored, with a new lesion in the brain. Interestingly, CTCs obtained on day 282, which was when a CT scan was taken, and PD was scored (LP25-9), showed a slightly decreased M-score, with a much lower intra-sample heterogeneity (37.51% ± 4.96%; **Figure 3.10b)**.

Patient LP38 had the highest expression of many genes in baseline CTCs (LP38-0), which somewhat decreased in CTCs isolated after 120 days of treatment (LP38-3), but with a significantly enhanced heterogeneity (**Figure 3.13d** and **Figure 3.10c**). Likewise, the tumor size was the largest at LP38-0 and decreased by 22% as the target lesion was scored SD (LP38-3). However, CTCs isolated after 155 days of treatment (LP38-4) again showed increased gene expression signals, which was consistent with the future clinical outcome and a PD score after 196 days of treatment. The EMT signature of individual CTCs was the strongest (82.39% ± 4.61%) at baseline (LP38-0), which dramatically decreased, with a high heterogeneity (39.24% ± 18.30%), in the LP38-3 CTCs and then remained at a similar level but with a lower heterogeneity (42.09% ± 8.31%) in the LP38-4 CTCs. Unfortunately, the amount of the blood sample obtained on day 196 was not sufficient for single-cell analysis, and the patient expired after 15 days.

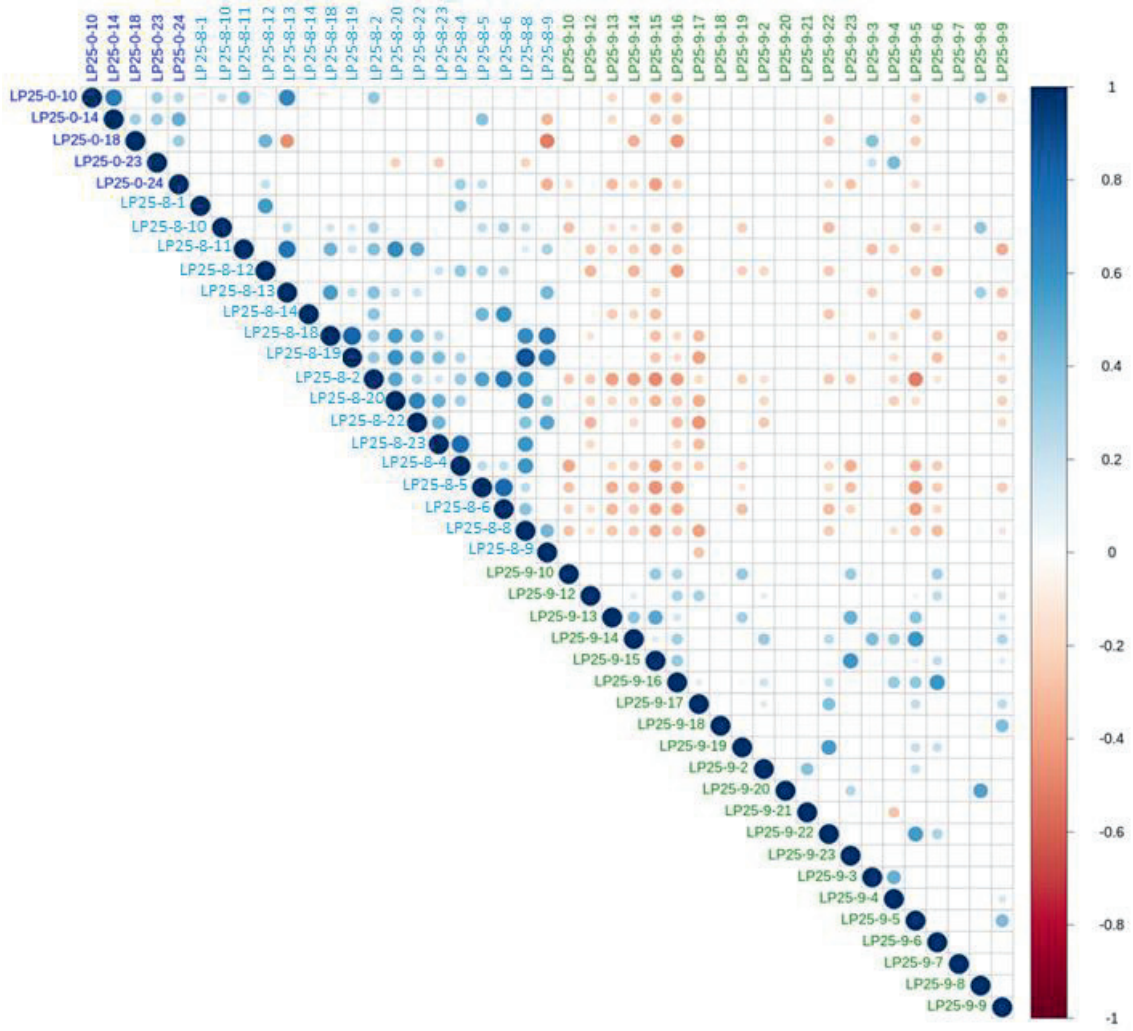

Figure 3.16. Correlation matrix plots of CTCs before and after treatment in patient LP25. Spearman correlation coefficients for sample characteristics. High and low similarity is indicated with blue and red color based on the scale bar, respectively. The circle size represents the magnitude of the correlation.

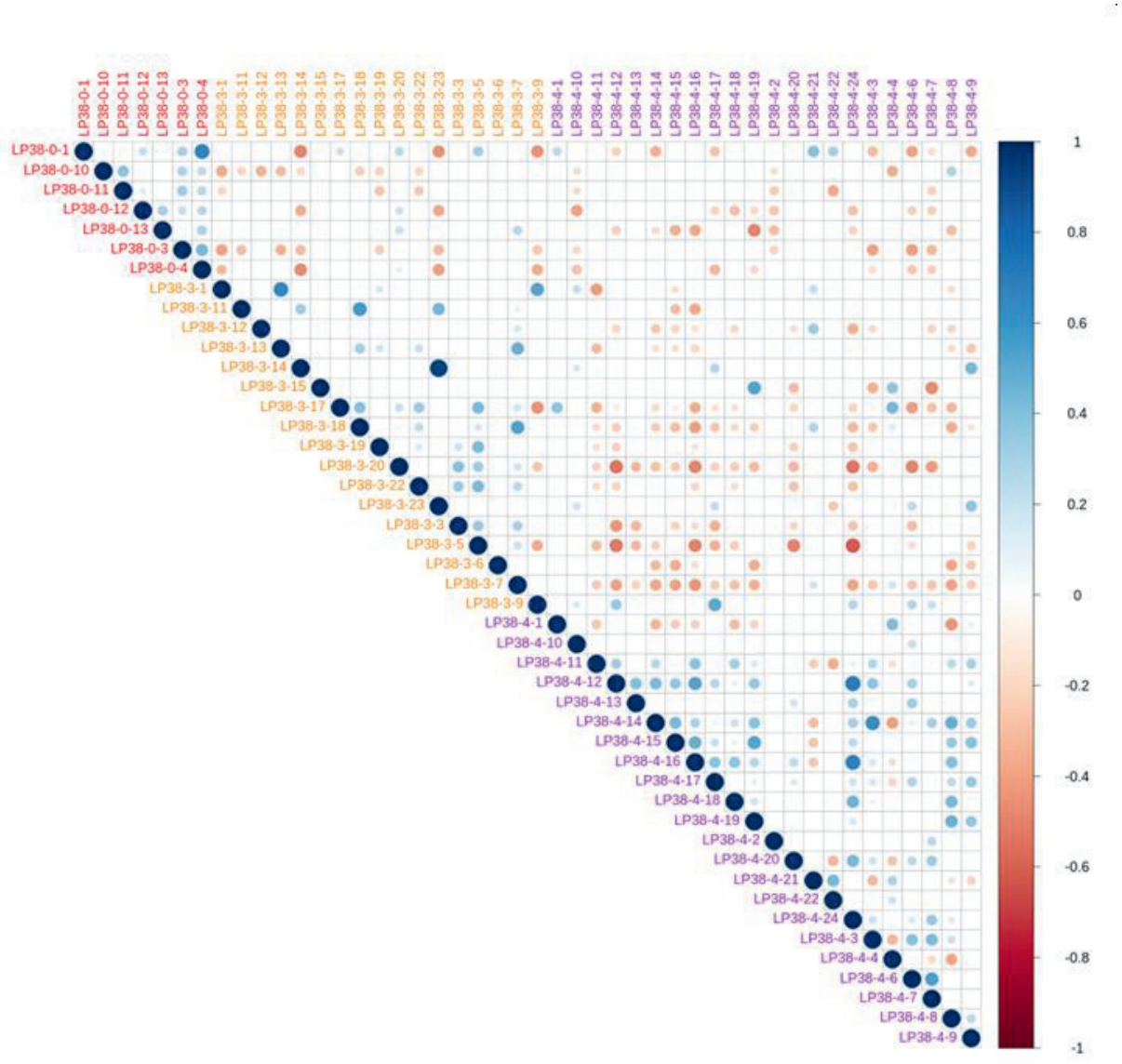

Figure 3.17. Correlation matrix plots of CTCs before and after treatment in patient LP38. Spearman correlation coefficients for sample characteristics. High and low similarity is indicated with blue and red color based on the scale bar, respectively. The circle size represents the magnitude of the correlation.

3.2.3 Conclusion

The availability of more facile methods for measuring the disease progression and identifying predictive biomarkers of therapeutic responses in patients with NSCLC would significantly contribute to clinical outcomes of patients. Recent advances in liquid biopsy technologies have enabled less invasive access to tumor materials, highlighting the prognostic value of CTCs in disease management [121-125]. However, frequent monitoring of CTCs has been limited by inconsistency in the enrichment yield of the extremely rare and heterogeneous cells, as well as by high costs and complexity of experimental protocols. Our study of prospectively collected blood samples from patients with NSCLC before and during EGFR-TKI therapy showed that longitudinal analysis of CTCs enumerated using a label-free isolation approach might provide early access to monitoring disease responses to targeted therapy.

Many studies have demonstrated that pretreatment CTC counts are highly relevant to PFS or OS of patients with advanced NSCLC [28, 95]. However, there have also been conflicting reports showing no statistical significance in the survival outcome depending on baseline CTC counts [100, 101]. A likely explanation for this discrepancy is the lack of standard enumeration methods for extremely rare and heterogeneous CTCs, as well as differences in the type of patients and the choice of treatment options. In our study, CTCs were detected in the majority of patients (85%), but the baseline CTC counts did not show an association with PFS or OS. On the other hand, dynamic changes in CTC counts were associated with CT scan-based tumor responses, suggesting a potential utility for early identification of responses to therapies. Although our data are consistent with those of a previous report [126], the number of patients was limited, and a further study, with a larger number of prospective patients in a setting with other targeted therapies or chemotherapy, is required to validate these findings.

Frequent monitoring of tumor mutations in patients with lung cancer is an urgent need to provide a clinically important guidance for disease management [36, 127-129]. For most patients with NSCLC, who harbor *EGFR* mutations, the treatment with an EGFR-TKIs therapy is beneficial. However, the T790M point mutation may arise soon, indicating the development of resistance to EGFR-TKI and the necessity to change the drug to third-generation EGFR-TKIs. Tissue biopsy is highly invasive, which prevents frequent monitoring of the development of mutations, and may not provide a representative mutation profile for patients with heterogeneous tumors at multiple sites. In this study, we demonstrated 100% concordance in the detection of *EGFR* mutations in tumor tissue and CTCs isolated from a total of 15 samples collected from 13 patients, including two cases of the emergence of the T790M mutation. These results present a promising outlook on the potential of routine analysis of CTCs to provide clinically relevant information for the timely selection of personalized therapies.

Other molecular information, such as gene expression data, can also be obtained by downstream analysis of a single CTC. Direct analysis of bulk cells may generate background signals from WBCs and other blood cells [130]. Furthermore, bulk cell-level analysis, based on signal averaging, leads to losing individual characteristics of heterogeneous CTCs, which are related to tumor biology and metastatic potential [131]. The importance of CTC characterization at a single-cell level has been highlighted by profiling multigene expression in individual CTCs in a heterogeneous population [102, 128], classifying CTC subpopulations [114], and studying an association of CTCs with the clinical outcome or tumor biology [132]. Herein, by using a label-free, high-throughput, clinical setting-friendly method for CTC isolation, based on the previously reported tabletop-sized FAST disc system [108], we were able to perform a longitudinal analysis of single-cell gene expression in CTCs isolated before and during targeted therapy. Our findings from single-cell gene expression analysis of four different lung cancer cell lines and three different patients indicated that the inter-heterogeneity among different cell lines or patients was much higher than the intra-heterogeneity within each group of CTCs.

EMT plays a key role in tumor progression and metastasis. EMT is associated with the loss of the epithelial phenotype, and increased invasion, migration, and cell proliferation are associated with the increased expression of mesenchymal markers. A number of studies have suggested that EMT may be associated with the resistance to EGFR-TKIs in patients with NSCLC [133, 134]. It was also suggested, based on liquid biopsy applications, that CTCs expressing EMT-related genes were associated with the disease progression and poor therapeutic responses in patients with breast [116], gastric [117], pancreatic [114], and lung [135] cancer. Gene expression in single cells has been studied to evaluate the heterogeneity of individual CTCs. Thus, Lin et al. [118] characterized single CTCs and demonstrated their inter- and intra-patient heterogeneity in four patients with pancreatic cancer. Ting et al. [136] conducted single-cell RNA sequencing of pancreatic CTCs and identified three distinct populations, with the data suggesting multiple pathways in the metastatic cascade. However, molecular analysis of single CTCs remains challenging because currently available platforms are expensive and not robust enough to be translated into the clinic. Consequently, there have been no reports on longitudinal monitoring of therapeutic responses via profiling of the EMT signature in individual CTCs based on a single-cell gene expression analysis.

EMT is crucial for cancer cells to acquire invasive and migratory abilities, eventually driving tumor metastasis. Recent studies have reported that EMT is not a step function, in which the change occurs from the E to the M state and that cells rather exhibit a hybrid E/M phenotype with a mix of E/M traits, which may be highly correlated with patient outcomes [134, 137, 138]. One important result of this study was that the E/M signature scores obtained by multigene expression analysis of single cells revealed substantial heterogeneity among individual cells and among cell lines. Despite their relatively small

intra-heterogeneity, the EMT scores of individual cells from four different NSCLC cell lines could predict the known characteristics of the specific cell types, which were categorized as mainly mesenchymal or epithelial, or a hybrid state, showing both traits [134, 139, 140]. Furthermore, analysis of EMT scores of individual pretreatment CTCs isolated from three patients with NSCLC indicated that the patients who showed relatively poor drug responses had CTCs with high M-scores, while the patient who showed a relatively good response to EGFR-TKI therapy had CTCs with high E-scores. Despite the heterogeneity in multigene expression and EMT scores among CTCs isolated from the patients, CTCs from the same source were clustered together, suggesting that the interpatient heterogeneity was higher than the intra-patient one.

We also monitored how multigene expression and EMT signatures evolved during EGFR-TKI therapy. Based on the data obtained using a limited number of CTCs isolated from two patients, the EMT scores of pretreatment CTCs were better associated with the drug response than were those of CTCs obtained during EGFR-TKI therapy. Even though the EMT scores of pretreatment CTCs were distinctly different (predominantly E or M), the EMT signatures of individual CTCs became more heterogeneous and then changed to a relatively uniform E/M hybrid signature during EGFR-TKI treatment. However, the meaning of the change in multigene expression profiles should be further validated in relation to drug responses in future studies, involving large cohorts of patients.

Although we only performed gene expression analysis using the Fluidigm technology, CTCs isolated without antibody selection bias can be applied for other types of molecular analysis at a single-cell level to unveil the tumor heterogeneity during disease progression upon personalized therapy. Despite the significantly reduced turnaround time and minimized manual operation steps, the CTC counting and picking process still require manual operation, which need to be automated for broader usage in clinical settings. A potentially important application of our technology is the isolation of CTC clusters, which are emerging as important players in metastasis. Though we could frequently observe CTC clusters from patients with other types of cancer, CTC clusters were rarely observed from patients with NSCLC (**Figure 3.2b**). In recent studies on inertial microfluidics-based CTC isolation using blood samples from patients with NSCLC, Zhou et al. did not observe CTC clusters [106], while Zeinali et al. detected CTC clusters from the majority of patients [107]. We believe that this discrepancy might be due to the different cohort of patients with relatively limited number of clinical samples.

In conclusion, we demonstrated that the label-free and clinical setting-friendly FAST disc platform enabled rapid enumeration of CTCs and their unbiased molecular analysis at a single-cell level. Our approach can be readily applied in future clinical studies for early detection of actionable mutations for therapy selection and disease monitoring. Our findings from an exploratory, small-scale, prospective

cohort study of *EGFR*-mutant patients with NSCLC support the importance of single-cell-level molecular analysis, including an EMT signature, to investigate the dynamics of disease progression and predict the drug response. We anticipate that the FAST disc system can become a clinical research tool to achieve comprehensive molecular profiling and assess the heterogeneity of CTCs from patients undergoing targeted therapy and to monitor the association with clinical outcomes. Overall, high-throughput, label-free isolation of CTCs from whole blood using the FAST disc platform may facilitate minimally invasive characterization and frequent monitoring of tumor progression for timely selection of a personalized medicine.

Chapter 4. General conclusions and future perspectives

4.1 General conclusions

Here, we demonstrated that the clog-free FAST disc platform enabled ultrafast enumeration of intact CTCs and their unbiased molecular analysis at a single-cell level. First of all, a robust centrifugal microfluidic platform, FAST disc, was developed and it can be used for the CTC enrichment from whole blood samples without clogging-issue. FAST disc achieved high sensitivity (95.9 ± 3.1% recovery rate) and selectivity (>2.5 log depletion of white blood cells), with rapid (>3 mL/min) operation. The results of numerical simulation and experiments supported that FAST disc provided clog-free uniform and rapid cell enrichment with much less pressure drops (1 kPa) than in the conventional size-based filtration. The utility of the point-of-care detection of CTCs with clinical samples was validated with 142 patients suffering from breast, stomach, or lung cancer.

Furthermore, a CTC-based liquid biopsy approach was used to examine the response of therapy and demonstrated the discovery of emergent drug resistance by longitudinal monitoring in a prospective cohort of 40 EGFR-mutant NSCLC patients with CTC counts, DNA mutations, and single-cell level gene expression. The change ratio of the CTC counts, based on each CTC count at baseline according to the patients, was significantly associated with clinical outcome which defined by CT scan images while the baseline CTC counts did not have any association with progression-free survival or overall survival. The detection of EGFR mutation was achieved a 100% concordance rate between tumor tissue and CTCs including emergence of T790M. Moreover, the data of mRNA profiling revealed the importance of the analysis to the epithelial/mesenchymal signature of individual CTCs to predict the response of drug in patients. The FAST disc enabled serial monitoring based on CTC counts, DNA mutations, as well as unbiased molecular characterization of patient-driven CTCs associated with tumor progression in NSCLC during targeted therapy.

Overall, our approach can be applied to future clinical studies for disease monitoring and early detection of actionable mutations related with therapy selection. From an exploratory, small-scale, prospective cohort study of EGFR-mutant NSCLC patients, our findings support the importance of single-cell level molecular analysis, including an EMT signature, to study the dynamics of disease progression and predict the drug responsiveness. We expect that the FAST disc can become a tool for clinical research to achieve comprehensive molecular profiling and investigate the heterogeneity of CTCs according to the patients who undergo targeted therapy and to predict the clinical outcomes based on the association with CTCs. High-throughput, label-free CTC isolation from whole blood using the FAST disc platform may induce frequent monitoring of tumor progression for timely selection of a personalized medicine via minimally invasive characterization.

4.2 Plan for future

In this thesis, we focus on the NSCLC as the application field of CTC based liquid biopsy. Another applicable field would be a pancreatic cancer due to its high incidence and mortality rate. Moreover, there is no specific marker for pancreatic cancer yet so CTCs are expected as a clue to understand unrevealed characteristics of pancreatic cancer.

Pancreatic cancer is a 5th leading cause of cancer mortality in Korea and a 4th leading cause in the United States [141-143]. Pancreatic cancer showed a dismal prognosis with a 5-year survival rate of below 9 % because most patients are detected in the late phase due to its characteristics such as rapid progression and early metastasis [144, 145]. Although recent advancements of therapeutic options such as FOLFIRINOX and nab-paclitaxel, pancreatic cancer may be refractory to these chemotherapeutic agents and rapidly progress resulting in early death. Therefore, better prognostic biomarkers are needed to select good candidates for chemotherapy in patients with unresectable pancreatic cancer.

CTCs are good candidates for prognostic biomarkers because these enable frequent analysis less invasively and provides the chance to study real-time dynamics of cancer. Although the efficient technologies for CTC analysis have been remarkably developed since 2007 [146-148], the isolation and characterization of CTCs are still challenging due to their rarity and heterogeneity and away from real-world use for evaluating the relationship between CTCs and clinical outcomes [149-152].

A few papers reported the significant relationship between CTC counts and survival in pancreatic cancer [153]. However, conventional CTC detection based on epithelial markers had limitation to detect heterogeneous pancreatic CTCs. Additional marker expression in pancreatic CTCs, including mesenchymal markers or stemness markers, were studied with survival [149, 154].

Moreover, few papers reported a heterogeneous gene expression of patient-driven CTCs in pancreatic cancer [114, 155, 156]. D.T. Ting et al characterized CTCs by dividing subgroup (classical CTC, platelet marker expressed CTC and proliferative CTC) based on the results of single cell RNA sequencing [155]. M. Lapin et al studied the subpopulation of CTCs according to the expression level of mRNA related to CTC phenotype [114]. C. Amantini et al found the change of marker expression among 19 genes according to treatment [156]. These reports contributed to understanding the characteristics of individual CTCs. But, advanced analysis with diverse aspects is required to extensive understand for heterogeneous CTC in pancreatic cancer.

One of the aspects is formation of CTCs. Formation of CTCs could be single CTCs or CTC clusters in circulation. The laters are interacting with circulating cells such as platelets, neutrophils, macrophages, and fibroblasts which are related to poor prognosis in various types of cancer. B.M. Szczerba et al reported the role of neutrophils in CTC cluster related to the metastatic potential in breast cancer [157]. However, the comprehensive characterization of the CTC clusters remains unknown.

Hereafter, downstream analysis of single CTCs and CTC clusters from each patient is needed for observing distinct characteristics related to clinical outcomes. Therefore, a robust CTC isolation system with high efficacy and a high-throughput molecular analysis of CTCs become increasingly necessary.

Our robust FAST disc enables a comprehensive characterization of CTCs through mRNA profiling by multiplex PCR with 48 RNA markers which already has been used to report about single CTCs and CTC clusters analysis [132, 158, 159].

We will investigate a strategy for the isolation of single CTCs and CTC clusters by FAST disc and the phenotypic characterization of CTC clusters based on mRNA profiling and demonstrate the correlation between mRNA expression of CTC clusters and clinical outcomes in patients with unresectable pancreatic cancer.

4.3 Future perspective

Active collaborations between clinics and academic research are necessary for clinical validation of new technologies for liquid biopsy. In this thesis, we suggest a robust device for CTC isolation which can be expected to expand the ability to utilize CTC based liquid biopsy in clinical routine and longitudinal surveillance of cancer therapy. If it is applied to run multicenter-large scale clinical trials, FAST disc can serve to clarify the clinical utility of CTCs in clinical routine.

For improving precision medicine, common implementation of single-cell analysis about CTC heterogeneity in clinical routine will be feasible with accompanying development of the technologies which can solve the problem of existing methods for molecular analysis, such as high cost and time-consuming process. Actualization of single-cell analysis will contribute to make affordable precision medicine for many patients.

On the other side, study about the relationship with other liquid biopsy markers, such as ctDNA and extracellular vesicle, allow better understanding of cancer progression and metastasis mechanism. For clinical applications, complementary use of multi-markers may be beneficial to improve the predictive accuracy in diagnostic and prognostic and to enhance the sensitivity and specificity of liquid biopsy.

References

1. Siegel, R. L.; Miller, K. D.; Jemal, A., Cancer statistics, 2017. *CA: A Cancer Journal for Clinicians* **2017,** *67* (1), 7-30.

2. Torre, L. A.; Bray, F.; Siegel, R. L.; Ferlay, J.; Lortet-Tieulent, J.; Jemal, A., Global cancer statistics, 2012. *CA: A Cancer Journal for Clinicians* **2015,** *65* (2), 87-108.

3. Mitsudomi, T.; Morita, S.; Yatabe, Y.; Negoro, S.; Okamoto, I.; Tsurutani, J.; Seto, T.; Satouchi, M.; Tada, H.; Hirashima, T., Gefitinib versus cisplatin plus docetaxel in patients with non-small-cell lung cancer harbouring mutations of the epidermal growth factor receptor (WJTOG3405): an open label, randomised phase 3 trial. *The lancet oncology* **2010,** *11* (2), 121-128.

4. Paez, J. G.; Jänne, P. A.; Lee, J. C.; Tracy, S.; Greulich, H.; Gabriel, S.; Herman, P.; Kaye, F. J.; Lindeman, N.; Boggon, T. J., EGFR mutations in lung cancer: correlation with clinical response to gefitinib therapy. *Science* **2004,** *304* (5676), 1497-1500.

5. Pao, W.; Chmielecki, J., Rational, biologically based treatment of EGFR-mutant non-small-cell lung cancer. *Nature Reviews Cancer* **2010,** *10* (11), 760-774.

6. Sequist, L. V.; Martins, R. G.; Spigel, D.; Grunberg, S. M.; Spira, A.; Ja¨nne, P. A.; Joshi, V. A.; McCollum, D.; Evans, T. L.; Muzikansky, A., First-line gefitinib in patients with advanced non–small-cell lung cancer harboring somatic EGFR mutations. *Journal of clinical oncology* **2008,** *26* (15), 2442-2449.

7. Yi, H. G.; Kim, H. J.; Kim, Y. J.; Han, S.-W.; Oh, D.-Y.; Lee, S.-H.; Kim, D.-W.; Im, S.-A.; Kim, T.-Y.; Kim, C. S., Epidermal growth factor receptor (EGFR) tyrosine kinase inhibitors (TKIs) are effective for leptomeningeal metastasis from non-small cell lung cancer patients with sensitive EGFR mutation or other predictive factors of good response for EGFR TKI. *Lung cancer* **2009,** *65* (1), 80-84.

8. Goss, G.; Tsai, C.-M.; Shepherd, F. A.; Bazhenova, L.; Lee, J. S.; Chang, G.-C.; Crino, L.; Satouchi, M.; Chu, Q.; Hida, T., Osimertinib for pretreated EGFR Thr790Met-positive advanced non-small-cell lung cancer (AURA2): a multicentre, open-label, single-arm, phase 2 study. *The Lancet Oncology* **2016,** *17* (12), 1643-1652.

9. Nagrath, S.; Sequist, L. V.; Maheswaran, S.; Bell, D. W.; Irimia, D.; Ulkus, L.; Smith, M. R.; Kwak, E. L.; Digumarthy, S.; Muzikansky, A., Isolation of rare circulating tumour cells in cancer patients by microchip technology. *Nature* **2007,** *450* (7173), 1235-1239.

10. Armstrong, A. J.; Marengo, M. S.; Oltean, S.; Kemeny, G.; Bitting, R.; Turnbull, J.; Herold, C. I.; Marcom, P. K.; George, D.; Garcia-Blanco, M., Circulating tumor cells from patients with advanced prostate and breast cancer display both epithelial and mesenchymal markers. *Molecular cancer research* **2011**, molcanres. 0490.2010.

11. Coumans, F. A.; van Dalum, G.; Beck, M.; Terstappen, L. W., Filter characteristics influencing circulating tumor cell enrichment from whole blood. *PloS one* **2013,** *8* (4), e61770.

12. Adams, D. L.; Alpaugh, R. K.; Tsai, S.; Tang, C.-M.; Stefansson, S., Multi-Phenotypic subtyping of circulating tumor cells using sequential fluorescent quenching and restaining. *Scientific reports* **2016,** *6*, 33488.

13. Swennenhuis, J. F.; Tibbe, A. G.; Levink, R.; Sipkema, R. C.; Terstappen, L. W., Characterization of circulating tumor cells by fluorescence in situ hybridization. *Cytometry Part A* **2009,** *75* (6), 520-527.

14. Renier, C.; Pao, E.; Che, J.; Liu, H. E.; Lemaire, C. A.; Matsumoto, M.; Triboulet, M.; Srivinas, S.; Jeffrey, S. S.; Rettig, M., Label-free isolation of prostate circulating tumor cells using Vortex microfluidic technology. *npj Precision Oncology* **2017,** *1* (1), 15.

15. Hodgkinson, C. L.; Morrow, C. J.; Li, Y.; Metcalf, R. L.; Rothwell, D. G.; Trapani, F.; Polanski, R.; Burt, D. J.; Simpson, K. L.; Morris, K., Tumorigenicity and genetic profiling of circulating tumor cells in small-cell lung cancer. *Nature medicine* **2014,** *20* (8), 897-903.

16. Torphy, R. J.; Tignanelli, C. J.; Kamande, J. W.; Moffitt, R. A.; Loeza, S. G. H.; Soper, S. A.; Yeh, J. J., Circulating tumor cells as a biomarker of response to treatment in patient-derived xenograft mouse models of pancreatic adenocarcinoma. *PloS one* **2014,** *9* (2), e89474.

17. Yu, M.; Bardia, A.; Aceto, N.; Bersani, F.; Madden, M. W.; Donaldson, M. C.; Desai, R.; Zhu, H.; Comaills, V.; Zheng, Z., Ex vivo culture of circulating breast tumor cells for individualized testing of drug susceptibility. *Science* **2014,** *345* (6193), 216-220.

18. Schwarzenbach, H.; Hoon, D. S. B.; Pantel, K., Cell-free nucleic acids as biomarkers in cancer patients. *Nat Rev Cancer* **2011,** *11* (6), 426-437.

19. Jahr, S.; Hentze, H.; Englisch, S.; Hardt, D.; Fackelmayer, F. O.; Hesch, R.-D.; Knippers, R., DNA Fragments in the Blood Plasma of Cancer Patients: Quantitations and Evidence for Their Origin from Apoptotic and Necrotic Cells. *Cancer Research* **2001,** *61* (4), 1659.

20. Jiang, P.; Chan, C. W. M.; Chan, K. C. A.; Cheng, S. H.; Wong, J.; Wong, V. W.-S.; Wong, G. L. H.; Chan, S. L.; Mok, T. S. K.; Chan, H. L. Y.; Lai, P. B. S.; Chiu, R. W. K.; Lo, Y. M. D., Lengthening and shortening of plasma DNA in hepatocellular carcinoma patients. *Proceedings of the National Academy of Sciences* **2015,** *112* (11), E1317.

21. Wan, J. C. M.; Massie, C.; Garcia-Corbacho, J.; Mouliere, F.; Brenton, J. D.; Caldas, C.; Pacey, S.; Baird, R.; Rosenfeld, N., Liquid biopsies come of age: towards implementation of circulating tumour DNA. *Nat Rev Cancer* **2017,** *17* (4), 223-238.

22. Chi, K. R., The tumour trail left in blood. *Nature* **2016,** *532* (7598), 269-271.

23. Siravegna, G.; Marsoni, S.; Siena, S.; Bardelli, A., Integrating liquid biopsies into the management of cancer. *Natute Reviews Clinical Oncology* **2017,** *14* (9), 531-548.

24. Alix-Panabières, C.; Pantel, K., Clinical Applications of Circulating Tumor Cells and Circulating Tumor DNA as Liquid Biopsy. *Cancer Discovery* **2016,** *6* (5), 479.

25. Krebs, M. G.; Sloane, R.; Priest, L.; Lancashire, L.; Hou, J.-M.; Greystoke, A.; Ward, T. H.; Ferraldeschi, R.; Hughes, A.; Clack, G., Evaluation and prognostic significance of circulating tumor cells in patients with non–small-cell lung cancer. *Journal of clinical oncology* **2011,** *29* (12), 1556-1563.

26. Punnoose, E. A.; Atwal, S.; Liu, W.; Raja, R.; Fine, B. M.; Hughes, B. G.; Hicks, R. J.; Hampton, G. M.; Amler, L. C.; Pirzkall, A., Evaluation of circulating tumor cells and circulating tumor DNA in non–small cell lung cancer: Association with clinical endpoints in a phase II clinical trial of pertuzumab and erlotinib. *Clinical Cancer Research* **2012,** *18* (8), 2391-2401.

27. Zhou, J.; Dong, F.; Cui, F.; Xu, R.; Tang, X., The role of circulating tumor cells in evaluation of prognosis and treatment response in advanced non-small-cell lung cancer. *Cancer chemotherapy and pharmacology* **2017,** *79* (4), 825-833.

28. Muinelo-Romay, L.; Vieito, M.; Abalo, A.; Nocelo, M. A.; Barón, F.; Anido, U.; Brozos, E.; Vázquez, F.; Aguín, S.; Abal, M., Evaluation of circulating tumor cells and related events as prognostic factors and surrogate biomarkers in advanced NSCLC patients receiving first-line systemic treatment. *Cancers* **2014,** *6* (1), 153-165.

29. Lindsay, C.; Faugeroux, V.; Michiels, S.; Pailler, E.; Facchinetti, F.; Ou, D.; Bluthgen, M.; Pannet, C.; Ngo-Camus, M.; Bescher, G., A prospective examination of circulating tumor cell profiles in non-small-cell lung cancer molecular subgroups. *Annals of Oncology* **2017,** *28* (7), 1523-1531.

30. Crosbie, P. A.; Shah, R.; Krysiak, P.; Zhou, C.; Morris, K.; Tugwood, J.; Booton, R.; Blackhall, F.; Dive, C., Circulating tumor cells detected in the tumor-draining pulmonary vein are associated with disease recurrence after surgical resection of NSCLC. *Journal of Thoracic Oncology* **2016,** *11* (10), 1793-1797.

31. Hofman, V.; Bonnetaud, C.; Ilie, M. I.; Vielh, P.; Vignaud, J. M.; Flejou, J.-F.; Lantuejoul, S.; Piaton, E.; Mourad, N.; Butori, C., Preoperative circulating tumor cell detection using the isolation by size of epithelial tumor cell method for patients with lung cancer is a new prognostic biomarker. *Clinical cancer research* **2010**, clincanres. 0445.2010.

32. Hofman, V.; Ilie, M. I.; Long, E.; Selva, E.; Bonnetaud, C.; Molina, T.; Vénissac, N.; Mouroux, J.; Vielh, P.; Hofman, P., Detection of circulating tumor cells as a prognostic factor in patients undergoing radical surgery for non-small-cell lung carcinoma: comparison of the efficacy of the CellSearch Assay™ and the isolation by size of epithelial tumor cell method. *International journal of cancer* **2011,** *129* (7), 1651-1660.

33. Stott, S. L.; Hsu, C.-H.; Tsukrov, D. I.; Yu, M.; Miyamoto, D. T.; Waltman, B. A.; Rothenberg, S. M.; Shah, A. M.; Smas, M. E.; Korir, G. K., Isolation of circulating tumor cells using a microvortex-generating herringbone-chip. *Proceedings of the National Academy of Sciences* **2010,** *107* (43), 18392-18397.

34. Sundaresan, T. K.; Sequist, L. V.; Heymach, J. V.; Riely, G. J.; Jänne, P. A.; Koch, W. H.; Sullivan, J. P.; Fox, D. B.; Maher, R.; Muzikansky, A., Detection of T790M, the acquired resistance EGFR mutation, by tumor biopsy versus noninvasive blood-based analyses. *Clinical Cancer Research* **2016,** *22* (5), 1103-1110.

35. Wang, S.; Liu, K.; Liu, J.; Yu, Z. T. F.; Xu, X.; Zhao, L.; Lee, T.; Lee, E. K.; Reiss, J.; Lee, Y. K., Highly efficient capture of circulating tumor cells by using nanostructured silicon

substrates with integrated chaotic micromixers. *Angewandte Chemie International Edition* **2011,** *50* (13), 3084-3088.

36. Ke, Z.; Lin, M.; Chen, J.-F.; Choi, J.-s.; Zhang, Y.; Fong, A.; Liang, A.-J.; Chen, S.-F.; Li, Q.; Fang, W., Programming thermoresponsiveness of NanoVelcro substrates enables effective purification of circulating tumor cells in lung cancer patients. *ACS nano* **2014,** *9* (1), 62-70.

37. Yeo, T.; Tan, S. J.; Lim, C. L.; Lau, D. P. X.; Chua, Y. W.; Krisna, S. S.; Iyer, G.; San Tan, G.; Lim, T. K. H.; Tan, D. S., Microfluidic enrichment for the single cell analysis of circulating tumor cells. *Scientific reports* **2016,** *6*, 22076.

38. Earhart, C. M.; Hughes, C. E.; Gaster, R. S.; Ooi, C. C.; Wilson, R. J.; Zhou, L. Y.; Humke, E. W.; Xu, L.; Wong, D. J.; Willingham, S. B., Isolation and mutational analysis of circulating tumor cells from lung cancer patients with magnetic sifters and biochips. *Lab on a Chip* **2014,** *14* (1), 78-88.

39. Park, S.-m.; Wong, D. J.; Ooi, C. C.; Kurtz, D. M.; Vermesh, O.; Aalipour, A.; Suh, S.; Pian, K. L.; Chabon, J. J.; Lee, S. H., Molecular profiling of single circulating tumor cells from lung cancer patients. *Proceedings of the National Academy of Sciences* **2016**, 201608461.

40. Murlidhar, V.; Zeinali, M.; Grabauskiene, S.; Ghannad-Rezaie, M.; Wicha, M. S.; Simeone, D. M.; Ramnath, N.; Reddy, R. M.; Nagrath, S., A Radial Flow Microfluidic Device for Ultra-High-Throughput Affinity-Based Isolation of Circulating Tumor Cells. *Small* **2014,** *10* (23), 4895-4904.

41. Murlidhar, V.; Reddy, R. M.; Fouladdel, S.; Zhao, L.; Ishikawa, M. K.; Grabauskiene, S.; Zhang, Z.; Lin, J.; Chang, A. C.; Carrott, P., Poor Prognosis Indicated by Venous Circulating Tumor Cell Clusters in Early-Stage Lung Cancers. *Cancer research* **2017,** *77* (18), 5194-5206.

42. Torga, G.; Pienta, K. J., Patient-Paired Sample Congruence Between 2 Commercial Liquid Biopsy Tests. *JAMA oncology* **2017**.

43. Ríos, Á.; Zougagh, M.; Avila, M., Miniaturization through lab-on-a-chip: Utopia or reality for routine laboratories? A review. *Analytica chimica acta* **2012,** *740*, 1-11.

44. Temiz, Y.; Lovchik, R. D.; Kaigala, G. V.; Delamarche, E., Lab-on-a-chip devices: How to close and plug the lab? *Microelectronic Engineering* **2015,** *132*, 156-175.

45. Gorjikhah, F.; Davaran, S.; Salehi, R.; Bakhtiari, M.; Hasanzadeh, A.; Panahi, Y.; Emamverdy, M.; Akbarzadeh, A., Improving "lab-on-a-chip" techniques using biomedical nanotechnology: a review. *Artificial cells, nanomedicine, biotechnology* **2016,** *44* (7), 1609-1614.

46. Lee, C.-C.; Sui, G.; Elizarov, A.; Shu, C. J.; Shin, Y.-S.; Dooley, A. N.; Huang, J.; Daridon, A.; Wyatt, P.; Stout, D., Multistep synthesis of a radiolabeled imaging probe using integrated microfluidics. *Science* **2005,** *310* (5755), 1793-1796.

47. Stachowiak, J. C.; Shugard, E. E.; Mosier, B. P.; Renzi, R. F.; Caton, P. F.; Ferko, S. M.; Van de Vreugde, J. L.; Yee, D. D.; Haroldsen, B. L.; VanderNoot, V. A., Autonomous microfluidic sample preparation system for protein profile-based detection of aerosolized bacterial cells and spores. *Analytical chemistry* **2007,** *79* (15), 5763-5770.

48. Hwang, H.; Kim, Y.; Cho, J.; Lee, J.-y.; Choi, M.-S.; Cho, Y.-K., Lab-on-a-disc for simultaneous determination of nutrients in water. *Analytical chemistry* **2013,** *85* (5), 2954-2960.

49. Strohmeier, O.; Keller, M.; Schwemmer, F.; Zehnle, S.; Mark, D.; von Stetten, F.; Zengerle, R.; Paust, N., Centrifugal microfluidic platforms: advanced unit operations and applications. *Chemical Society Reviews* **2015,** *44* (17), 6187-6229.

50. Nagy, E., *Basic equations of mass transport through a membrane layer*. 2nd edition ed.; Elsevier: 2019.

51. Ferreira, M. M.; Ramani, V. C.; Jeffrey, S. S., Circulating tumor cell technologies. *Molecular oncology* **2016,** *10* (3), 374-394.

52. Cristofanilli, M.; Budd, G. T.; Ellis, M. J.; Stopeck, A.; Matera, J.; Miller, M. C.; Reuben, J. M.; Doyle, G. V.; Allard, W. J.; Terstappen, L. W., Circulating tumor cells, disease progression, and survival in metastatic breast cancer. *N. Engl. J. Med.* **2004,** *351* (8), 781-791.

53. de Bono, J. S.; Scher, H. I.; Montgomery, R. B.; Parker, C.; Miller, M. C.; Tissing, H.; Doyle, G. V.; Terstappen, L. W. W. M.; Pienta, K. J.; Raghavan, D., Circulating Tumor Cells Predict Survival Benefit from Treatment in Metastatic Castration-Resistant Prostate Cancer. *Clin. Cancer Res.* **2008,** *14* (19), 6302-6309.

54. Alix-Panabières, C.; Pantel, K., Challenges in circulating tumour cell research. *Nat. Rev. Cancer* **2014,** *14* (9), 623-631.

55. Kling, J., Beyond counting tumor cells. *Nat. Biotechnol.* **2012,** *30* (7), 578-580.

56. Green, B. J.; Saberi Safaei, T.; Mepham, A.; Labib, M.; Mohamadi, R. M.; Kelley, S. O., Beyond the Capture of Circulating Tumor Cells: Next-Generation Devices and Materials. *Angew. Chem. Int. Ed.* **2016,** *55* (4), 1252-1265.

57. Hosokawa, M.; Yoshikawa, T.; Negishi, R.; Yoshino, T.; Koh, Y.; Kenmotsu, H.; Naito, T.; Takahashi, T.; Yamamoto, N.; Kikuhara, Y., Microcavity array system for size-based enrichment of circulating tumor cells from the blood of patients with small-cell lung cancer. *Anal. Chem.* **2013,** *85* (12), 5692-5698.

58. Hosokawa, M.; Kenmotsu, H.; Koh, Y.; Yoshino, T.; Yoshikawa, T.; Naito, T.; Takahashi, T.; Murakami, H.; Nakamura, Y.; Tsuya, A., Size-based isolation of circulating tumor cells in lung cancer patients using a microcavity array system. *PLoS One* **2013,** *8* (6), e67466.

59. Negishi, R.; Hosokawa, M.; Nakamura, S.; Kanbara, H.; Kanetomo, M.; Kikuhara, Y.; Tanaka, T.; Matsunaga, T.; Yoshino, T., Development of the automated circulating tumor cell recovery system with microcavity array. *Biosens. Bioelectron.* **2015,** *67*, 438-442.

60. Adams, D. L.; Zhu, P.; Makarova, O. V.; Martin, S. S.; Charpentier, M.; Chumsri, S.; Li, S.; Amstutz, P.; Tang, C.-M., The systematic study of circulating tumor cell isolation using lithographic microfilters. *RSC Adv.* **2014,** *4* (9), 4334-4342.

61. Adams, D. L.; Martin, S. S.; Alpaugh, R. K.; Charpentier, M.; Tsai, S.; Bergan, R. C.; Ogden, I. M.; Catalona, W.; Chumsri, S.; Tang, C. M.; Cristofanilli, M., Circulating giant macrophages as a potential biomarker of solid tumors. *Proc Natl Acad Sci U S A* **2014,** *111* (9), 3514-9.

62. Lim, L. S.; Hu, M.; Huang, M. C.; Cheong, W. C.; Gan, A. T. L.; Looi, X. L.; Leong, S. M.; Koay, E. S.-C.; Li, M.-H., Microsieve lab-chip device for rapid enumeration and fluorescence in situ hybridization of circulating tumor cells. *Lab Chip* **2012,** *12* (21), 4388-4396.

63. Zhou, M.-D.; Hao, S.; Williams, A. J.; Harouaka, R. A.; Schrand, B.; Rawal, S.; Ao, Z.; Brennaman, R.; Gilboa, E.; Lu, B., Separable bilayer microfiltration device for viable label-free enrichment of circulating tumour cells. *Sci. Rep.* **2014,** *4*, 7392.

64. Sarioglu, A. F.; Aceto, N.; Kojic, N.; Donaldson, M. C.; Zeinali, M.; Hamza, B.; Engstrom, A.; Zhu, H.; Sundaresan, T. K.; Miyamoto, D. T., A microfluidic device for label-free, physical capture of circulating tumor cell clusters. *Nat. Methods* **2015,** *12*, 685 - 691.

65. Coumans, F.; van Dalum, G.; Beck, M.; Terstappen, L., Filter characteristics influencing circulating tumor cell enrichment from whole blood. *PLoS One* **2013,** *8* (4), e61770.

66. Lee, A.; Park, J.; Lim, M.; Sunkara, V.; Kim, S. Y.; Kim, G. H.; Kim, M.-H.; Cho, Y.-K., All-in-one centrifugal microfluidic device for size-selective circulating tumor cell isolation with high purity. *Anal. Chem.* **2014,** *86* (22), 11349-11356.

67. Coumans, F. A.; van Dalum, G.; Beck, M.; Terstappen, L. W., Filtration parameters influencing circulating tumor cell enrichment from whole blood. *PLoS One* **2013,** *8* (4), e61774.

68. Seal, S., Silicone flotation: A simple quantitative method for the isolation of free-floating cancer cells from the blood. *Cancer* **1959,** *12* (3), 590-595.

69. Weitz, J.; Kienle, P.; Lacroix, J.; Willeke, F.; Benner, A.; Lehnert, T.; Herfarth, C.; von Knebel Doeberitz, M., Dissemination of tumor cells in patients undergoing surgery for colorectal cancer. *Clin. Cancer Res.* **1998,** *4* (2), 343-348.

70. Park, E. S.; Jin, C.; Guo, Q.; Ang, R. R.; Duffy, S. P.; Matthews, K.; Azad, A.; Abdi, H.; Todenhöfer, T.; Bazov, J., Continuous Flow Deformability-Based Separation of Circulating Tumor Cells Using Microfluidic Ratchets. *Small* **2016,** *12* (14), 1909-1919.

71. Shim, S.; Stemke-Hale, K.; Tsimberidou, A. M.; Noshari, J.; Anderson, T. E.; Gascoyne, P. R., Antibody-independent isolation of circulating tumor cells by continuous-flow dielectrophoresis. *Biomicrofluidics* **2013,** *7* (1), 011807.

72. Moon, H.-S.; Kwon, K.; Kim, S.-I.; Han, H.; Sohn, J.; Lee, S.; Jung, H.-I., Continuous separation of breast cancer cells from blood samples using multi-orifice flow fractionation (MOFF) and dielectrophoresis (DEP). *Lab Chip* **2011,** *11* (6), 1118-1125.

73. Huang, S.-B.; Wu, M.-H.; Lin, Y.-H.; Hsieh, C.-H.; Yang, C.-L.; Lin, H.-C.; Tseng, C.-P.; Lee, G.-B., High-purity and label-free isolation of circulating tumor cells (CTCs) in a microfluidic platform by using optically-induced-dielectrophoretic (ODEP) force. *Lab Chip* **2013,** *13* (7), 1371-1383.

74. Chen, J.; Li, J.; Sun, Y., Microfluidic approaches for cancer cell detection, characterization, and separation. *Lab Chip* **2012,** *12* (10), 1753-1767.

75. Qian, W.; Zhang, Y.; Chen, W., Capturing Cancer: Emerging Microfluidic Technologies for the Capture and Characterization of Circulating Tumor Cells. *Small* **2015,** *11* (32), 3850-3872.

76. Hyun, K.-A.; Jung, H.-I., Advances and critical concerns with the microfluidic enrichments of circulating tumor cells. *Lab Chip* **2014,** *14* (1), 45-56.

77. Hyun, K.-A.; Kim, J.; Gwak, H.; Jung, H.-i., Isolation and enrichment of circulating biomarkers for cancer screening, detection, and diagnostics. *Analyst* **2016,** *141* (2), 382-392.

78. Adams, D.; Zhu, P.; Makarova, O.; Li, S.; Amstutz, P.; Tang, C.-M., HER-2 FISH analysis and H & E staining of circulating tumor cells pre-isolated using high porosity precision microfilters. *Cancer Res.* **2012,** *72* (8), 2395-2395.

79. Desitter, I.; Guerrouahen, B. S.; Benali-Furet, N.; Wechsler, J.; Jaenne, P. A.; Kuang, Y.; Yanagita, M.; Wang, L.; Berkowitz, J. A.; Distel, R. J., A new device for rapid isolation by size and characterization of rare circulating tumor cells. *Anticancer Res.* **2011,** *31* (2), 427-441.

80. Hou, X.; Hu, Y.; Grinthal, A.; Khan, M.; Aizenberg, J., Liquid-based gating mechanism with tunable multiphase selectivity and antifouling behaviour. *Nature* **2015,** *519* (7541), 70-73.

81. Strohmeier, O.; Keller, M.; Schwemmer, F.; Zehnle, S.; Mark, D.; von Stetten, F.; Zengerle, R.; Paust, N., Centrifugal microfluidic platforms: advanced unit operations and applications. *Chem. Soc. Rev.* **2015,** *44* (17), 6187-6229.

82. Ozkumur, E.; Shah, A. M.; Ciciliano, J. C.; Emmink, B. L.; Miyamoto, D. T.; Brachtel, E.; Yu, M.; Chen, P.-i.; Morgan, B.; Trautwein, J., Inertial focusing for tumor antigen–dependent and–independent sorting of rare circulating tumor cells. *Sci. Transl. Med.* **2013,** *5*, 179ra47.

83. Aggarwal, C.; Meropol, N.; Punt, C.; Iannotti, N.; Saidman, B.; Sabbath, K.; Gabrail, N.; Picus, J.; Morse, M.; Mitchell, E., Relationship among circulating tumor cells, CEA and overall survival in patients with metastatic colorectal cancer. *Ann. Oncol.* **2013,** *24* (2), 420-428.

84. Janni, W. J.; Rack, B.; Terstappen, L. W.; Pierga, J.-Y.; Taran, F.-A.; Fehm, T.; Hall, C.; de Groot, M. R.; Bidard, F.-C.; Friedl, T. W., Pooled analysis of the prognostic relevance of circulating tumor cells in primary breast cancer. *Clin. Cancer Res.* **2016,** *22* (10), 2583-2593.

85. Rack, B.; Schindlbeck, C.; Jückstock, J.; Andergassen, U.; Hepp, P.; Zwingers, T.; Friedl, T. W.; Lorenz, R.; Tesch, H.; Fasching, P. A., Circulating tumor cells predict survival in early average-to-high risk breast cancer patients. *J. Natl. Cancer Inst.* **2014,** *106* (5), dju066.

86. Siegel, R. L.; Miller, K. D.; Jemal, A., Cancer statistics, 2019. *CA Cancer J Clin* **2019,** *69*, 7-34.

87. Wong, M. C. S.; Lao, X. Q.; Ho, K. F.; Goggins, W. B.; Tse, S. L. A., Incidence and mortality of lung cancer: global trends and association with socioeconomic status. *Sci Rep* **2017,** *7* (1), 14300.

88. Kapeleris, J.; Kulasinghe, A.; Warkiani, M. E.; Vela, I.; Kenny, L.; O'Byrne, K.; Punyadeera, C., The prognostic role of circulating tumor cells (CTCs) in lung cancer. *Front Oncol* **2018,** *8*, 311.

89. Pao, W.; Chmielecki, J., Rational, biologically based treatment of EGFR-mutant non-small-cell lung cancer. *Nat Rev Cancer* **2010,** *10* (11), 760-774.

90. Greig, S. L., Osimertinib: first global approval. *Drugs* **2016,** *76* (2), 263-273.

91. Goss, G.; Tsai, C.-M.; Shepherd, F. A.; Bazhenova, L.; Lee, J. S.; Chang, G.-C.; Crino, L.; Satouchi, M.; Chu, Q.; Hida, T.; Han, J.-Y.; Juan, O.; Dunphy, F.; Nishio, M.; Kang, J.-H.;

Majem, M.; Mann, H.; Cantarini, M.; Ghiorghiu, S.; Mitsudomi, T., Osimertinib for pretreated EGFR Thr790Met-positive advanced non-small-cell lung cancer (AURA2): a multicentre, open-label, single-arm, phase 2 study. *Lancet Oncol* **2016,** *17* (12), 1643-1652.

92. Cohen, S. J.; Punt, C.; Iannotti, N.; Saidman, B. H.; Sabbath, K. D.; Gabrail, N. Y.; Picus, J.; Morse, M.; Mitchell, E.; Miller, M. C., Relationship of circulating tumor cells to tumor response, progression-free survival, and overall survival in patients with metastatic colorectal cancer. *J Clin Oncol* **2008,** *26*, 3213-3221.

93. Hayes, D. F.; Cristofanilli, M.; Budd, G. T.; Ellis, M. J.; Stopeck, A.; Miller, M. C.; Matera, J.; Allard, W. J.; Doyle, G. V.; Terstappen, L. W. J. C. C. R., Circulating tumor cells at each follow-up time point during therapy of metastatic breast cancer patients predict progression-free and overall survival. *Clin Cancer Res* **2006,** *12* (14), 4218-4224.

94. De Bono, J. S.; Scher, H. I.; Montgomery, R. B.; Parker, C.; Miller, M. C.; Tissing, H.; Doyle, G. V.; Terstappen, L. W.; Pienta, K. J.; Raghavan, D., Circulating tumor cells predict survival benefit from treatment in metastatic castration-resistant prostate cancer. *Clin Cancer Res* **2008,** *14* (19), 6302-6309.

95. Hofman, V.; Bonnetaud, C.; Ilie, M. I.; Vielh, P.; Vignaud, J. M.; Flejou, J.-F.; Lantuejoul, S.; Piaton, E.; Mourad, N.; Butori, C., Preoperative circulating tumor cell detection using the isolation by size of epithelial tumor cell method for patients with lung cancer is a new prognostic biomarker. *Clin Cancer Res* **2010,** *17* (4), 827-35.

96. Crosbie, P. A.; Shah, R.; Krysiak, P.; Zhou, C.; Morris, K.; Tugwood, J.; Booton, R.; Blackhall, F.; Dive, C., Circulating tumor cells detected in the tumor-draining pulmonary vein are associated with disease recurrence after surgical resection of NSCLC. *J Thorac Oncol* **2016,** *11* (10), 1793-1797.

97. He, W.; Li, W.; Jiang, B.; Chang, L.; Jin, C.; Tu, C.; Li, Y., Correlation between epidermal growth factor receptor tyrosine kinase inhibitor efficacy and circulating tumor cell levels in patients with advanced non-small cell lung cancer. *Onco Targets Ther* **2016,** *9*, 7515-7520.

98. Zhang, Z.; Xiao, Y.; Zhao, J.; Chen, M.; Xu, Y.; Zhong, W.; Xing, J.; Wang, M., Relationship between circulating tumour cell count and prognosis following chemotherapy in patients with advanced non-small-cell lung cancer. *Respirology* **2016,** *21* (3), 519-525.

99. Tong, B.; Xu, Y.; Zhao, J.; Chen, M.; Xing, J.; Zhong, W.; Wang, M., Prognostic significance of circulating tumor cells in non-small cell lung cancer patients undergoing chemotherapy. *Oncotarget* **2017,** *8* (49), 86615-86624.

100. Juan, O.; Vidal, J.; Gisbert, R.; Munoz, J.; Macia, S.; Gomez-Codina, J., Prognostic significance of circulating tumor cells in advanced non-small cell lung cancer patients treated with docetaxel and gemcitabine. *Clin Transl Oncol* **2014,** *16* (7), 637-643.

101. Chudasama, D.; Barr, J.; Beeson, J.; Beddow, E.; Mcgonigle, N.; Rice, A.; Nicholson, A.; Anikin, V., Detection of circulating tumour cells and survival of patients with non-small cell lung cancer. *Anticancer Res* **2017,** *37* (1), 169-173.

102. Ozkumur, E.; Shah, A. M.; Ciciliano, J. C.; Emmink, B. L.; Miyamoto, D. T.; Brachtel, E.; Yu, M.; Chen, P.-i.; Morgan, B.; Trautwein, J., Inertial focusing for tumor antigen–dependent and–independent sorting of rare circulating tumor cells. *Sci Transl Med* **2013,** *5* (179), 179ra47.

103. Varillas, J. I.; Zhang, J.; Chen, K.; Barnes, I. I.; Liu, C.; George, T. J.; Fan, Z. H., Microfluidic isolation of circulating tumor cells and cancer stem-like cells from patients with pancreatic ductal adenocarcinoma. *Theranostics* **2019,** *9* (5), 1417-1425.

104. Hvichia, G.; Parveen, Z.; Wagner, C.; Janning, M.; Quidde, J.; Stein, A.; Müller, V.; Loges, S.; Neves, R.; Stoecklein, N., A novel microfluidic platform for size and deformability based separation and the subsequent molecular characterization of viable circulating tumor cells. *Int J Cancer* **2016,** *138* (12), 2894-2904.

105. Yagi, S.; Koh, Y.; Akamatsu, H.; Kanai, K.; Hayata, A.; Tokudome, N.; Akamatsu, K.; Endo, K.; Nakamura, S.; Higuchi, M., Development of an automated size-based filtration system for isolation of circulating tumor cells in lung cancer patients. *PLoS One* **2017,** *12* (6), e0179744.

106. Zhou, J.; Kulasinghe, A.; Bogseth, A.; O'Byrne, K.; Punyadeera, C.; Papautsky, I., Isolation of circulating tumor cells in non-small-cell-lung-cancer patients using a multi-flow microfluidic channel. *Microsyst Nanoeng* **2019,** *5*, 8.

107. Zeinali, M.; Lee, M.; Nadhan, A.; Mathur, A.; Hedman, C.; Lin, E.; Harouaka, R.; Wicha, M. S.; Zhao, L.; Palanisamy, N.; Hafner, M.; Reddy, R.; Kalemkerian, G. P.; Schneider, B. J.; Hassan, K. A.; Ramnath, N.; Nagrath, S., High-throughput label-free isolation of heterogeneous circulating tumor cells and CTC clusters from non-small-cell lung cancer patients. *Cancers* **2020,** *12* (1), 127.

108. Kim, T.-H.; Lim, M.; Park, J.; Oh, J. M.; Kim, H.; Jeong, H.; Lee, S. J.; Park, H. C.; Jung, S.; Kim, B. C., FAST: size-selective, clog-free isolation of rare cancer cells from whole blood at a liquid–liquid interface. *Anal Chem* **2017,** *89* (2), 1155-1162.

109. Kang, Y. T.; Kim, Y. J.; Lee, T. H.; Cho, Y. H.; Chang, H. J.; Lee, H. M., Cytopathological study of the circulating tumor cells filtered from the cancer patients' blood using hydrogel-based cell block formation. *Sci Rep* **2018,** *8* (1), 15218.

110. Kim, M.; Suh, D. H.; Choi, J. Y.; Bu, J.; Kang, Y. T.; Kim, K.; No, J. H.; Kim, Y. B.; Cho, Y. H., Post-debulking circulating tumor cell as a poor prognostic marker in advanced stage ovarian cancer: a prospective observational study. *Medicine* **2019,** *98* (20), e15354.

111. Lu, Y.; Liang, H.; Yu, T.; Xie, J.; Chen, S.; Dong, H.; Sinko, P. J.; Lian, S.; Xu, J.; Wang, J., Isolation and characterization of living circulating tumor cells in patients by immunomagnetic negative enrichment coupled with flow cytometry. *Cancer* **2015,** *121* (17), 3036-3045.

112. Lowe, A. C.; Pignon, J. C.; Carvo, I.; Drage, M. G.; Constantine, N. M.; Jones, N.; Kroll, Y.; Frank, D. A.; Signoretti, S.; Cibas, E. S., Young investigator challenge: application of cytologic techniques to circulating tumor cell specimens: detecting activation of the oncogenic transcription factor STAT3. *Cancer Cytopathol* **2015,** *123* (12), 696-706.

113. Krebs, M. G.; Sloane, R.; Priest, L.; Lancashire, L.; Hou, J.-M.; Greystoke, A.; Ward, T. H.; Ferraldeschi, R.; Hughes, A.; Clack, G., Evaluation and prognostic significance of circulating tumor cells in patients with non–small-cell lung cancer. *J Clin Oncol* **2011,** *29* (12), 1556-1563.

114. Lapin, M.; Tjensvoll, K.; Oltedal, S.; Javle, M.; Smaaland, R.; Gilje, B.; Nordgård, O., Single-cell mRNA profiling reveals transcriptional heterogeneity among pancreatic circulating tumour cells. *BMC cancer* **2017,** *17* (1), 390.

115. Eisenhauer, E. A.; Therasse, P.; Bogaerts, J.; Schwartz, L. H.; Sargent, D.; Ford, R.; Dancey, J.; Arbuck, S.; Gwyther, S.; Mooney, M., New response evaluation criteria in solid tumours: revised RECIST guideline (version 1.1). *Eur J Cancer* **2009,** *45* (2), 228-247.

116. Yu, M.; Bardia, A.; Wittner, B. S.; Stott, S. L.; Smas, M. E.; Ting, D. T.; Isakoff, S. J.; Ciciliano, J. C.; Wells, M. N.; Shah, A. M., Circulating breast tumor cells exhibit dynamic changes in epithelial and mesenchymal composition. *Science* **2013,** *339* (6119), 580-584.

117. Li, T.-T.; Liu, H.; Li, F.-P.; Hu, Y.-F.; Mou, T.-Y.; Lin, T.; Yu, J.; Zheng, L.; Li, G.-X., Evaluation of epithelial-mesenchymal transitioned circulating tumor cells in patients with resectable gastric cancer: relevance to therapy response. *World J Gastroenterol* **2015,** *21* (47), 13259-67.

118. Lin, E.; Rivera-Báez, L.; Fouladdel, S.; Yoon, H. J.; Guthrie, S.; Wieger, J.; Deol, Y.; Keller, E.; Sahai, V.; Simeone, D. M., High-throughput microfluidic labyrinth for the label-free isolation of circulating tumor cells. *Cell Syst* **2017,** *5* (3), 295-304. e4.

119. Voena, C.; Varesio, L. M.; Zhang, L.; Menotti, M.; Poggio, T.; Panizza, E.; Wang, Q.; Minero, V. G.; Fagoonee, S.; Compagno, M., Oncogenic ALK regulates EMT in non-small cell lung carcinoma through repression of the epithelial splicing regulatory protein 1. *Oncotarget* **2016,** *7* (22), 33316.

120. Mitra, A.; Mishra, L.; Li, S., EMT, CTCs and CSCs in tumor relapse and drug-resistance. *Oncotarget* **2015,** *6* (13), 10697-10711.

121. Lim, M.; Kim, C.-J.; Sunkara, V.; Kim, M.-H.; Cho, Y.-K., Liquid biopsy in lung cancer: clinical applications of circulating biomarkers (CTCs and ctDNA). *Micromachines* **2018,** *9* (3), 100.

122. Sundling, K. E.; Lowe, A. C., Circulating tumor cells: overview and opportunities in cytology. *Adv Anat Pathol* **2019,** *26* (1), 56-63.

123. Wu, L.; Xu, X.; Sharma, B.; Wang, W.; Qu, X.; Zhu, L.; Zhang, H.; Song, Y.; Yang, C., Beyond capture: circulating tumor cell release and single-cell analysis. *Small Methods* **2019,** *3* (5), 1800544.

124. Hong, B.; Zu, Y., Detecting circulating tumor cells: current challenges and new trends. *Theranostics* **2013,** *3* (6), 377-394.

125. Chen, L.; Bode, A. M.; Dong, Z., Circulating tumor cells: moving biological insights into detection. *Theranostics* **2017,** *7* (10), 2606-2619.

126. Punnoose, E. A.; Atwal, S.; Liu, W.; Raja, R.; Fine, B. M.; Hughes, B. G.; Hicks, R. J.; Hampton, G. M.; Amler, L. C.; Pirzkall, A., Evaluation of circulating tumor cells and circulating tumor DNA in non–small cell lung cancer: association with clinical endpoints in a phase II clinical trial of pertuzumab and erlotinib. *Clin Cancer Res* **2012,** *18* (8), 2391-2401.

127. Sundaresan, T. K.; Sequist, L. V.; Heymach, J. V.; Riely, G. J.; Jänne, P. A.; Koch, W. H.; Sullivan, J. P.; Fox, D. B.; Maher, R.; Muzikansky, A., Detection of T790M, the acquired resistance EGFR mutation, by tumor biopsy versus noninvasive blood-based analyses. *Clin Cancer Res* **2016,** *22* (5), 1103-1110.

128. Park, S.-M.; Wong, D. J.; Ooi, C. C.; Kurtz, D. M.; Vermesh, O.; Aalipour, A.; Suh, S.; Pian, K. L.; Chabon, J. J.; Lee, S. H., Molecular profiling of single circulating tumor cells from lung cancer patients. *Proc Natl Acad Sci U SA* **2016,** *113* (52), 8379-8386.

129. Yeo, T.; Tan, S. J.; Lim, C. L.; Lau, D. P. X.; Chua, Y. W.; Krisna, S. S.; Iyer, G.; San Tan, G.; Lim, T. K. H.; Tan, D. S., Microfluidic enrichment for the single cell analysis of circulating tumor cells. *Sci Rep* **2016,** *6*, 22076.

130. Sieuwerts, A. M.; Kraan, J.; Bolt-de Vries, J.; van der Spoel, P.; Mostert, B.; Martens, J. W.; Gratama, J.-W.; Sleijfer, S.; Foekens, J. A., Molecular characterization of circulating tumor cells in large quantities of contaminating leukocytes by a multiplex real-time PCR. *Breast Cancer Res Treat* **2009,** *118* (3), 455.

131. Haber, D. A.; Velculescu, V. E., Blood-based analyses of cancer: circulating tumor cells and circulating tumor DNA. *Cancer Discov* **2014,** *4* (6), 650-61.

132. Chen, C. L.; Mahalingam, D.; Osmulski, P.; Jadhav, R. R.; Wang, C. M.; Leach, R. J.; Chang, T. C.; Weitman, S. D.; Kumar, A. P.; Sun, L., Single-cell analysis of circulating tumor cells identifies cumulative expression patterns of EMT-related genes in metastatic prostate cancer. *The Prostate* **2013,** *73* (8), 813-826.

133. Byers, L. A.; Diao, L.; Wang, J.; Saintigny, P.; Girard, L.; Peyton, M.; Shen, L.; Fan, Y.; Giri, U.; Tumula, P. K.; Nilsson, M. B.; Gudikote, J.; Tran, H.; Cardnell, R. J. G.; Bearss, D. J.; Warner, S. L.; Foulks, J. M.; Kanner, S. B.; Gandhi, V.; Krett, N.; Rosen, S. T.; Kim, E. S.; Herbst, R. S.; Blumenschein, G. R.; Lee, J. J.; Lippman, S. M.; Ang, K. K.; Mills, G. B.; Hong, W. K.; Weinstein, J. N.; Wistuba, I. I.; Coombes, K. R.; Minna, J. D.; Heymach, J. V., An epithelial-mesenchymal transition gene signature predicts resistance to EGFR and PI3K inhibitors and identifies Axl as a therapeutic target for overcoming EGFR inhibitor resistance. *Clin Cancer Res* **2012,** *19* (1), 279-290.

134. Schliekelman, M. J.; Taguchi, A.; Zhu, J.; Dai, X.; Rodriguez, J.; Celiktas, M.; Zhang, Q.; Chin, A.; Wong, C. H.; Wang, H.; McFerrin, L.; Selamat, S. A.; Yang, C.; Kroh, E. M.; Garg, K. S.; Behrens, C.; Gazdar, A. F.; Laird-Offringa, I. A.; Tewari, M.; Wistuba, I. I.; Thiery, J. P.; Hanash, S. M., Molecular portraits of epithelial, mesenchymal, and hybrid states in lung adenocarcinoma and their relevance to survival. *Cancer Res* **2015,** *75* (9), 1789-1800.

135. Milano, A.; Mazzetta, F.; Valente, S.; Ranieri, D.; Leone, L.; Botticelli, A.; Onesti, C. E.; Lauro, S.; Raffa, S.; Torrisi, M. R., Molecular detection of EMT markers in circulating tumor cells from metastatic non-small cell lung cancer patients: potential role in clinical practice. *Anal Cell Pathol* **2018,** *2018*.

136. Ting, D. T.; Wittner, B. S.; Ligorio, M.; Jordan, N. V.; Shah, A. M.; Miyamoto, D. T.; Aceto, N.; Bersani, F.; Brannigan, B. W.; Xega, K., Single-cell RNA sequencing identifies

extracellular matrix gene expression by pancreatic circulating tumor cells. *Cell Rep* **2014,** *8* (6), 1905-1918.

137. George, J. T.; Jolly, M. K.; Xu, S.; Somarelli, J. A.; Levine, H., Survival outcomes in cancer patients predicted by a partial EMT gene expression scoring metric. *Cancer Res* **2017,** *77* (22), 6415-6428.

138. Jia, D.; George, J. T.; Tripathi, S. C.; Kundnani, D. L.; Lu, M.; Hanash, S. M.; Onuchic, J. N.; Jolly, M. K.; Levine, H., Testing the gene expression classification of the EMT spectrum. *Phys Biol* **2019,** *16* (2).

139. Walter, K.; Holcomb, T.; Januario, T.; Du, P.; Evangelista, M.; Kartha, N.; Iniguez, L.; Soriano, R.; Huw, L.; Stern, H.; Modrusan, Z.; Seshagiri, S.; Hampton, G. M.; Amler, L. C.; Bourgon, R.; Yauch, R. L.; Shames, D. S., DNA methylation profiling defines clinically relevant biological subsets of non-small cell lung cancer. *Clin Cancer Res* **2012,** *18* (8), 2360-2373.

140. Witta, S. E.; Gemmill, R. M.; Hirsch, F. R.; Coldren, C. D.; Hedman, K.; Ravdel, L.; Helfrich, B.; Dziadziuszko, R.; Chan, D. C.; Sugita, M.; Chan, Z.; Baron, A.; Franklin, W.; Drabkin, H. A.; Girard, L.; Gazdar, A. F.; Minna, J. D.; Bunn, P. A., Restoring E-cadherin expression increases sensitivity to epidermal growth factor receptor inhibitors in lung cancer cell lines. *Cancer Res* **2006,** *66* (2), 944-950.

141. Habib, J. R.; Yu, J., Circulating tumor cells in pancreatic cancer: a review. *Journal of Pancreatology* **2019,** *2* (2), 54-59.

142. Siegel, R. L.; Miller, K. D.; Jemal, A., Cancer statistics, 2019. *CA: a cancer journal for clinicians* **2019**.

143. Society, A. C., Cancer Facts & Figures 2019. American Cancer Society Atalanta, GA: 2019.

144. Cen, P.; Ni, X.; Yang, J.; Graham, D. Y.; Li, M., Circulating tumor cells in the diagnosis and management of pancreatic cancer. *Biochimica et Biophysica Acta -Reviews on Cancer* **2012,** *1826* (2), 350-356.

145. Effenberger, K. E.; Schroeder, C.; Hanssen, A.; Wolter, S.; Eulenburg, C.; Tachezy, M.; Gebauer, F.; Izbicki, J. R.; Pantel, K.; Bockhorn, M., Improved risk stratification by circulating tumor cell counts in pancreatic cancer. *Clinical Cancer Research* **2018,** *24* (12), 2844-2850.

146. Uenishi, T.; Kubo, S.; Yamamoto, T.; Shuto, T.; Ogawa, M.; Tanaka, H.; Tanaka, S.; Kaneda, K.; Hirohashi, K., Cytokeratin 19 expression in hepatocellular carcinoma predicts early postoperative recurrence. *Cancer science* **2003,** *94* (10), 851-857.

147. Gabriel, M. T.; Calleja, L. R.; Chalopin, A.; Ory, B.; Heymann, D., Circulating tumor cells: a review of non–EpCAM-based approaches for cell enrichment and isolation. *Clinical chemistry* **2016,** *62* (4), 571-581.

148. Millner, L. M.; Linder, M. W.; Valdes, R., Circulating tumor cells: a review of present methods and the need to identify heterogeneous phenotypes. *Annals of Clinical & Laboratory Science* **2013,** *43* (3), 295-304.

149. Poruk, K. E.; Blackford, A. L.; Weiss, M. J.; Cameron, J. L.; He, J.; Goggins, M.; Rasheed, Z. A.; Wolfgang, C. L.; Wood, L. D., Circulating tumor cells expressing markers of tumor-

initiating cells predict poor survival and cancer recurrence in patients with pancreatic ductal adenocarcinoma. *Clinical cancer research* **2017,** *23* (11), 2681-2690.

150. Gemenetzis, G.; Groot, V. P.; Yu, J.; Ding, D.; Teinor, J. A.; Javed, A. A.; Wood, L. D.; Burkhart, R. A.; Cameron, J. L.; Makary, M. A., Circulating tumor cells dynamics in pancreatic adenocarcinoma correlate with disease status: results of the prospective CLUSTER study. *Annals of surgery* **2018,** *268* (3), 408-420.

151. Okubo, K.; Uenosono, Y.; Arigami, T.; Mataki, Y.; Matsushita, D.; Yanagita, S.; Kurahara, H.; Sakoda, M.; Kijima, Y.; Maemura, K., Clinical impact of circulating tumor cells and therapy response in pancreatic cancer. *European Journal of Surgical Oncology* **2017,** *43* (6), 1050-1055.

152. Poruk, K. E.; Vicente Valero III, T. S.; Blackford, A. L.; Griffin, J. F.; Poling, J.; Hruban, R. H.; Anders, R. A.; Herman, J.; Zheng, L.; Rasheed, Z. A., Circulating tumor cell phenotype predicts recurrence and survival in pancreatic adenocarcinoma. *Annals of surgery* **2016,** *264* (6), 1073.

153. Lee, J. S.; Park, S. S.; Lee, Y. K.; Norton, J. A.; Jeffrey, S. S., Liquid biopsy in pancreatic ductal adenocarcinoma: current status of circulating tumor cells and circulating tumor DNA. *Molecular oncology* **2019,** *13* (8), 1623-1650.

154. Wei, T.; Zhang, X.; Zhang, Q.; Yang, J.; Chen, Q.; Wang, J.; Li, X.; Chen, J.; Ma, T.; Li, G., Vimentin-positive circulating tumor cells as a biomarker for diagnosis and treatment monitoring in patients with pancreatic cancer. *Cancer letters* **2019,** *452*, 237-243.

155. Ting, D. T.; Wittner, B. S.; Ligorio, M.; Jordan, N. V.; Shah, A. M.; Miyamoto, D. T.; Aceto, N.; Bersani, F.; Brannigan, B. W.; Xega, K., Single-cell RNA sequencing identifies extracellular matrix gene expression by pancreatic circulating tumor cells. *Cell reports* **2014,** *8* (6), 1905-1918.

156. Amantini, C.; Morelli, M. B.; Nabissi, M.; Piva, F.; Marinelli, O.; Maggi, F.; Bianchi, F.; Bittoni, A.; Berardi, R.; Giampieri, R., Expression profiling of circulating tumor cells in pancreatic ductal adenocarcinoma patients: biomarkers predicting overall survival. *Frontiers in oncology* **2019,** *9*, 874.

157. Szczerba, B. M.; Castro-Giner, F.; Vetter, M.; Krol, I.; Gkountela, S.; Landin, J.; Scheidmann, M. C.; Donato, C.; Scherrer, R.; Singer, J., Neutrophils escort circulating tumour cells to enable cell cycle progression. *Nature* **2019,** *566* (7745), 553.

158. Ozkumur, E.; Shah, A. M.; Ciciliano, J. C.; Emmink, B. L.; Miyamoto, D. T.; Brachtel, E.; Yu, M.; Chen, P.-i.; Morgan, B.; Trautwein, J., Inertial focusing for tumor antigen–dependent and–independent sorting of rare circulating tumor cells. *Science translational medicine* **2013,** *5* (179), 179ra47-179ra47.

159. Wong, K. H.; Tessier, S. N.; Miyamoto, D. T.; Miller, K. L.; Bookstaver, L. D.; Carey, T. R.; Stannard, C. J.; Thapar, V.; Tai, E. C.; Vo, K. D., Whole blood stabilization for the microfluidic isolation and molecular characterization of circulating tumor cells. *Nature communications* **2017,** *8* (1), 1-11.

Acknowledgements

I would like to express my sincere appreciations to my advisor, Professor Yoon-Kyoung Cho, for thoughtful guidance, encouragement, and patience throughout not only to my thesis research but also to my life. Although there were many hardships and difficulties in my doctoral course, I was able to overcome them with her heartfelt advices.

I would also like to thank all my dissertation committee members, Professor Semin Lee, Professor Taejoon Kwon, Professor Mi-Hyun Kim, and Professor Dong Uk Kim for sharing their knowledge, giving good inspiration and suggesting valuable comments to complete this thesis.

All of FRUITS group members have helped me a lot and special thanks to Juhee Park for her precious comments and co-works about CTC research, Dr. Tae-Hyeong Kim, Ada Younglim Lee, and Dr. Yubin Kim for teaching me about the technical skills for the disc when I was a junior. Dr. Jung Min Oh for the supports in numerical simulation of FAST disc. Also, I appreciate all of researchers and students, Dr. Vijaya Sunkara, Dr. Sumit Kumar, Dr. Jonathan Sabate del Rio, Dr. Chi-ju Kim, Dr. Yang-Seok Park, Dr. Hyun-Kyung Woo, Dr. Issac Micheal, Hye-yeon Ha, JunYoung Kim, Sunmin Yu, Yongjun Choi, Chaeeun Lee, Mamata Karmacharya, Oleksandra Gulenko, Jungmin Kim and Jooyoung Ro.

Additionally, I was lucky to involve in the R&D project from the Ministry of Health & Welfare during my doctoral degree and not only I could motivate myself but also I could have many colleagues. I would like to thank all the project team members in Pusan National University Hospital, Keimyung University Dongsan Hospital, Samsung Medical Center and Clinomics.

Finally, I deeply thank my family members, mother and sister for the continuous support and dedication, utmost faith and encouragement throughout tough time. I also thank my soulmates, Dr. Minhee Kim, fresh Dr. Jiuk Jang and In Un Kim for their emotional supports. For the very last part, I really appreciated BTS because their song brightened up my youth which dotted with frustrations. Based on these supports, I was able to endure hard times and become a mature person.